# Experimental and Numerical Investigation of Fire Whirl's Impact on the Firebrand's Lofting Mechanism

This thesis is submitted to the University of Sheffield for the degree of Doctor of Philosophy in the faculty of Engineering.

**Yuchen Zhang**

**Combustion and Energy Research Group**

**Department of Mechanical Engineering**

**November 2022**

# DECLARATION

The work presented in this thesis is that of the Author and has not been submitted for the award of any degree at the University of Sheffield or any other university or insinuation where other sources of information or help from other parties used in this thesis have been acknowledged.

# ACKNOWLEDGEMENT

Firstly, I would like to express my love to my parents who taught me to be brave and honest. I cannot finish my PhD without their support. It is my great fortune to be their son.

I also want to show my gratitude to my supervisor, Professor Yang Zhang. He not only guides my study and research, but also, more importantly, as a role model of a scientist and shows me how to think and persist. With the help of his kind support, I get through the rough time of the PhD.

Also, I appreciate the help from my colleague, Ahmed Albadi and Xiao Wang. You have helped me so much in both the research side and the skill of English writing in the past four years. Without your help, the Language barriers will last for a much longer time.

Moreover, I would like to say thank you to my colleague, Hangxu Zhou. After I failed to pass the Confirmation review, the objectives of my research had to be adjusted. It is my pleasure to continue doing your research and find the research gap in your research area.

Finally, I want to thank my colleagues in the combustion group, Houshi Jiang, Ahmad Fuad, Ahmed Albadi, Muyi Pan, Jing Zhang, Xuanqi liu, Haibo Zhou. I feel so happy and inspired to work together with you.

# Abstract

Wildfire, which is one of the most destructive phenomena on earth, is known as very difficult to suppress, especially in large-scale fires such as forest fires in dry season. Countless acres of land and properties are destroyed due to it are reported each year. One of the most important reasons for its difficulty to control is its spreading mechanism. Among all of the spreading mechanisms for wildland fire, the spotting phenomenon is the most remarkable. The spotting phenomenon is defined as the discontinuous spread of the wildland fire caused by a firebrand, which could be a burning particle generated from a burning tree. With the help of wind, a firebrand could travel miles away from the main fire zone and cause a secondary ignition far from the initial wildland fire. In order to study the spotting phenomenon, a huge amount of publications have focused on the spotting distance of the firebrand under different conditions. However, another topic about the firebrand's takes off mechanism is quite limited. And the taking off mechanism for firebrand is called lofting. As the fact of the maximum spotting, the distance could be more than 10 miles away, the current understanding of the detailed physics of the spotting is not accurate.

In this thesis, the lofting of the firebrands is investigated. The investigation is being undertaken from both experimental and numerical sides. In the experimental study about the firebrand's lofting, a setup for collecting data about the firebrand's lofting mechanism in a fire whirl generator has been developed. In order to qualitatively understand the fire whirl that is being utilized in the experiment, the PIV test was also conducted on the fire whirl generator. Based on the experimental result,

a hypothesis that aerodynamic lift might be one of the key points to the hyper-long spotting distance.

Then, in the numerical study about the firebrand's lofting, a developed mathematic model for predicting the lofting trajectory of the firebrand was developed. The comparisons about including aerodynamic lift and other factors are also included. Meanwhile, a semi-theoretical approach to solving mathematical models has also been developed. After then, the modified approach is proven to be reliable after testing it with the traditional Runge-Kutta method.

Based on the modelling of the lofting mechanism, the impact of aerodynamic lift, tumbling effect, and mass loss effect has been studied. Among the three aspects, the mass loss effect is the less important one, and the aerodynamic lift is the most important one. This conclusion also fits the result of the experimental study.

This study helps build the inner connection between the fire whirl and hyper-long-distance spotting, which deepens the understanding of the detailed physics of the firebrand's lofting mechanism, which could be helpful for firefighters in controlling the wildland fire.

# Table of Contents

[8]

# List of Figure

[12]

[14]

[15]

[18]

[19]

# NOMENCLATURE

| | | |
|:---:|:---:|:---:|
| $A$ | [m²] | Aera |
| $D_{eff}$ | [m] | Effective mass diameter |
| $F$ | [kg·m/s²] | Force |
| $Fall$ | [-] | Number of Fall group cases |
| $Float$ | [-] | Number of Float group cases |
| $Fly$ | [-] | Number of Fly group cases |
| $L$ | [kg·m²/s] | Angular momentum |
| $M$ | [kg·m²/s²] | Moment |
| $Pr$ | [-] | Prandtl number |
| $Re$ | [-] | Reynolds number |
| $V$ | [m/s] | Velocity of an object |
| $W$ | [m/s] | Velocity of the surrounding flow |
| $X$ | [m] | Displacement in horizontal direction |
| $Y$ | [m] | Displacement in vertical direction |
| $b$ | [m] | Coefficient of radius of the plume |
| $c$ | [m] | Chord length |
| $c_p$ | [J/kg·K] | specific heat capacity |
| $g$ | [m/s²] | Acceleration of gravity |
| $k$ | [W/(m·K)] | thermal conductivity |
| $l$ | [m] | Length of the particle |
| $m$ | [kg] | Mass |
| $p$ | [kg/m²] | Radius |
| $r$ | [m] | Radius |
| $t$ | [s] | Time |
| $u$ | [m/s] | X-axis projected velocity of an object |
| $v$ | [m/s] | Y-axis projected velocity of an object |
| $w$ | [m/s] | Z-axis projected velocity of an object |

## NOMENCLATURE (Greek letter)

| | | |
|---|---|---|
| $\alpha$ | [º] | **Angle of attack** |
| $\theta$ | [º] | **Angle in polar coordinate system** |
| $\mu$ | N·s/m² | **Dynamic Viscosity** |
| $\rho$ | [kg/m³] | **Density** |
| $\varphi$ | [º] | **Angle of inclination** |
| $\omega$ | [1/s] | **Angular velocity** |

# ABBREVIATION

| | | |
|---|---|---|
| *AP* | **Affected Percentage** | **A scale to measure the firebrand's motion** |
| *AR* | **Aspect Ratio** | **A scale to measure the shape of a plate** |
| *CFD* | **Computational Fluid Dynamic** | **[-]** |
| *DNS* | **Direct Numerical Simulation** | **[-]** |
| *FDS* | **Fire Dynamic Simulator** | **An open-source wildland fire simulation software** |
| *LES* | **Large Eddy Simulation** | **[-]** |
| *NIFC* | **National Interagency Fire Center** | **[-]** |
| *ODE* | **Ordinal Differential Equation** | **[-]** |
| *PIV* | **Particle Image Velocimetry** | **[-]** |

# SUBCRIPTS

| | |
|---|---|
| $x$ | x-axis |
| $y$ | y-axis |
| $z$ | z-axis |
| $D$ | Aerodynamic drag term |
| $L$ | Aerodynamic Lift term |
| $Flow$ | Flow |
| $Relative\ or\ R$ | Relative |
| $a$ | Absolute |
| $VM$ | Virtual mass term |
| $PG$ | Pressure gradient term |
| $G$ | Gravity |
| $B$ | Buoyancy |

# 1. Introduction

## 1.1. Motivation

Wildfires, also known as bushfires and forest fires, threaten people's life and property [9]. It has increasingly drawn the attention of the public in recent years due to its destructiveness and difficulty to control.



*Figure 1.1. A typical photo of a wildland fire published on the official website of*

*Washoe County, Emergency Management and Homeland Security [83].*

The record of wildfire's destructiveness can be traced back to the Great Fire of Rome in 64 ADS [39]. Every year, trillions of pounds of economic losses are caused unavoidably by wildfires globally [40]. Hundreds of thousands of people have been left homeless since their homes were destroyed by the wildfire. For example, more than 7500 dwellings were destroyed in the 2016 Fort McMurray [13], which caused over

USD 12 billion in numerical costs [69]. The Great Fire of Rome lasted six days and seven-night; seventy per cent of the city was ruined in such tremendous disaster. Research shows that changes in climate create warmer, drier conditions, which extend the fire season and increase the wildfire risk. Therefore, studying the methodology of controlling it turns out to be a critical topic. Currently, the only effective method to handle wildfires is to address the root causes of wildfires. Nature ignitions caused by lighting are a vital factor. However, human-caused fires are usually more severe. According to the National Interagency Fire Centre's statistic, in 2021, 52641 over 52985 wildfires was caused by human activities in the USA, and 3023759 acres over 7125643 acres of land was destroyed by human-caused wildfire [69]. Human-caused fires may result from campfires and negligently discarded cigarettes. Take one of the most sever victims of wildfire as an example. In the USA, the 'Smokey bear' act of educating the public about the dangers of human-caused wildfires can be traced back to 1944.

However, strict rules may not stop the wildfire thoroughly. Some researchers believe that climate change will also increase the wildfire risk. Since the ignition of wildfires is inevitable, it is necessary to study the detailed physics of it and find appropriate ways to control the wildfire and eventually put it out.

The history of studying wildfires can be called back to 1911. In such year, Coert Dubois, who is assumed to be the early-stage leadership of fire researchers, made the first case study on wildfire [67]. He also made the first use of statistical methods in analysing wildfires in 1914. Furthermore, the first fire behaviour and fire effects research in around 1915. In such kinds of research, he called for developing a method

not only for quantifying fire danger but also for determining the rate of the wildfire burning uncontrollably [67]. Based on his study, there are six factors, which are inflammability, season, risk, controllability, liability, and safety, were used to measure the overall fire danger [21]. Thus, most of the research on wildland fires is to focus on their control.

Empirical or semi-empirical models are widely used in justification to support decision-making on the wildland fire control process. Cruz & Alexander reviewed the performance of the operational fire models and pointed out the importance of estimating the free-burning fire spread rate to those empirical models [14]. Sharples [91] pointed out that such operational models are developed with quasi-steady state assumptions which may not be present in the wildfire that existed in reality and is the reason for the difficulty of predicting the wildfire behaviours.

Therefore, knowing the physics of the spread and building the physical model of the wildfire spread will be necessary to predict the behaviours and control the wildfire. As Tarifa and Torralbo [11] stated that heat is the crucial factor in the process of the flame propagation mechanism, in which the radiations and convections are both significant characteristics. Focusing on the radiations and convections could be helpful to build a physical model of the speed of spread of the wildfire. However, the wildfire is more than just a free-burning fire spread model. A more challenge property of wildfire is its discontinuous spread, especially the hyper-long-distance ones, which is difficult to predict.

*Figure 1.2. A typical photograph of a firebrand in a real wildland fire observed in the*

*eucalyptus forest near Melbourne, Australia[81].*

Spot fire distance is used to define the discontinuous firebrand's distribution [93]. It is

known that the spot fire distance becomes more significant with increasing intensity

and size of the wildfire. However, it still lacks a basic understanding of the mechanism

of firebrand transport. Moreover, a few contradictions have been found during the

critical review of the experimental study of firebrand transport. The following chapter

will introduce and analyse such contradictions to provide a brand-new understanding

of the firebrand spotting mechanism.
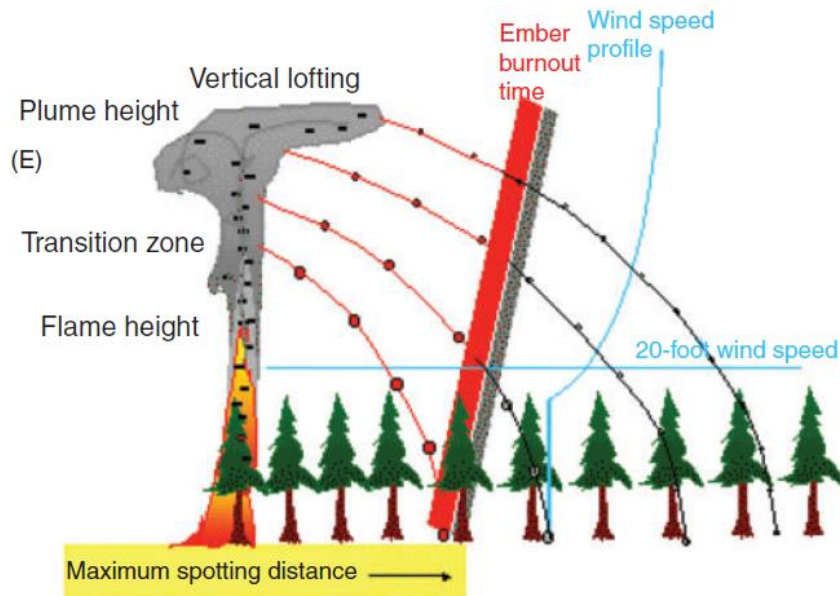
*Figure 1.3. Traditional understanding about the mechanism of firebrand's transport [40]. The first stage is lofting by the vertical wind, in which the lift force's effect can be neglected [36]. Moreover, the second one is horizontal transport, in which a rare study about modelling with the lift effect has been reported.*

The previous study of firebrands was mainly divided into three topics: generation, transport, and the mechanism of its ignition of exposed fuel. Of all these three topics, most studies have focused on firebrand transport.

In 1965, Tarifa [11], for the first time, investigation the transport of firebrands. By neglecting the influence of the firebrand's shape and surrounding wind velocity's change, he built the first aerodynamic model for firebrand transport. Other researchers improved his model in several different aspects, such as the shape of the firebrand, the angle of attack, and the flow condition from the wildland fire, which will be discussed in the following chapters.

Until now, due to difficulties in measuring transport, much of the study of firebrand

transport comes from mathematical modelling of lofting and downwind transport [41]. However, these models lack experimental validation [80], leading to a wrong solution to some extent.

By analysing the limited number of experiments which study the firebrand transport, it is clear that the present models neglect some important factors which are vital to understanding firebrand transport.

Most of the transport models are based on previous research about windborne debris [23]. However, the basic assumptions of windborne debris do not fit the situation of firebrands [92]. While the windborne debris is lifted by strong winds such as hurricanes and tornadoes, [2]the firebrand is lifted by the vertical plume generated from the wild-fire [11][36]. The wind condition is different. Therefore, the windborne debris theory will be misleading when studying the firebrands' transport phenomenon.

One piece of evidence about the limitation of windborne debris theory in explaining firebrand transport comes from the contradiction between A. Muraszew's [3] and Ali Tohidi's [80][76][77] experiment results. Ali Tohidi pointed out that a 12m/s velocity air jet is not able to loft the wooden firebrand, while A. Muraszew is able to lift the wooden firebrand by using a fire whirl with a vertical velocity of 9.2 m/s [2]. The details about comparing these two experiments will be undertaken in the following paragraphs. Moreover, a similar result has been obtained by our experiment that is taken in Spain, which will also be discussed in the following paragraphs.
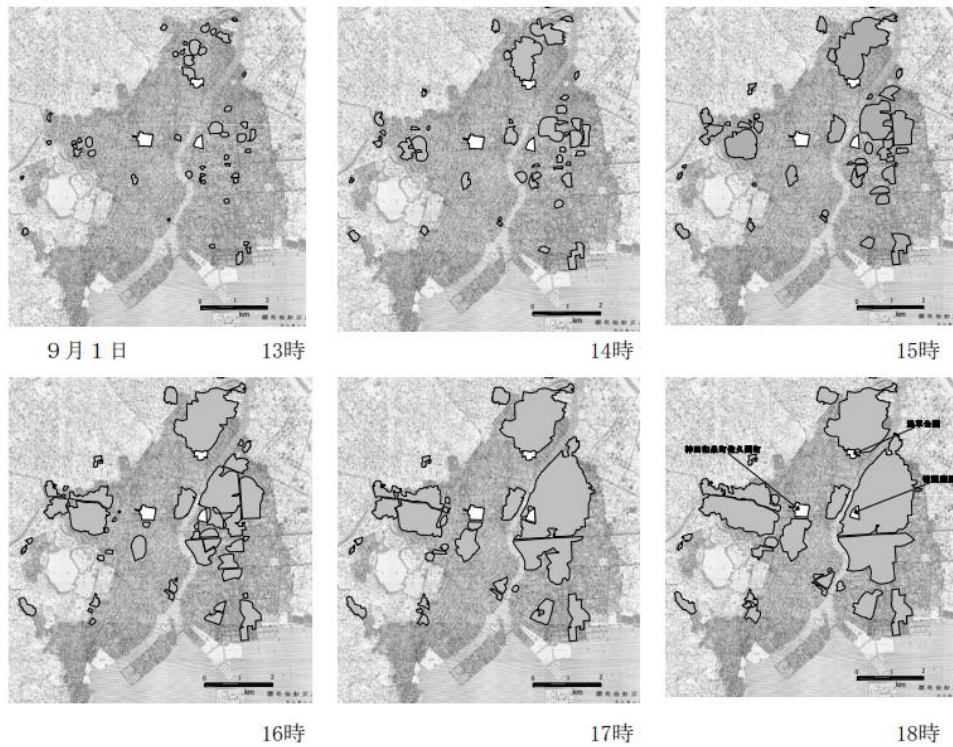
*Figure 1.4. The data of fire spotting distance at different times of the 1923 Tokyo Fire was provided by the report published by the Government of Japan [90].*

Another piece of evidence comes from the statistics from the 1923 Tokyo Fire, which spread rapidly owing to a strong typhoon. By checking the weather record, the velocity speed for the first day ranged from 10.7 to 21.8 m/s, which is higher than that of the plume generated by wildland fire. However, the maximum spot distance is about 4km, which is not far compared to other wildland fires without the impact of typhoons [90].

7
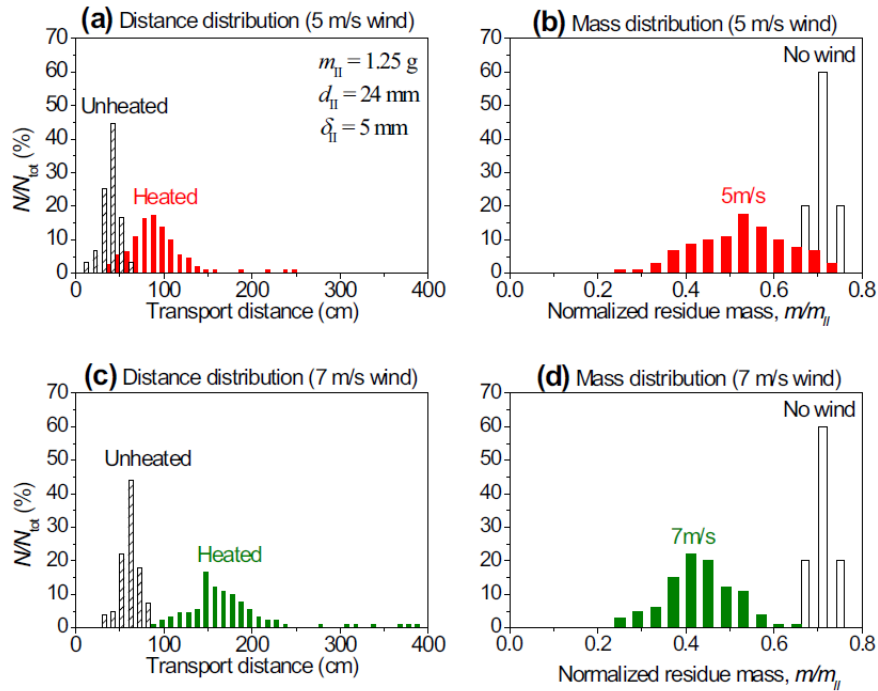
*Figure 1.5. The experiment data of disk-shaped particles with a diameter of 24 mm and thickness of 5 mm of spotting distance with or without ignited in different speeds of wind flow [38]. Such results indicate that the burning effect on the spotting distance is a complicated topic [38].*

In Jiayun Song's experiment[38], the burning of the firebrand will also affect transport. From their experiment, statistics show that the spotting distance will extend compared with the unburned firebrand. Moreover, the mode of burning will also affect the spotting distance. However, in the mathematical models, the effect of burning is neglected or only assumed to affect the mass of the firebrand during transport.

From a brief review of the previous publication on the firebrand's transportation, it is clear that the fundamental mechanism of the firebrand's transportation in the wildland fire is still not clear enough. Whatsmore, there are some research gaps about

the hyper-long-distance transportation of the firebrand.

Therefore, my PhD study aims to improve the understanding of the mechanism of lofting the firebrand from both experimental and numerical sides. In the numerical side of studying the firebrand's lofting mechanism, a serial of the model will be introduced to compare the result, eventually building a better model to predict the transport of the firebrand. Meanwhile, some brand-new data-collecting procedures were introduced in the experimental side of studying the firebrand's lofting mechanism. The collected data has also been used to validate the numerical model.

## 1.2. Aim and Objectives

### 1.2.1. Aim of research

The aim of my PhD studying is to understand the primary mechanism of firebrand transport. To further investigate the detailed dynamics of the firebrand, the previous transport model should be investigated, and several experiments for collecting the data should be designed. By critical reviewing the previous study, the limitation of previous models has been discussed. A few hypotheses have been made to explain the phenomenon of firebrand lofting. Moreover, from the previous study, it is clear that for a specific shape and density of firebrand, the initial angle of attack will affect the mode of motion seriously[35], which eventually will influence the flying path of the firebrand. However, only a limited understanding of how the firebrand's burning affects its transport has been studied. Thus, in order to study the transport of firebrands, the experiment of tracking the path and rotation mode of a firebrand should be made. In order to investigate in more detail about firebrand transport, a

real wildfire experiment will be conducted. With its complicated flow condition, more phenomena will be overserved. Therefore, collecting the data for firebrands in real wildland fire would be not only a good contribution to investigating the aerodynamics of firebrands but also a new method for researching the topics about particles in flow fields. Then, the new design of the experiment set-up should be developed to fit the requirement of real wild-fire experiments.

## 1.2.2. Objectives

a) Review current literature relating to mechanisms of firebrand's transport, the influence of the angle of attack on the flying path, and the method of collecting the data during its transport.

b) Study the effect of fire whirl on the firebrand's lofting and its self-rotation effect.

c) Collect the data about the fire whirl that is being utilized to study the firebrand's motion.

d) Analyse the data of firebrands and establish a better transport model to predict the transport of firebrands.

e) Develop a new methodology to solve the governing equations about the firebrand's motion.

## 1.3. Thesis outline

In Chapter 1, The motivation for author to undertake the investigation about the

wildland fire is being given directly with main objectives. The thesis outline is also being mentioned in this chapter.

In Chapter 2, the critical review of the firebrands and spotting phenomenon in large-scale wildfires are given. In this chapter, the basic combustion model for firebrands is reviewed. Then, the review of the aerodynamic properties for the rectangular-shaped firebrands are placed. After analysing the forces that exerted on the firebrands, the coefficients of both drag and lift are discussed in detail. After then, the generation system of fire whirl will be reviewed. Four types of the fire whirl generator will be reviewed, and the appropriate one was chosen.

In Chapter 3, the experimental study of the firebrand's lofting mechanism will be introduced. Two sections will be provided. For the first one, a brand-new method of studying the fire whirl's additional impact on the firebrand's lofting mechanism has been introduced. The statistical approach to analyse such additional impact will also be discussed. In the second section, the Particle Image Velocimetry technique will be utilized to provide a qualitative analysis of the generated fire whirl by the chosen fire whirl generator.

In Chapter 4, A detailed introduction to the numerical method of the firebrand will be introduced. The aerodynamic forces, such as drag and lift, are focused on in the introduction. A brand-new indirect method of measuring the direction of the aerodynamic force in a three-dimensional domain has been introduced and analysed in this chapter. After then, the governing equations of the motion of firebrands were introduced. A brand-new method for solving differential equations semi-theoretically has been introduced in this section.

Based on the mathematical models introduced in Chapter 4 and in Chapter 5, a detailed study of the lofting performance of the firebrand under a simulated fire whirl has been undertaken. The Fire Dynamic Simulator (FDS) has been utilized as the simulation software. The impacts of multiple factors, such as aerodynamic lift, tumbling, and mass loss effect, were investigated. Each factor's impact on the lofting performance has been discussed in detail in this chapter.

In the end, the main conclusions of the studies in this thesis are presented in Chapter 6, and the main findings from the studies are also concluded. For the next steps of the investigation, the corresponding future works are highlighted in Chapter 7.

# 2. Literature review

## 2.1. Wildland fire and spotting phenomenon

A wildland fire is an uncontrolled fire burning in a rural area of vegetation. It can burn in woods, grasslands, and other ecosystems and have a history of at least millions of years. From its definition, it is clear that the combustion of vegetation in a rural area could be positive effects on human life, such as the secondary succession of the plants, accelerated farming, and military usage. This could be called back to the land-use fire in German Odenwald in 1290 and the Black Forest in 1344. However, once mentioned uncontrolled, the hazards of wildland fire turned out to be more destructive than their positive part to human life. As one of the most severe civilisation disasters worldwide, human life and property have been threatened by wildland fire for a long history, from the Great fire of Rome in 64 AD [39] to the long-lasting California fire in November 2018 [12]. Once the combustion turns into an uncontrolled fire, it is almost impossible to put it out of humankind's strength.

Such tragedies also attract quantities of researchers' attention. Their studies cover a wide range of topics regarding the mechanism of wildland fire, such as the formation[20], propagation[41][6][61], and secondary ignition of the wildland fire[48], which eventually helps the firefighters to deal with the wildland fire more effectively and more efficiently.

Based on NIFC's statistics[69], there are two major causes of the formation of the wildland fire, the lightning-caused of wildland fires and the Human-caused wildland fire. Meanwhile, there are also several minor causes, such as volcanic eruptions and

extreme weather. From all these causes of wildland fire, human activities cause most of the wildland fires. Thus, it is unavoidable for humans to live with the threaten of wildland fire. Furthermore, Whatmore, studying the mechanism of wildland fire is significantly important for human beings.
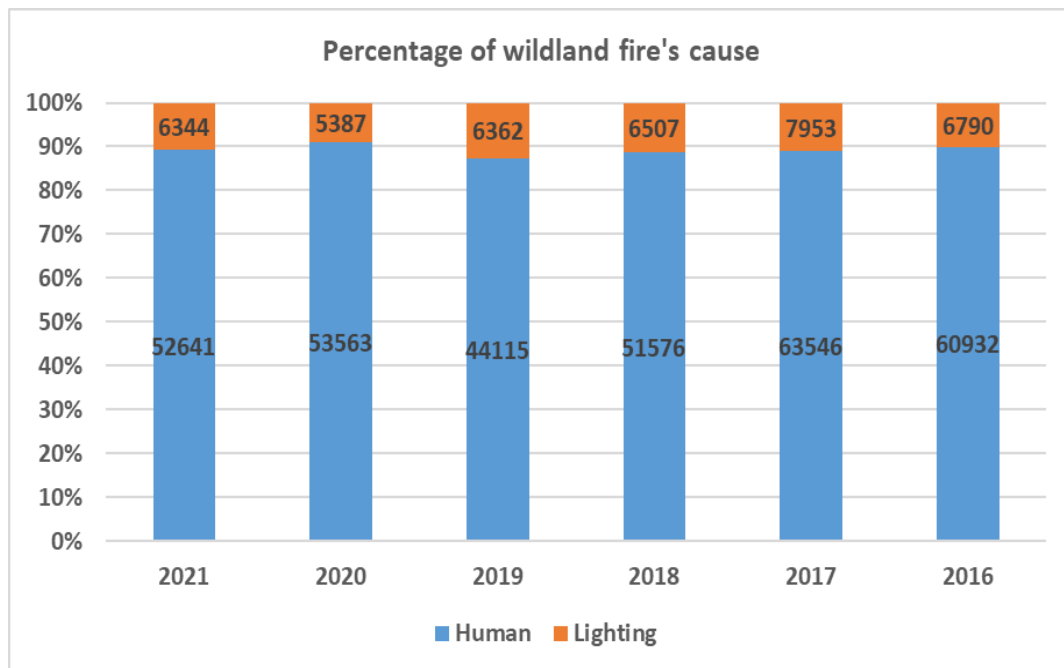


*Figure 2.1. The data of recorded wildland fire cause from 2016 to 2021 [69]. From the figure, it is clear that the frequency of human causes of the wildland fire is significantly higher than that of the nature cause. Therefore, Studying the strategy for understanding and controlling the wildland fire is quite necessary.*

For the propagation of wildland fire, it is an interdisciplinary study that covers Combustion, Pyrolysis, Heat Transfer, Fluid Dynamics, Aerodynamics, etc. There are great amounts of investigations focused on this topic by different approaches and models. The McArthur's statistical model was developed in 1966 and to characterise the wildland fire of the bush [45]. Williams' empirical model was developed in 1977, which focused on investigating the relationship between heat flux to the speed of

propagation of wildland fire [84]. Weber's physical model was developed in 1991 to study the mechanisms of conductive, convective, and radiative heat transfer [82]. They are both examples of the investigation into the wildland fire's propagation.

However, since the objective of the thesis is to focus on the firebrand's spotting phenomenon, there would not be a further review of other transporting mechanisms. In the following chapter, the history and details of firebrands and spotting phenomenon investigation are reviewed, together with their fundamental characterises.

## 2.2. Firebrand and spotting phenomenon

### 2.2.1. Firebrand

Firebrands, commonly known as burning embers, are one of the most significant reasons for fire spread mechanisms under the condition of wildland fire. It can be a piece of wood, leaves or charcoal etc. The history of this word could be called back to 1965. Tarifa [11] firstly introduced it as a kind of particle that is lofted by the fire plume from the wildland fire and transported by wind to generate a secondary ignition far from the main fire zone. An example of the extinguished firebrand, which was found in the position 1 km away from the centre zone of the Oakland Hill fire in 1991, is presented in Figure 2.2 [40].

*Figure 2.2. A real firebrand from Oakland Wildfire. About 50mm in diameter, 5mm in thickness, and 2.3g in weight [40]. As it had burnt during transportation, the initial size of it should be larger. And this dimensional information of the firebrand will be utilized in the following mathematical modelling. And in the comparison of the experimental study of the firebrand.*

Since it is the very first published real firebrand, the geometry of the firebrand is utilized in the mathematical model. Another reason is that the geometry of a firebrand is extremely random. Therefore, it can be concluded that most of the real firebrands are irregularly shaped from the current publications. In real wildland fire, the firebrand is generated from various types of wood species. Therefore, a typical firebrand's density ranges from 250 kg/m3 to 950 kg/m3 [20]. However, due to the post-reaction, the density of a firebrand also depends on its combustion and the period of burning. The firebrand, shown as the example in Figure 2.3, was produced from a cedar shingle, where its original density was 385 kg/m3. The generated firebrand's measured density was about 250 kg/m3. It seems that with a longer period of combustion, the density

of firebrands tends to be lighter due to the long-time burning and carbonization. From Figure 2.2., the sample of the firebrand's diameter is around 50mm * 50mm * 3 mm.

A typical life cycle for a firebrand can be mainly separated into three steps: generation, transportation, and ignition [40]. There are huge amounts of investigation for the three topics of firebrands. However, this thesis is mainly focusing on its transportation part, and more specifically, the lofting stage. The firebrand's generation and secondary ignition will be briefly introduced in the following paragraphs.

The generation of firebrands is the process of converting from part of trees to burning particles [20]. And as an important topic of firebrand investigation, the size distribution of firebrands also has attracted plenty of researchers' attention. That is because the size of firebrands significantly affects the firebrand's behaviour, such as lofting, transporting, and secondary ignition. Both experimental study and numerical simulation have been applied to the size distribution of firebrands. In comparison, the experimental studies occupied the majority position of such investigation.

*Figure 2.3. The firebrand samples were collected in a prescribed fire conducted in a pine forest [20]. The variety of the shape and size indicate that in real wildland fire, the firebrand's shape is complicated. However, most of them are shown as a plat that has a relatively large cross-section area with a little thickness. Therefore, in the investigation of this thesis, the shape of the firebrand is simplified as a rectangular plate.*

Collecting from full-scale experiments, Figure 2.4 demonstrates the collected samples of a firebrand. Three times the experiment was conducted in the Pinelands National Reserve (New Jersey, USA.) [20]. By analysing the data of the sample collected from the experiment, the size distribution was able to be generated. Three different plots represented different types of particles, which were the bark slices, pine, and shrub branches.
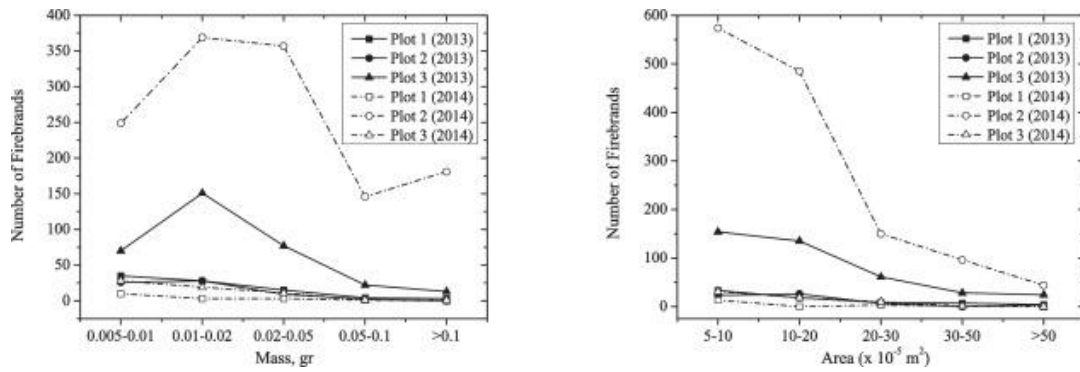
*Figure 2.4. The firebrand simple's distribution of the mass range and area range [20]. The size indicates that the approximate size range of the firebrand is around $10^{-5}$ m, which is fit for the size of the firebrand that is being utilized in the numerical modelling.*

There were also limited publications that used numerical simulation to study the size distribution. Tohidi's research was one of the examples [78]. The Monte-Carlo method was applied to predict the generation of the size distribution of firebrands.
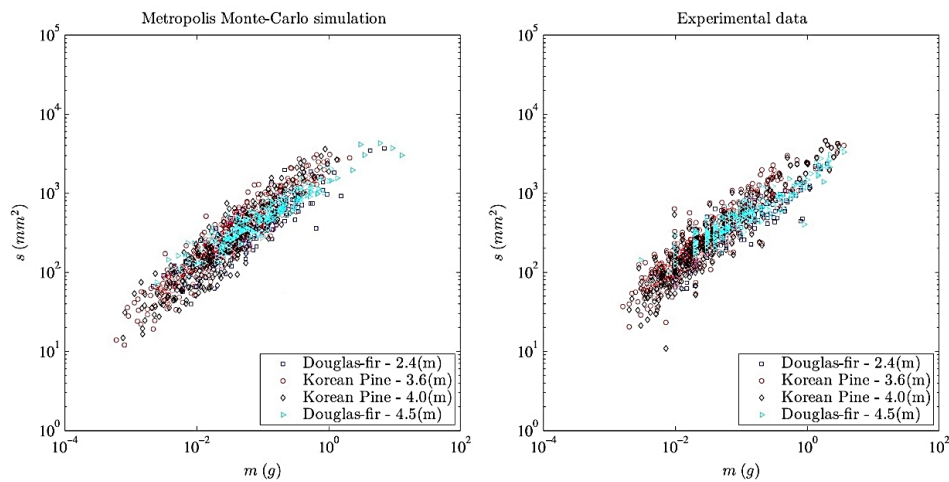


*Figure 2.5. The numerical simulation and experimental data about the firebrand [78].*

From the previous publications, it is clear that the size of generated firebrand from a real burning tree mainly varied between $10^2$ to $10^3$ mm². Such conclusions could be

applied to the following study of the simulation directly. In order to simplify the calculation, the surface area of the firebrand was set to $10^2$ mm$^2$, which means that the firebrand is a 1cm * 1cm square disk. Although the firebrand being observed from the experiment also covered the shape of the cylinder and bar, the bigger surface area usually indicated a strong relationship with the spotting ignition. Therefore, in the simulation, only the disk-shaped firebrand was utilized.

## 2.2.2. Spotting phenomenon

The phenomenon of discontinuous fire spread that is related to the firebrand is called spotting. It was firstly introduced by Byram in 1954 [67]. About two years later, a more precious definition was given by the USDA Forest Service 'Spot fire is the fire set outside the perimeter of the main fire by flying sparks or embers' and 'Spotting is the behaviour of a fire producing sparks or embers that are carried by the wind and start new fires beyond the zone of direct ignition by the main fire' [67].
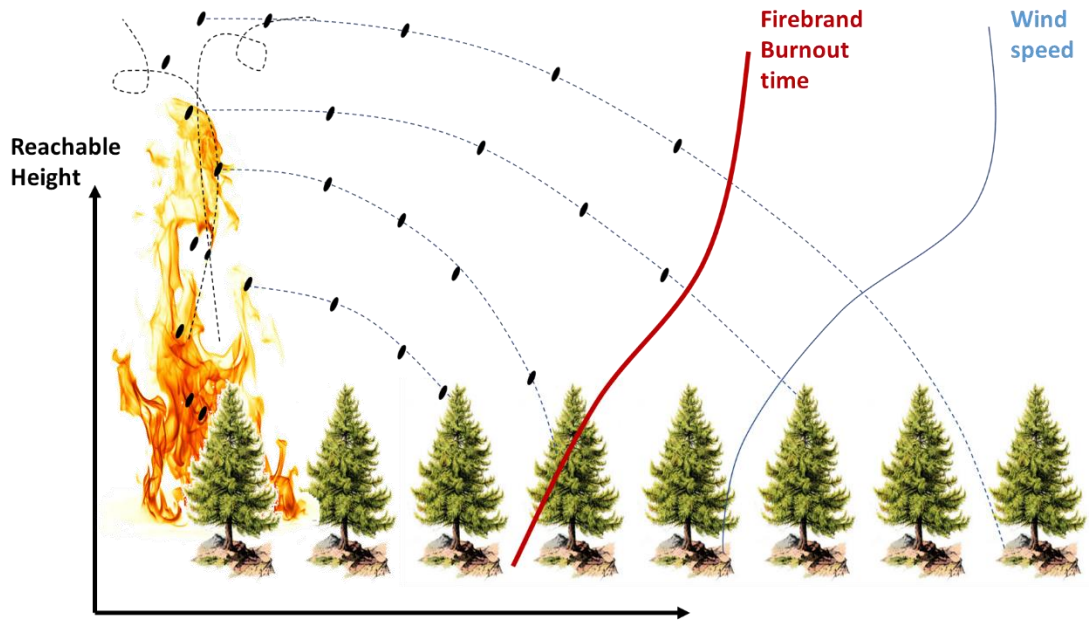
*Figure 2.6. A typical lift of a firebrand generated from wildland fire. The vertical fire plume lifted the firebrand into the sky. And from a certain height, the horizontal wind speed will transfer the firebrand into a far distance, which eventually ignites the secondary fire. Also, as the firebrand keeps burning during transportation, the firebrand may burnout before landing.*

As mentioned before, the process of spotting can be mainly divided into three stages, generation, transportation, and secondary ignition [40]. The generation stage has been introduced in the previous paragraphs. In the part of the firebrand's transportation, researchers focused on the firebrand's aerodynamic properties, burning model, and surrounding flow with wind profiles. For the secondary ignition, the heat transfer and chemical reaction between the firebrand to the recipient fuel were the most popular topic for study. In this thesis, the transporting of a firebrand is one of the main objectives is focused. Figure 2.6, produced by the author, is presented to show the spotting with firebrands.

One of the most significant factors for spotting is distance [68]. Based on the magnitude of firebrands' travelling area, the spotting phenomenon is able to be divided into two conceptions, short-distance spotting and long-distance spotting. The short-distance spotting could cause new ignition about 0.5 km away from the main fire zone. At the same time, the long-distance spotting's magnitude is about several miles. The longest record for the spotting distance was 29 km [53]. The statistic study for it by determining the spotting distances has been undertaken several times for different wildland fires.

It is apparent that the long-distance spotting phenomenon is much more destructive. One of the main objectives of this thesis is to study the mechanisms of long-distance spotting. The following chapters will mainly focus on introducing the current study of the firebrand's transportation.

## 2.2.3. Transportation model and spotting distance

Since the 1960s, the relevant work of studying the transportation of firebrands has been started. A huge number of papers have been published as well as a huge number of models that are used to predict the trajectories and the maximum spotting distance of a firebrand. The following chapters will review the inspiring research in chronological order.

***Tarifa's model [11]***
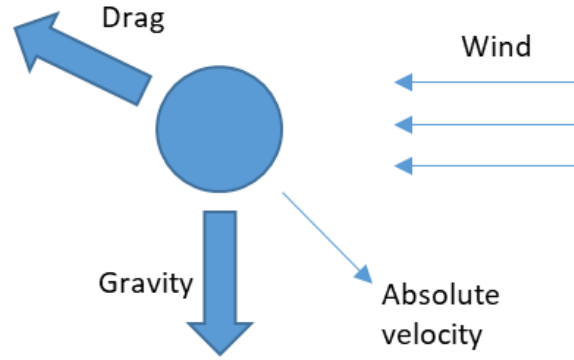
*Figure 2.7. A schematic of the spherical and drag-only model built by Tarifa. In this model, the only aerodynamic force that is being considered is the aerodynamic drag, which is pointed opposite to the relative velocity of the surrounding flow.*

As the very beginning study for firebrand transportation, Tarifa [11] provides the most fundamental transportation model, which is being improved many times in the following few decades. By analysing the data collected from the burning experiments for spherical firebrands in a vertical wind tunnel. The model of a spherical firebrand under the constant flow field could be expressed as:

$$m\,\frac{dV_x}{dt} = -\frac{1}{2}\,\rho_a\,A\,C_D\,W^2\,\frac{W_x}{W} \qquad \text{(Eq. 2-1)}$$

$$m\,\frac{dV_y}{dt} = -\frac{1}{2}\,\rho_a\,A\,C_D\,W^2\,\frac{W_y}{W} + mg \qquad \text{(Eq. 2-2)}$$

where $C_D$ indicates the coefficient of drag, $\rho_a$ is the density of surrounding air, $A$ and $m$ are the reference area and the mass of the firebrand. $\overrightarrow{W}$ is the relative velocity of the wind with respect to the motion of the firebrand, and $\vec{g}$ is the acceleration of gravity. For this very beginning model, the buoyancy force was not introduced, neither the lift force. The experimental objectives were idealized as spherical particles. For the trajectory of the firebrands in a flow field, the expressions were given as follows:

23

$$X = \int_0^t (u_x - W_x)\, dt \qquad \text{(Eq. 2-3)}$$

$$Y = \int_0^t (u_y - W_y)\, dt \qquad \text{(Eq. 2-4)}$$

where $u$ is the wind velocity around the firebrand, and the subscripts $x$ and $y$ indicate initiate the horizontal and vertical directions, respectively. By integrating the absolute velocity of the firebrand in its relative direction, the trajectories and the maximum spotting distance is able to be calculated.

As the most basic transportation model, it is no doubt that there are a lot of limitations in it, such as the spherical assumption, constant wind speed, and neglecting of aerodynamic lift. However, it provided a simple but clear method for predicting the firebrand's propagation. Overall, most of the later model is developed based on it.

### Lee's model

In 1969, Lee [44] improved Tarifa's model by introducing the swirling model to the firebrand transportation model by replacing the constant wind speed assumption. The fire-swirling model Lee used is shown in the following Figure.
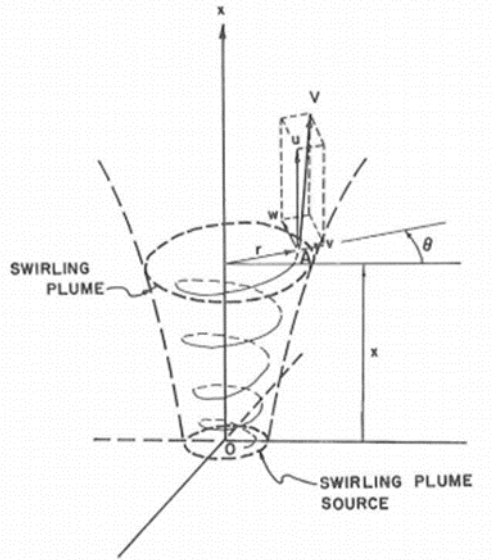
*Figure 2.8. the swirling plume model under the cylindrical coordinate system that was introduced in Lee's model[44]. The aerodynamic model for the firebrand is not verified a lot. However, due to the introduction of a swirling plume source, the performance changes significantly.*

The asymmetrical turbulent swirling natural-convection plume model, of which the velocity field can be written as:

$$u(x,r) = u(x) * e^{(-\frac{r^2}{b^2})} \qquad \text{(Eq. 2-5)}$$

$$w(x,r) = w(x) * f\left(\frac{r}{b}\right) \qquad \text{(Eq. 2-6)}$$

In the previous equations, $u(x,r)$ and $w(x,r)$ represent the axial and swirling velocity. $b = b(x)$ is the equation of a characteristic radius of the plume. $f\left(\frac{r}{b}\right)$ indicated the profile of the swirling velocity.

Together with the continuity equation:

$$\frac{\partial p}{\partial t} + \frac{1}{r}\frac{\partial \rho v r}{\partial r} + \frac{1}{r}\frac{\partial \rho w}{\partial \theta} + \frac{\partial \rho u}{\partial x} = 0 \qquad \text{(Eq. 2-7)}$$

25

The radial velocity $v$ is achievable, which is:

$$rv = bu(x)\left[e^{-\frac{r^2}{b^2}} - 1\right]\frac{db}{dx} + \frac{b^2}{2}\left[e^{-\frac{r^2}{b^2}} - 1\right]\frac{du(x)}{dx}$$

$$+ \frac{r^2u(x)}{b}e^{-\frac{r^2}{b^2}}\frac{db}{dx}$$

(Eq. 2-8)

And by converting Tarifa's model [11] into cylindrical coordinates, the governing equation is:

$$\ddot{x} = \frac{3}{8}\left(\frac{\rho}{\rho_p}\right)C_D(r_0 - ct)^{-\frac{1}{2}}(u - v_x)^2 - g + \frac{\rho}{\rho_p}g$$

(Eq. 2-9)

$$\ddot{r} - r\dot{\theta}^2 = \frac{3}{8}\left(\frac{\rho}{\rho_p}\right)C_D(r_0 - ct)^{-\frac{1}{2}}(v - v_r)^2$$

(Eq. 2-10)

$$r\ddot{\theta} + 2\dot{r}\dot{\theta} = \frac{3}{8}\left(\frac{\rho}{\rho_p}\right)C_D(r_0 - ct)^{-\frac{1}{2}}(w - v_\theta)^2$$

(Eq. 2-11)

Lee's model also contained several limitations that were not able to be neglected. Although the complicated fire plume model has been introduced to replace Tarifa's constant velocity field, it still keeps the spherical assumption and neglects the aerodynamic life effect. The other two assumptions will be released in the following few years of studying.

***Albini's model [5][6]***

Since 1979, Albini [5][6] has become one of the most popular researchers on the topic of firebrand research. His investigation covered a wide range of areas, from the prediction of spotting distance under various conditions to the wind-blown flame models. He also investigated the firebrand behaviour experimentally; various shapes of firebrands were applied in the experiments, such as plates, cylinders, and spheres.

As a later relative model for the firebrand's transportation, Albini's model considered

the shape of the firebrand together with a more complicated flow field that drove the firebrand. The governing equations for firebrand motion could be expressed as follows:

$$\ddot{x} = \frac{1}{m}f - gj$$

where $\ddot{x}$ is the acceleration vector of the firebrands in a global translating but non-rotating coordinate reference. $f$ is the overall force vector being applied to the firebrands. $m$ is the mass of the firebrand, $g$ is the gravity acceleration that is being applied to the firebrand. $j$ represents the unit vector along the vertical direction under the global coordinate reference.
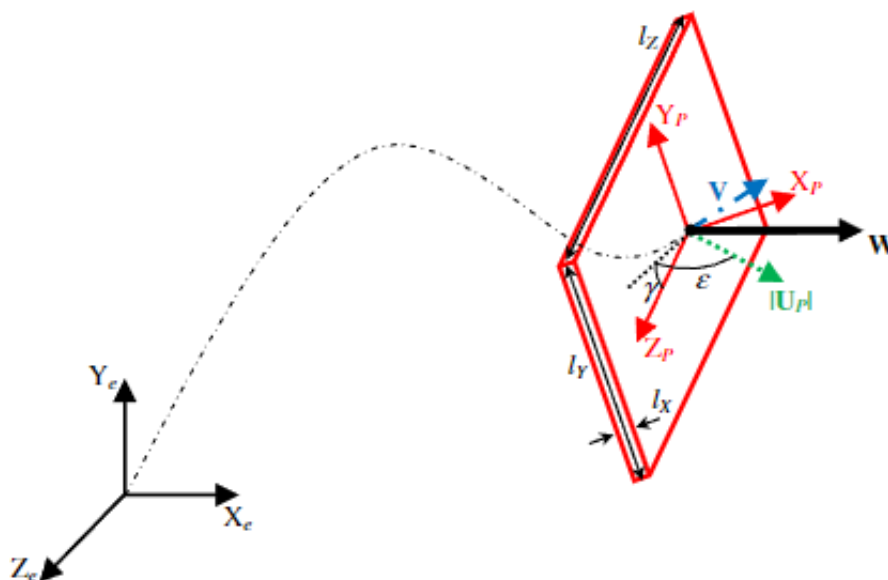


Figure 2.9. The schematic is about a rectangular plate-like firebrand's definition of aerodynamic angles [23]. That in Albini's most complicated model utilized.

A breakthrough point from Albini's model is that the three dimensions of motion have been considered, together with the rotation. The reaction from the flow to the firebrand along its principal axes is as follows:

$$F_p = C_F \frac{1}{2} \rho_a \left| U_p \right|^2 A_r \qquad \text{(Eq. 2-13)}$$

where $F_p$ is the external force applied to the firebrands along the principal axes, $C_F$ is the force coefficients measured from experiments. $\rho_a$ is the density of the surrounding flow of the firebrands. $A_r$ is the referencing area of the plate. $U_p$ is the relative velocity components along the firebrand's principal axes. By considering its three dimensions, the moments of the firebrands could be expressed as below:

$$M_p = M_E + M_D \qquad \text{(Eq. 2-14)}$$

where $M_p$ is the applied moment vector along the principal axes, $M_E$ is the externally applied moment, and $M_D$ is the damping moment.

$$M_E = C_{EM} \frac{1}{2} \rho_a \left| U_p \right|^2 V_r \qquad \text{(Eq. 2-15)}$$

$$M_D = C_{DM} \frac{1}{2} \rho_a \left( \left| U_p \right| + \frac{1}{2} |\omega| \sqrt[2]{l^2} \right) V_r \omega \sqrt[2]{l^2} \qquad \text{(Eq. 2-16)}$$

$C_{EM}$ is the externally applied moment coefficients measured from experiments. $C_{DM}$ is the damping moment coefficient measured from experiments. $V_r$ is the referencing volume for the firebrand. $l$ is the referencing length for the firebrand. $\omega$ is the angular velocity vector for the firebrand.

Then by using Euler's equation for rigid body dynamic. The angular momentum of the debris could be defined as:

$$\dot{L}_p = M_p - \omega \times L_p \qquad \text{(Eq. 2-17)}$$

$L_p$ is the angular momentum of the debris.

There are also many other researchers that build plenty of other inspiring models that

predict the firebrand's transportation, such as Muraszew [3][2] and Woycheese [41]. This thesis was just focusing on some representative models to introduce the timeline of mathematical models of firebrand's research. From the literature review made above, the trend of developing the firebrand's model is apparent. The model was developed more complicated and fit for more general conditions. As a popular topic in studying firebrand transportation, the current model has been modified and improved step by step annually. This improvement should also consider the development of computing science. The complicated model could be solved numerically with the help of powerful modern servers, As well as the complicated flow field compared with the most basic constant velocity field. Therefore, using these models to study the spotting phenomenon is a reliable choice.

## 2.2.4. Experimental study for spotting phenomenon

Apart from the mathematical model that is being used to study spotting, several experiments have also been introduced to investigate the firebrand's transporting mechanism. The following section will be mainly focused on the previous investigation of the experimental study of the spotting phenomenon.

***Tarifa's experiment [11]***

At the very beginning, experimentally study firebrand transportation. Tarifa's experiment [11] was undertaken in a suction-intake wind tunnel in which the air speed is controlled by the average of the lateral-air intakes and with a throttle valve. In this study, the spherical wooden sample was chosen to study its mechanism.
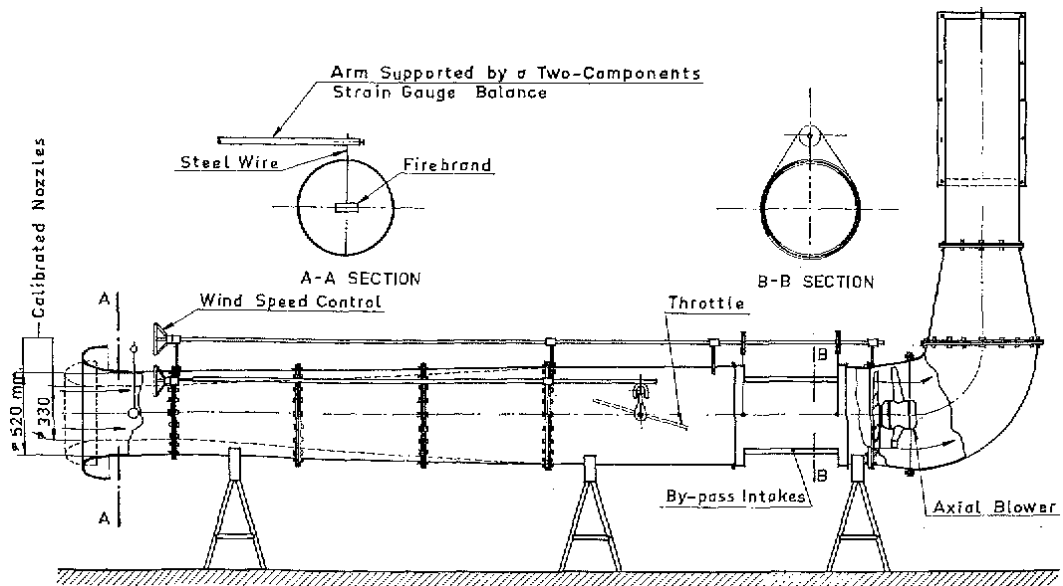
*Figure 2.10 The experimental setup of the wind tunnel test about the firebrand's*

*terminal velocity during transportation [11]. This setup could also be utilized in the*

*data collection of the mass loss effect of the firebrand during transportation. The A-A*

*section is designed to measure the change of mass during combustion. And the*

*vertical section is used to measure the firebrand's terminal velocity.*

There were mainly two experiments undertaken in Tarifa's experiment. For the first

one, a steel wire was used to sustain the firebrand and measure its varying during the

time. The data of weight, diameter, and magnitude of aerodynamic drag were

measured. This is also the first experiment studying the firebrand's combustion

process during transportation. However, as the main objective is not focusing on its

combustion effect, this thesis will not extend this topic to give a more detail discussion.

The other experiments used the vertical part of the wind tunnel. By controlling the

wind speed in the wind tunnel, Tarifa is trying to keep the wind continuously equal to

the terminal velocity of the fall of the firebrand. Since the firebrand burned, the wind

speed was continuously reduced.

From the observation of these experiments, serval conclusions had been made.

- The flight paths of firebrands may be studied, in all practical cases, by assuming that they always travelled under their falling terminal velocity.

- The firebrand could travel for a long distance while still burning from the fire front.

- The great distance is reached when the firebrand keeps within the main zone of the convection plume up to a critical height.

- The shape of firebrands is an important factor in the spotting process.
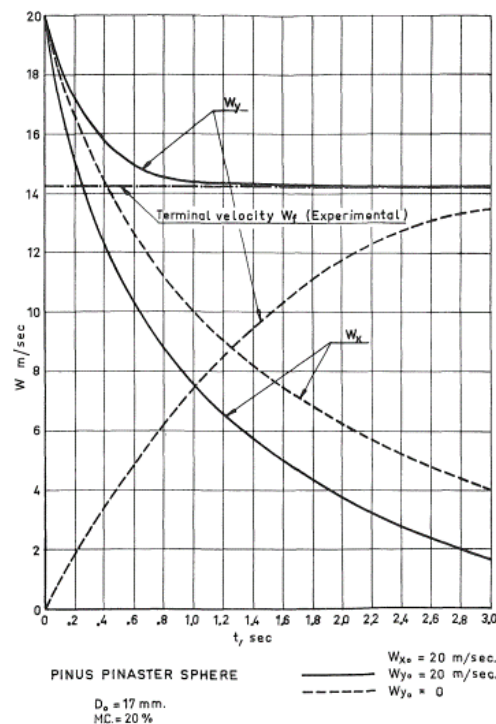


*Figure 2.11. The data collected form Tarifa's experiment about the terminal velocity*

*for firebrands under the different speeds of wind tunnels [11].*

Of all these conclusions, the most significant one is the first one, the terminal velocity assumption, which affected the following researchers vitally. Even today, there is still some basic spotting distance prediction software using the terminal assumption.

More importantly, Tarifa's experiment provided an example for the following

researchers to investigate the firebrand experimentally.

***Muraszw's experiment [3][2]***
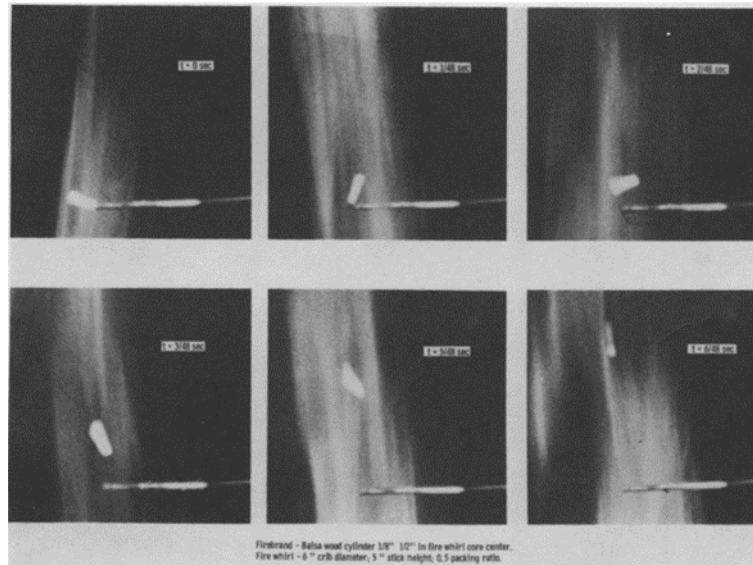


*Figure 2.12. The video snapshot about the fire whirl's lofting effect on a balsa wood*

*cylinder[3]. In this experiment, the capability of a weak fire whirl to lift the balsa*

*wood sample is proved.*

Muraszw's research topic is mainly focused on the fire whirl [2]. As an extreme

phenomenon in wildland fire, fire whirl is usually related to more destructive wildland

fires and severe combustion. Therefore, he pointed out that a long-distance firebrand

might be related to the fire whirl

A 6-inch crib diameter, 5-inch stick height, and 0.5 packing ratio fire whirl had been

applied in his experiment. A balsa wood cylinder with a 1/16 inch and 1/8 inch crossing

section, ½ inch long, was introduced at various points of the core of the fire whirl.

Its motion was recorded with a movie camera at 48 frames/s.

## Firebrand Subscale Trajectory, Height vs Time

1/8 in. x 1/8 in. x 1/2 in. BALSA
RELEASED AT CENTERLINE
— — EXPERIMENT
——— CALCULATION
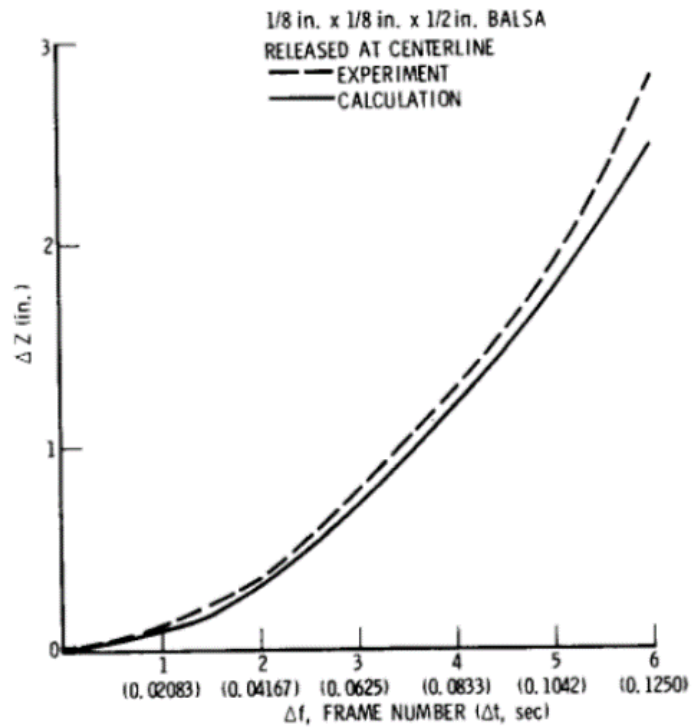
*Figure 2.13. The processed data about firebrand's lofting with respect to the time [3].*

*The data collected from the experiment was also compared with the calculation*

*result, which indicates that the calculation is quite accurate.*

The idea of Muraszw's experiment inspired the authors' thesis significantly. As it created a contradiction with a later experiment that formed a research gap that led the author to study with, which pointed out that the most destructive long-distance spotting phenomenon might be due to the fire whirl generated in the wildland fire.

Another phenomenon is that a high-speed jet flame is not able to sustain the rod-like firebrand also points out that the lofting mechanism of the firebrand still requires some sort of effort to study.

**Ali Tohidi's experiment [78][7][76]**

33

Tohidi's experiment focuses on the combination of firebrand's vertical lofting and horizontal transport [80]. As the previous experiments were only focused on one aspect. Such as, Tarifa's vertical wind tunnel experiment was only studying the falling terminal velocity. In contrast, Muraszew's experiment was only focusing on the fire whirl's effect on the firebrand's lofting. Other experiments were studying the spotting distance of firebrands in various conditions. Therefore, an overall experimental study was necessary to undertake.



*Figure 2.14. The air jet is utilized in the firebrand transportation experimental [80].*

*Such type of air jet could generate a wind speed of which's centerline exit velocity*

*range of 0-12 m/s. However, in the publication, it is cited that such a strong jet is not*

*able to lift a wooden firebrand. Therefore, the polyurethane sample was utilized in*

*the experiment, and it is impossible to study the burning effect on the firebrand's*

*transportation.*

For the lofting stage of a firebrand, an air jet was used to loft the samples. The jet

centreline exit velocity in this experiment was adjusted between 0-12 m/s, which is a reasonable range generated from the fire plume from the wildland fire. Among all the test cases, three jet velocity had been applied to loft the sample of a firebrand, 12 m/s, 8.05 m/s, and 9m/s

After the firebrand is lifted by the air jet, it would turn into the transport area. A horizontal wind tunnel which is classified as a low-speed boundary layer was applied to the experiments.



*Figure 2.15. Two side views about the setup of Ali Tohidi's experiment [80]. In the left-hand figure, in the horizontal wind tunnel, the roughness elements and spire elements have been introduced to generate a turbulence boundary layer. In the right-hand figure, a side view camera has been utilized to track the trajectory of firebrands.*

A 60-fps video camera was used to capture the motion of the firebrand in this experiment. Several image processing algorithms were utilized to trace the firebrand's

motion, such as the Gaussian filter and Morphological.
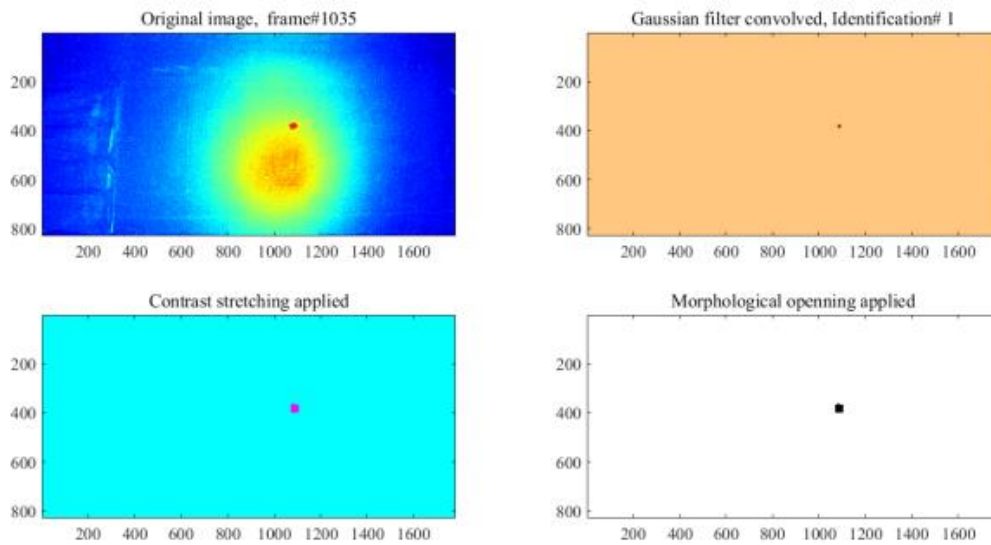


*Figure 2.16. The image processing algorithms are being used in detecting the position*

*of the firebrand in the captured video [80].*

After processing the raw video captured during the experiment, the location data of the firebrand versus time could be collected automatically. Then, the data on the trajectory of firebrands were used to validate the models of firebrand motion.
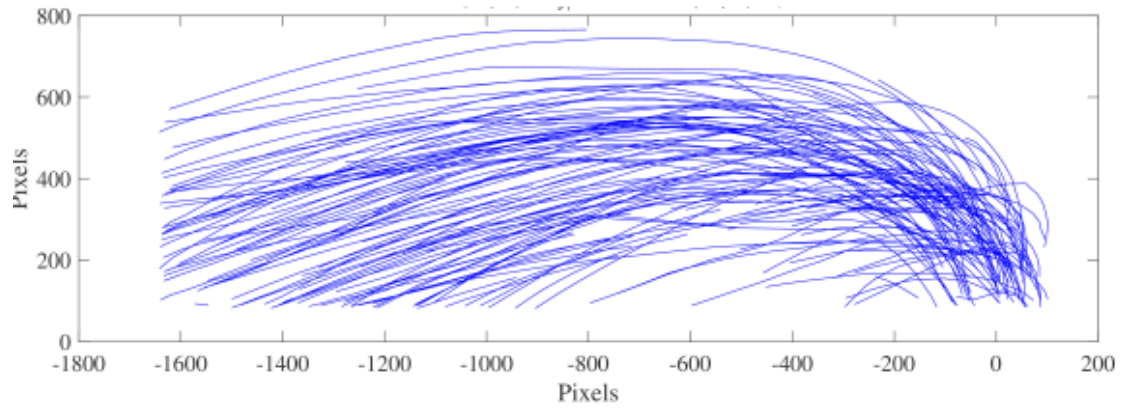
*Figure 2.17. The trajectory of the firebrand after the image processing [80]. The data is collected in the aspect ratio of the sample to be 1, with the horizontal velocity being 2.23 m/s and the vertical jet's velocity of 8.05 m/s.*

However, the reason for introducing this experiment is not for the setup and methodology but for the comment mentioned in the publication.

The interesting point of this experiment is the material of the firebrands sample. Tohidi pointed out that the balsa wood sample is not able to be lofted by the air jet, even under the 12 m/s velocity wind speed. Therefore, polyurethane was chosen to be the material for making the samples.

*Figure 2.18. the polyurethane-made sample of a firebrand, with the aspect ratio*

*μ=1,4,6 [80].*

In his experiments, the non-combusting polyurethane model of firebrand with a density of 30 kg/m$^3$, the side aspect ratio was 1, and the longitudinal aspect ratio was set to be 1, 4, and 6. For the longitudinal aspect ratio of 1, the three dimensions of the firebrand were 1 cm × 1 cm × 1 cm. and for the other aspects ratio, the short edge is 0.5 cm.

The size of the sample compared with the real firebrand collected from the wildland fire seemed to be reasonable. However, its density of it was totally far from the truth. As mentioned in the previous paragraph, the real firebrand's density is about 250 kg/m$^3$. The tested samples were about ten times lighter than the real firebrand. Moreover, a slightly lighter sample compared with the real firebrand, which was made of balsa wood, was still not able to be lofted by the air jet, which points out that the current understanding of the large size of the firebrand's lofting mechanism is limited. However, in Murazew's experiment, a similar size of balsa wood sample was able to be lofted by the fire whirl. This contradiction inspired the author to a neglected part

of the firebrand's lofting mechanism, which will be fully discussed in the following paragraphs.

### *Manzello's experiment [47][46][49]*

Manzello is one of the most popular researchers that focused on firebrands recently and still working on it [48][51][50][47][46][49]. He worked for NIST (National Institute of Standards and Technology) and developed a Baby Dragon, which is a firebrand releaser. His study covered a huge range of this topic, such as the transportation model, transportation experiments, and most recently, the experimental study of secondary ignition.
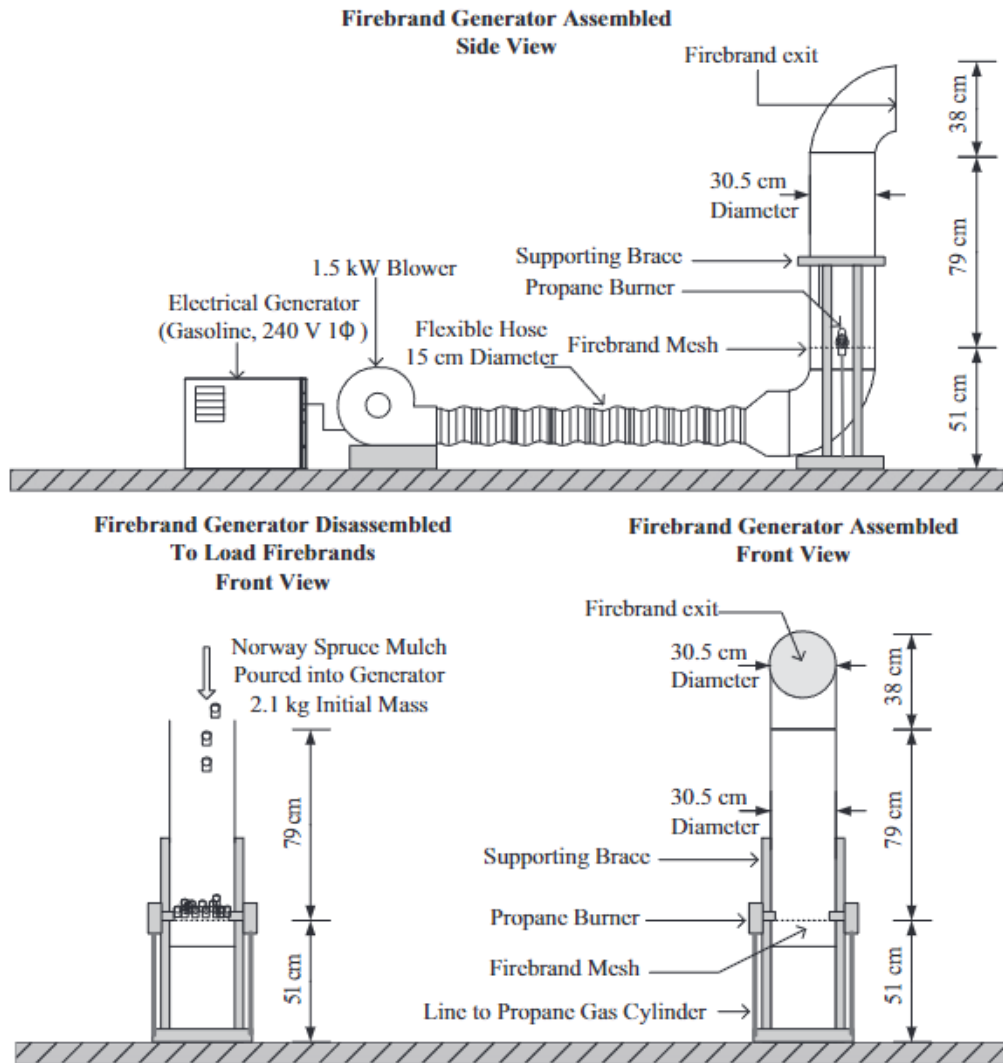
*Figure 2.19. The schematic of 'Baby Dragon', the firebrand shower generator [47].*

*Such device has been utilized in most of Manzello's research[48][51][50][47][46][49].*

*The firebrand mesh sustains the firebrand and also controls the minimal size of the*

*firebrand being generated.*

Figure 2.19 shows a schematic of the 'baby dragon', the firebrand shower generator.

The structure of the baby dragon could mainly separate into two parts. The burning

firebrand generator and the horizontal exit of the firebrand.

For the firebrand generator, a burner with two stainless steel mesh screens. The mesh

screen filtered out the firebrand larger than 25 mm in diameter and supported the firebrand pieces. A 1.5 kW blower was used to provide the wind to lift the firebrand pieces. The mulch pieces kept burning on the mesh screens. Since the weight and diameter kept decreasing while it was burning, the large mulch pieces could become lighter enough to be blown up by the blower with enough burning period.

For the horizontal releaser part of the baby dragon, a 30.5 cm diameter pipe was used to release the burning pieces of the firebrands. The mesh screen made sure that the firebrand won't be larger than 25 mm so that such burning ash would travel with the wind. With the help of a video camera, the trajectory of the firebrand in these experiments could be measured. Developed from this baby dragon device, Manzello studied the spotting phenomenon with various parameters, such as the material of the firebrand, the size of a firebrand, a different obstacle that generated different flow fields, and some post phenomena generated from spotting.

*Figure 2.20. A long exposure photo about the firebrand shower's trajectory generated by the 'Baby Dragon'[73].*

In the Figure 2.20. A long exposure photo about the firebrand shower's trajectory generated by the 'Baby Dragon'[73]. Figure 2.20 the trajectory of the firebrand showed clearly. The circulation around the obstacle could be observed as well as the path of the firebrand also shows that the lift effect is quite obvious due to the turning about the firebrand's direction of the motion.

One thing needs to be mentioned the sample of firebrand generated from the baby dragon is not that similar to the real firebrand collected from the wildland fire. The test scenario was a relatively strong blow with the relatively small size of the sample. The inappropriate size of the sample indicates that the mechanism might be different. Therefore, to study the detailed physics of the firebrand's transportation, the scenario should be modified slightly.

*Figure 2.21. The generated firebrand landing around the obstacle[50].*

The scale of the generated firebrand is relatively small compared to the real firebrand shown in Figure 2.2. The physical mechanism of the motion will be slightly different due to its smaller size. Therefore, to understand the physical mechanism of the firebrand's lofting, the setup should be modified.

## 2.3. Aerodynamics of rectangular-shaped firebrands

As mentioned in the previous paragraphs, mathematical modelling is a fundamental tool for studying the spotting phenomenon. The research gap in studying the lofting mechanism of the firebrand in the firewhirl also required mathematical modelling of the firebrand. Therefore, the aerodynamic analysis of a firebrand's transportation will be reviewed in this section. The two periods of the motion of firebrand have been introduced before. The horizontal transportation model has been well developed compared with the vertical lofting model. However, the two periods of motion's mechanism share the same fundamental aerodynamic theory. The main objectives of

43

this thesis are focused on the lofting stage of a firebrand transporting in the flow field.

Compared with the gliding stage, the vertical lofting stage is much shorter. Thus, neglecting the burning effect for those few seconds is reasonable.

A Brief introduction about the previous firebrand transporting model is being summarized as the following table.

*Table 1. The previous firebrand transporting model.*

| Model | Gravity | Aerodynamic Force | Other Force |
|---|---|---|---|
| *1965 Tarifa* | Yes | Spherical drag | No |
| *1979 Albini* | Yes | Semi-empirical aerodynamic force | No |
| *2003 Yin* | Yes | Stokes drag, Buoyancy, pressure gradient, and virtual mass | Basset history term |
| *2010 Mando and Rosendahl* | Yes | Drag, Lift, buoyancy | minor issue |

In this section, the fundamental aerodynamic theory of the firebrand lofted mechanism is reviewed. The fundamental aerodynamic theory is based on the aerodynamic forces applied to the firebrands together with Newton's second law. For the detail about the aerodynamic forces, the aerodynamic coefficients of lift, darg, and damping moment based on different conditions will be introduced. As the discovered real firebrand from real wildland fire is about disk-shape, all the coefficients and details of models are utilized for rectangular-shaped firebrands. Considering the Reynolds number of the firebrand is related to the velocity of the

firebrand, the relation between coefficients and Reynolds number will be illustrated in this chapter.

## 2.3.1. Basic properties of the rectangular-shaped firebrand

As mentioned before, the simulation of the firebrand is based on a real firebrand that finds in a real wildland fire. A rectangular-shaped firebrand will be used to study the lofting mechanism.
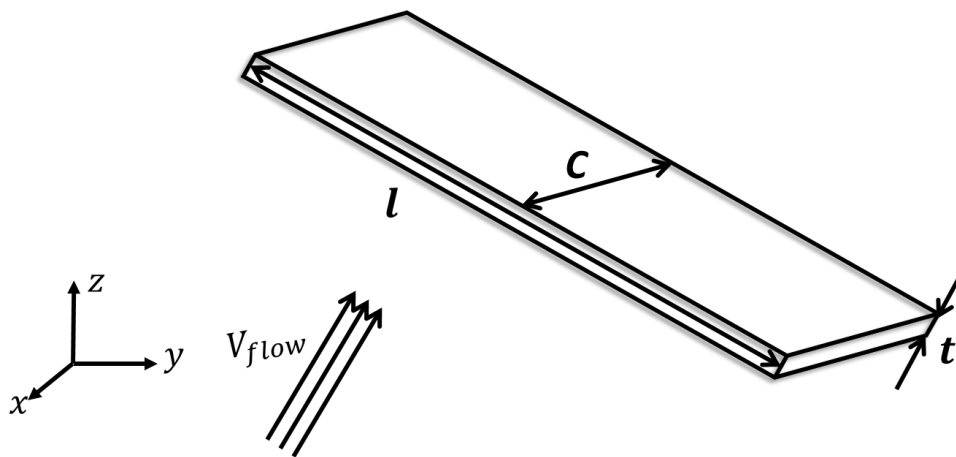


*Figure 2.22. The schematic of a rectangular-shape plate-like firebrand's motion in a flow field.*

For a general rectangular-shaped firebrand, there are three dimensions for it. The $l$ indicate the length of the particle, $c$ and $t$ represents the chord length and the thickness of the rectangular-shaped firebrand. The reference area of the rectangular-shaped plate is formed with length and chord length, more specifically, $A_r = l \times c$.

The shape of a rectangular plate is measured by a parameter, which is called the aspect ratio. The aspect ratio has been used wildly in application such as screen, image,

and video. For the case of a firebrand, the aspect ratio is defined as the ratio of the dimension for the firebrand [35], and it can be expressed as:

$$AR = \frac{l}{c}$$

(Eq. 2-18)

where $l$ indicate the length of the particle, $c$ represents the chord length.

Since the firebrand is travelling within the effect of flow, the condition of the fluid is not able to be neglected. The Reynolds number (Re) is a dimensionless value to represent the fluid condition, which was firstly introduced by Sir George Stoke in 1851 [71]. In fluid mechanics, it is used to determine the flow regime from laminar to turbulence and indicate the similarity between the real case and the laboratory-scale case. For the case of a firebrand lofted by a flow field, the calculation of the Reynolds number is shown as:

$$Re = \frac{\rho_a V_f l}{\mu}$$

(Eq. 2-19)

In the equation, $\rho_a$ and $\mu$ indicate the density and the dynamic viscosity of the ambient fluid of the firebrand, $V_f$ and $c$ represent the relative velocity and characteristic length (length) of the firebrand.

## 2.3.2. Aerodynamic forces and moment for the firebrand

The aerodynamic analysis is one of the most important steps for predicting the trajectory of a firebrand in a flow field. From the previous introduction, many works have been made to study the aerodynamic effect of the firebrand from both experimental side and analytical studies. In this chapter, a brief but systematic

introduction to aerodynamic analysis will be provided.

As the introduction of the aerodynamic calculation, the governing equation for the velocity of the spherical particle in a nonuniform flow field is chosen. This equation was published by Yin in 2003 [85]. And it can be expressed as:

$$m_p \frac{d\vec{v}}{dt} = \underbrace{V_p \left(\rho_p - \rho_F\right)\vec{g}}_{gravity} + \underbrace{6\pi d\mu(\vec{u} - \vec{v})}_{viscous\ Stokes\ drag} + \underbrace{\rho_F V_p \frac{D\vec{u}}{D\vec{t}}}_{\substack{pressure \\ gradient}}$$

$$+ \underbrace{\frac{1}{2} \rho_F V_p \frac{d\left(\vec{u} - \vec{v}\right)}{dt}}_{\substack{virtual \\ mass}} \qquad (Eq.\ 2\text{-}20)$$

$$- \underbrace{6\pi d^2\ \mu \int_0^t \left\{ \frac{\left(\frac{d}{d\tau}\right)(\vec{v} - \vec{u})}{[\pi\mu\,(t - \tau)/\rho_F]^{1/2}} \right\} dt}_{Basset\ history\ term}$$

where respectively, $m_p$, $V_p$, $\rho_p$, $d$ and $\vec{v}$ are the mass, volume, density, diameter, and velocity of particle, and $\rho_F$, $\vec{u}$ and $\mu$ are the density, velocity and viscosity of the ambient fluid. $\vec{g}$ is the gravity acceleration and $\tau$ is a constant. The left-hand term represents the inertia of the firebrand, which is linear to the change rate of the velocity. From the acceleration of the firebrand, the velocity and displacement are able to be calculated by integration. The right-hand terms can be separate into five parts. For the first term, gravity also considered the effect of buoyancy [35]. The second term represents the Stokes viscous drag, which means the force of viscosity on a moving spherical objective through fluid that is not able to neglect the viscosity [70]. And it is also related to the objective's diameter, ambient fluid viscosity, and objective's relative velocity to its ambient flow. The third term is the pressure gradient, which indicates that the pressure difference across the objective presents as a force

applied to the objective [35]. The fourth term, virtual mass,[59] is the inertia added to a system due to the space moved by an accelerating or decelerating objective through the surrounding fluid. And the last term, Basset force,[34][1] donates the aerodynamic force due to the lagging boundary layer effect generated from the change of relative velocity of an objective with respect to the surrounding fluid. However, one thing needs to be mentioned the last two-term, virtual mass and Basset history term, are relatively small in magnitude compared to the first three terms. Meanwhile, for those non-spherical shape objectives, the first three terms occupied the majority position. Therefore, in the case of this thesis analysis, the last two terms will be neglected.

From the equation, the fluid velocity $\vec{u}$ is the velocity vector at the same point of the objective's centre of mass, and by using the chain rule, the time derivative can be expressed as:

$$\frac{d\overrightarrow{u(x,y,z)}}{dt} = \left(\frac{\partial\vec{u}}{\partial t} + \frac{\partial\vec{u}}{\partial x}\frac{dx}{dt} + \frac{\partial\vec{u}}{\partial y}\frac{dy}{dt} + \frac{\partial\vec{u}}{\partial z}\frac{dz}{dt}\right)$$

*(Eq. 2-21)*

$$= \left(\frac{\partial\vec{u}}{\partial t} + u\frac{\partial\vec{u}}{\partial x} + v\frac{\partial\vec{u}}{\partial y} + w\frac{\partial\vec{u}}{\partial z}\right)$$

$$\overrightarrow{u(x,y,z)} = (u,v,w) \qquad \textit{(Eq. 2-22)}$$

$u, v, w$ are velocity vectors projection to $x, y, z$ axes. The material derivation for the fluid velocity is:

$$\frac{Du}{Dt} = \left(\underbrace{\frac{\partial\vec{u}}{\partial t}}_{local\ derivation} + \underbrace{\vec{u}\cdot\nabla\vec{u}}_{convective\ rate\ of\ change}\right) \qquad \textit{(Eq. 2-23)}$$

The first term on the right-hand side of the equation is defined as the local rate of change [35]. For steady flow, the local derivation is kept at zero. The second term

stands for the variation due to the change in the position of a fluid particle. If there is no gradient, the second term will be zero. Therefore, there will be no convective change.

Further, according to the study of the particle in a turbulent flow by Lázaro and Lasheras in 1989 [42], it was found that the drag and the inertia effects were significantly larger than the effects of the other terms for their magnitude. Moreover, the simplification of the equations for a small particle in a thin layer was undertaken by Martin and Meiburg in 1994 [52] and Raju and Meiburg in 1995 [60]. From their studies, the drag, gravity and inertial effects play dominant roles in a spherical objective movement in a flow field.

However, it is necessary to mention that the real firebrand is not a sphere. Thus, applying the spherical objective's analysis is not accurate enough to predict the motion of a real firebrand. The following chapter will be focused on the review of non-spherical particles. More specifically, the rectangular-shaped plate-like objective motion in a flow field. One of the most significant differences in aerodynamic analysis between rectangular-shaped objects and the sphere is the aerodynamic lift effect.

The earliest study on the aerodynamic force for an objective's motion in a flow field that considered the aerodynamic lift effect might be found in Sir George Cayley's work in the 18th century [65], that he pointed out the four fundamental forces of the flight including lift, drag, thrust, and weight. The very detailed research of the aerodynamic lift on a non-spherical object could trace back to 1965, which was published by Hoerner [30]. Even today, the study of the lift force of an objective in the flow field is still being carried out.

One of the most basic points in studying the firebrand's motion is to focus on the aerodynamic analysis of a rectangular-shaped plate-like object. The governing equation was developed by Yin [85] and shown as follows:

$$m_p \frac{d\vec{v}}{dt} = \vec{F}_D + \vec{F}_L + V_p (\rho_p - \rho_F)\vec{g} + \vec{F}_{PG} + \vec{F}_{VM}$$ 

(Eq. 2-24)

where $\vec{F}_D$, $\vec{F}_L$ , $\vec{F}_{PG}$, and $\vec{F}_{VM}$ denote drag, lift, and force due to the pressure gradient and virtual mass force. The third term in right-hand equations represents the gravity that considers the effect of buoyancy. As mentioned in the previous paragraph, compared with the other forces, the virtual mass forces and pressure gradient are relatively small in magnitude. Then following the simplification from Lázaro and Lasheras [42], it was only necessary to consider the inertia, drag, and gravity term for a small and heavy particle in a flow field.

The aerodynamic drag force for a non-spherical object in the flow field could be expressed as:

$$F_D = \frac{1}{2} C_d \cdot \rho \cdot V_r^2 \cdot A_c$$

(Eq. 2-25)

In this equation, $F_D$ is the aerodynamic drag. $C_d$ represents the drag coefficient, which depends on the shape of the object and the Reynolds number of the system. $V_r$ is the relative velocity of the firebrand to the surrounding flow. $A_c$ is the firebrand's cross-sectional area. The direction of the aerodynamic drag is the same as that of the relative motion.

At the early stage of studying the lift force, the relationship between lift and drag was considered. The very beginning equation of the relationship was developed in 1965 by Hoerner [30]:

$$\frac{|\vec{F}_L|}{|\vec{F}_D|} = |sin^2(\alpha_i)\cos(\alpha_i)|$$

where $\alpha_i$ , also called the angle of attack, indicates the angle of incidence between the relative velocity of wind with respect to particle [35], and the major particle axis, as it is shown in the following Figure 2.23.
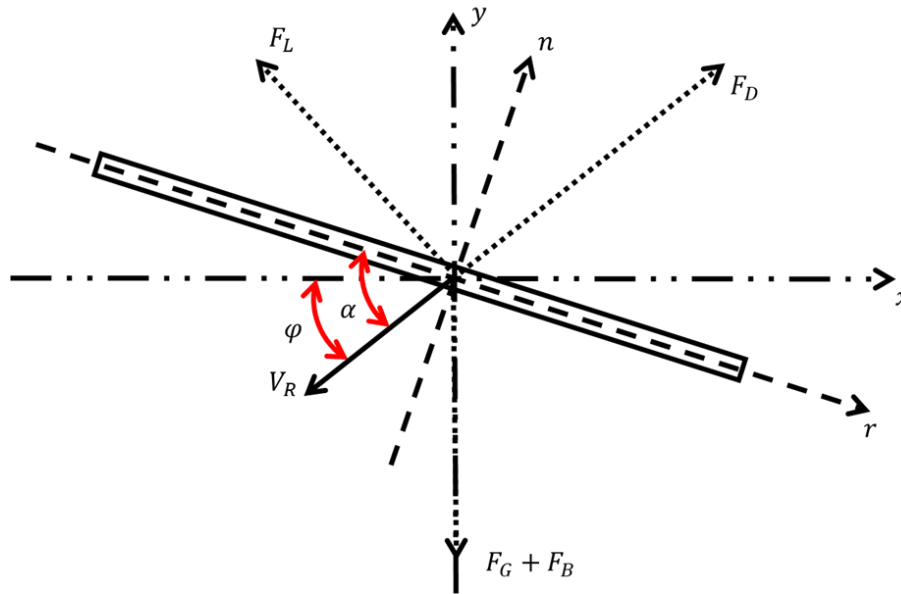


*Figure 2.23. The schematic about the forces exerted on the firebrand and the definition of the angle of attack α, and angle of inclination φ. Such a schematic is defined in a two-dimensional domain.*

However, in the past half-century study of aerodynamic life, it is found that the aerodynamic lift is able to be calculated separately by using a similar formula with aerodynamic drag [35]. The equation for aerodynamic life force exerted on a non-spherical particle could be expressed as:

$$F_L = \frac{1}{2}C_l \cdot \rho \cdot V_r^2 \cdot A$$

In this equation, $F_L$ represents the aerodynamic lift. $C_l$ represents the lift coefficient,

which is related to the firebrand's shape, inclination, and some flow conditions. $V_r$ is the relative velocity of the firebrand to the surrounding flow. $A$ represents the firebrand's area. And the direction of the aerodynamic lift is perpendicular to the relative velocity [35].

Similarly, the damping moment applied to a rectangular-shaped plat that prevents it from rotating could also be given [29]:

$$M_\alpha = -\frac{1}{2} C_M \cdot A_{ref} \cdot l_{ref} \cdot \rho |V_r|^2 \frac{\omega_R}{|\omega_R|} \qquad \text{(Eq. 2-28)}$$

A further discussion about the coefficient will be discussed in the next section.

## 2.3.3. Coefficient of drag and lift and damping moment

As a dimensionless scale, the coefficients of drag, lift, and damping moment are important values for determining drag, lift forces, and damping moment exerted on the particle in a fluid field. For the drag force, the simplest form of the drag coefficient is applied to a spherical particle since it is the only function of the particle's Reynolds number after simplifications. Nonetheless, other assumptions, such as the shape, of non-spherical particles, must be made in order to measure the drag coefficient for other cases. The orientation of non-spheres should also be considered in order to get a more accurate measurement. For the lift force exerted on a particle, it is not necessary to considerate the lift on a sphere since the symmetric shape prevents the existence of aerodynamic lift. Measuring the coefficient of lift is more complicated for a non-spherical particle, and many factors must be considered, such as Reynolds number, shape, and angle of attack.

In this section, the drag coefficients for both the spherical and rectangular plates are

reviewed. The influence of orientation on the drag coefficient is discussed as well. Meanwhile, the lift coefficients of rectangular-shaped plate-like particles are introduced.

### *Fundamental analysis of the aerodynamic force on a particle*

For an object moving through a fluid field, due to the fraction and viscous shear stress over the body surface, eventually, a resultant force is exerted on that object, which is defined as a drag force. Since the drag force is obtained from the fraction and viscous shear stress, the magnitude and direction of the drag force need to be indicated. From Stokes' Law [70], the total drag force on a sphere can be presented as:

$$\vec{F_D} = -6\pi\mu\vec{u_r}R \qquad \text{(Eq. 2-29)}$$

where $\mu$, $\vec{u_r}$ and $R$ indicate the dynamic fluid viscosity, the object's relative velocity with respect to the ambient flow and the radius of the sphere. The direction of the drag is defined as the opposite of the object's relative velocity, or in other words, the direction that prevents the relative motion. As the flow pattern is related to the Reynolds number, the magnitude of the fraction and viscous shear stress are also highly affected by the flow pattern.

Different Reynolds number represents different pattern for the flow field, at the situation of a very low Reynolds number ($Re < 10$), the creeping flow can be assumed. In such conditions, the viscosity can be neglected, and no boundary layer effect. With the increase of the Reynolds number, a pair of vortices are generated at the downstream side. In the beginning, such vortices are small and stable. When Reynolds numbers keep increasing, the downstream vortices become unstable.
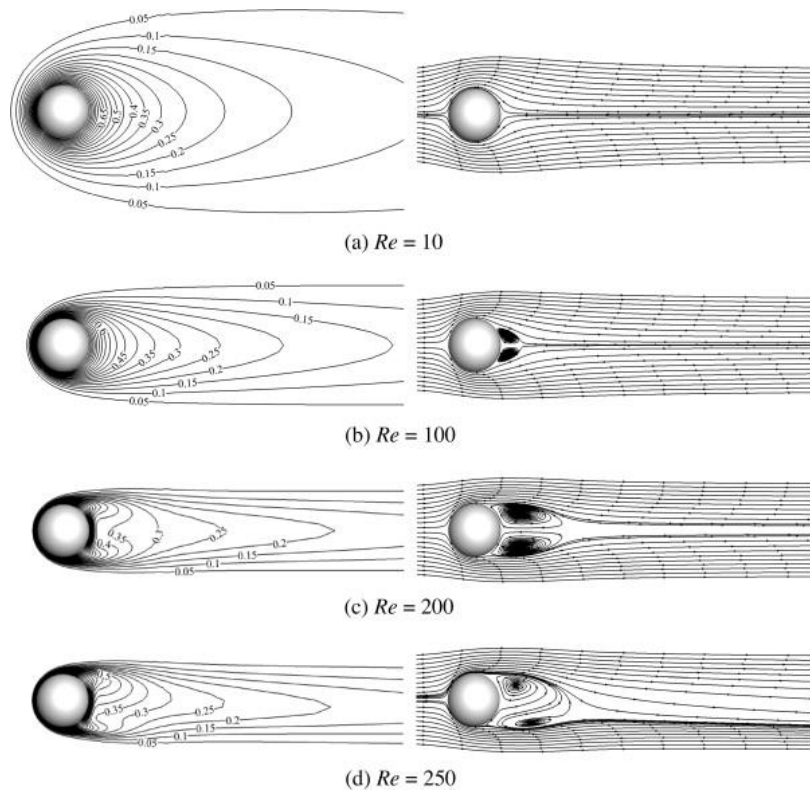
*Figure 2.24. The temperature field (left) and streamline (right) are about the flow around a sphere [61]. Both of them show the impact of the Reynolds number on the flow, which eventually will impact the aerodynamic forces.*

Such observations clearly state that with different Reynolds numbers, the coefficients definitely obeyed different rules. Following that idea, previous researchers measured the coefficients under different Reynolds numbers with various shaped of objects.
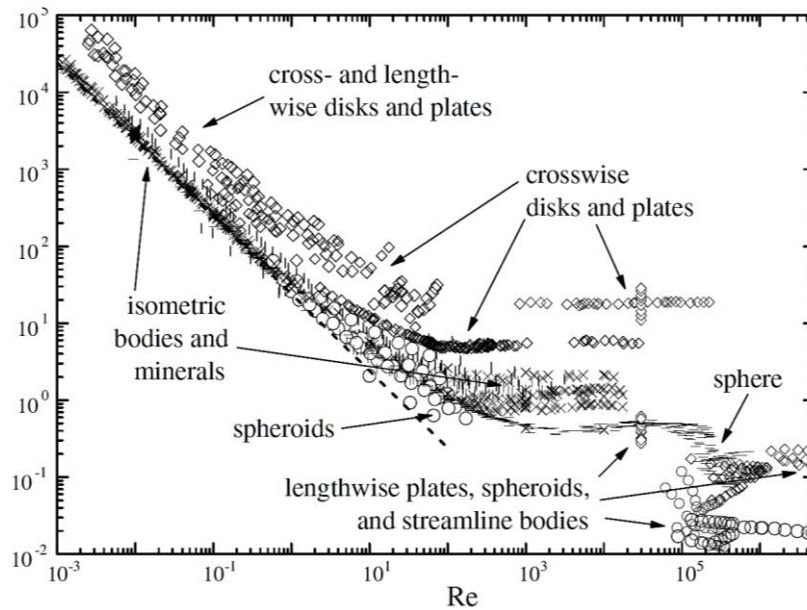
*Figure 2.25. The drag coefficient for different shapes of the object under different*

*Reynolds numbers [33].*

As the firebrand cannot be simplified as a sphere, another important factor that is not able to be neglected is the angle of attack. For a non-spherical body moving through a flow field, the flow's pattern changed significantly due to the velocity difference between the upper surface and lower surface of the body. The pressure of the upper layer and the bottom layer is different, which generates a force that is perpendicular to the body's relative velocity with respect to the ambient flow.

In Figure 2.25, different shapes' objects' coefficient of drag shows a different trend, which indicates that different shapes' firebrands might obey the different rules of the lofting mechanism. Thus, in this thesis investigation of the firebrand's lofting mechanism, the firebrand is assumed to be a rectangular-shape plate-like object.
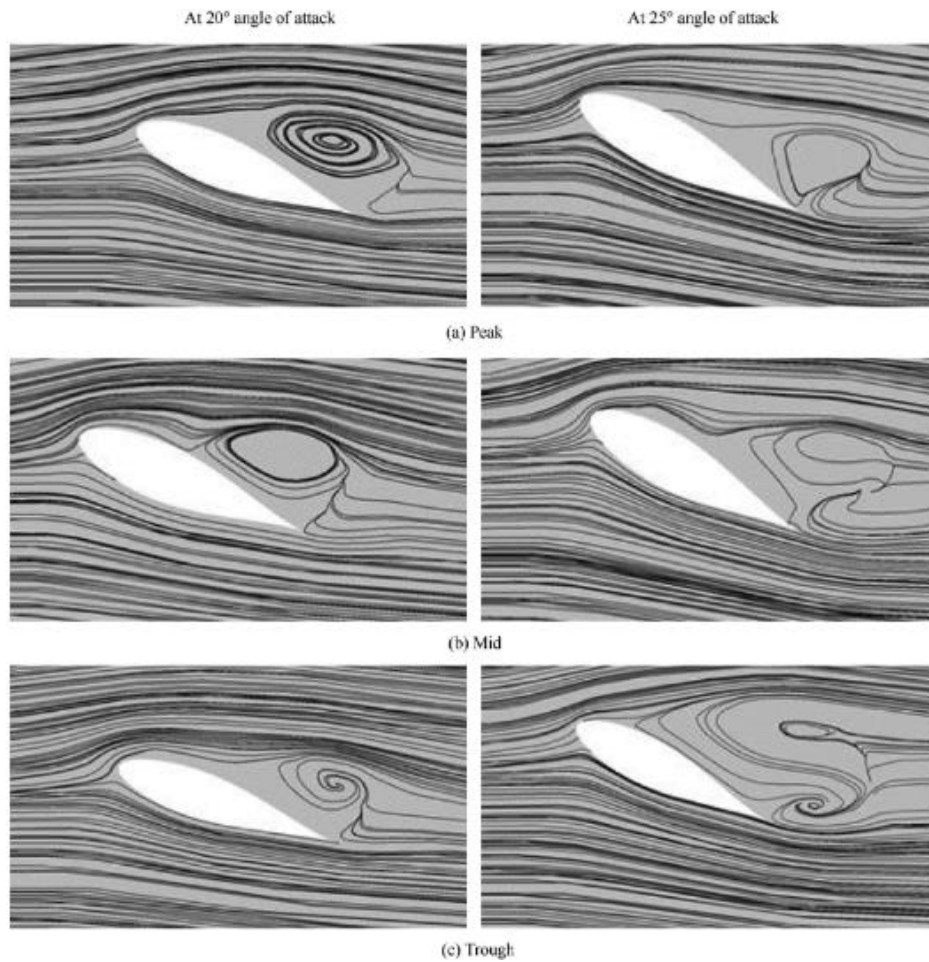
*Figure 2.26. The streamline pattern around an airfoil with different angles of attack [22]. It shows that the change in the angle of attack will affect the flow pattern significantly, which will also affect the aerodynamic forces exerted on the firebrand.*

A slightly change in the angle of attack results in a significant variation in the flow pattern. This indicates that for a non-spherical object's motion in a flow field, the coefficients for the aerodynamic drag, aerodynamic lift, and damping moment are quite sensitive to the variation in the angle of attack. There are multiple research studies have already published on this topic. The following chapter will introduce it in detail.
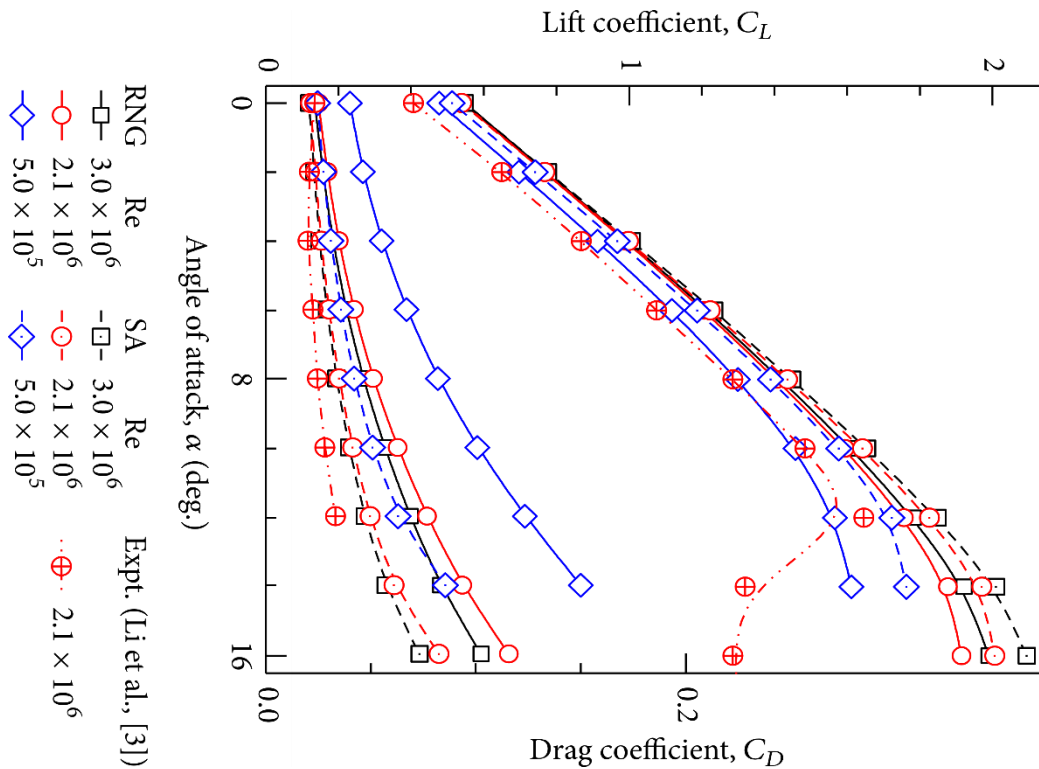
*Figure 2.27. Variation of Lift coefficient and Drag coefficient with angle of attack in various turbulence model's simulation results [37].*

### Drag coefficient

The research on measuring the coefficient of drag empirically and theoretically has been undertaken for several years. A huge amount of the equations has been established with a different application range of the Reynolds numbers. Among all shapes of objects, the sphere is the simplest type. The drag coefficient of the sphere shape of objects is related and only related to the Reynolds number. Some of the equations for measuring the coefficient for the spherical particles will be reviewed in the following paragraph.

The simplest relationship was formed by Stokes [70] in 1851, which only fit for non-viscous flow, and the equation can be expressed as:

$$C_D = \frac{24}{Re} \qquad \text{(Eq. 2-30)}$$

A more general relationship that covered the range of Reynolds number $Re < 10^4$ was formed by Fair and Geyer in 1954 [19]. The equation can be expressed as:

$$C_D = \frac{24}{Re} + \frac{3}{\sqrt{Re}} + 0.34 \qquad \text{(Eq. 2-31)}$$

After Fair and Geyer [19], most of the later equations follow a similar rule but with different details of the parameter. The basic rules can be expressed as follows:

$$C_D = \sum a_i \times Re^{-i} \qquad \text{(Eq. 2-32)}$$

Such as Yow et al. published in 2005 [86] the equation which fits the range of Reynolds number $Re < 2 \times 10^4$ can be expressed as:

$$C_D = \frac{23.5}{Re} + \frac{4.6}{\sqrt{Re}} + 0.3 \qquad \text{(Eq. 2-33)}$$

And Terfous et al. published in 2013 [75], for the range of Reynolds number $0.1 < Re < 5 \times 10^4$. The equation is:

$$C_D = 2.689 + \frac{21.683}{Re} + \frac{0.131}{Re^2} - \frac{10.616}{Re^{0.1}} + \frac{12.216}{Re^{0.2}} \qquad \text{(Eq. 2-34)}$$

However, a firebrand cannot be assumed as a sphere. Therefore, the rectangular-shaped plate-like object's coefficient of drag will be reviewed in the following paragraph.

In 2006, Holmes et al. published an equation for the coefficient of drag for squared plate [31][32], which is suitable for the range of Reynolds number $Re < 10^5$.

$$\text{(Eq. 2-35)}$$
$$C_D = 0.1 + C_N \sin(\alpha)$$

where $C_N$ is the coefficient of normal force on the plate, and $\alpha$ is the angle of attack

between flow and plate. The detail about the coefficient of normal force on the plate is expressed:

$$\alpha < 40°, C_N = 1.7(\frac{\alpha}{40})$$

$$40° \leq \alpha < 140°, C_N = 1.15 \qquad \text{(Eq. 2-36)}$$

$$40° \leq \alpha \leq 180°, C_N = 1.7\frac{180 - \alpha}{40}$$

Zastawny et al. also published the relationships for the coefficient of drag for disks in 2012 [88]. The suitable range for the Reynolds number is $Re < 10^3$. And the equation is:

$$C_D = \frac{5.82}{Re^{0.44}} + \frac{15.56}{Re^{1.068}}$$

$$+ \left(\frac{35.41}{Re^{0.96}} + \frac{3.63}{Re^{0.05}} - \frac{5.82}{Re^{0.44}}\right. \qquad \text{(Eq. 2-37)}$$

$$\left. + \frac{15.56}{Re^{1.068}}\right) [\sin(\alpha)]^{1.96}$$

From the previous two equations, the importance of the angle of attack to the coefficients has been introduced. As per the previous chapter's description, the slight change in the angle of attack will verify the flow pattern severely, and then the angle of attack to all aerodynamic effects is not able to be neglected.

### Lift coefficient

The basic structure of the equation of the lift forces is built from the equation of aerodynamic drag. Therefore, the relationship between its coefficient and other parameters is also similar to that of aerodynamic drag. The Reynolds number, shape, and angle of attack will significantly affect the coefficient of aerodynamic lift. Since the aerodynamic lift is usually smaller than drag by one or more orders of magnitude,

there are only limited investigations being undertaken to determine the lift coefficient for non-spherical objects.

And among all non-spherical objects, rectangular-shaped plate-like objects are used to simulate the firebrand. Therefore, the equations of the lift coefficient for such types of objects will be reviewed in the following paragraph.

In 2012, Zastawny's research [88] had been published the equation for lift coefficient, which is being applied to the range of $Re < 10^3$. The equation can be expressed as:

$$C_L = \left(\frac{b_1}{Re^{b_2}} + \frac{b_3}{Re^{b_4}}\right)[\sin(\alpha)]^{b_5+b_6 Re^{b_7}}[\cos(\alpha)]^{b_8-b_9 Re^{b_{10}}} \qquad \textit{(Eq. 2-38)}$$

In this equation, for the shape of rectangular-shaped plate-like objects, $b_1 = 12.112, b_2 = 1.035, b_3 = 3.887, b_4 = 0.109, b_5 = 0.811, b_6 = 0.248, b_7 = -0.198, b_8 = 5.822, b_9 = -4.718, b_{10} = 0.0007$.

Similarly, Sanjeevi et al. [64][63][62] published the relationship in more detail and investigated Zastawny's research. The new equation is suitable for the range of $0.1 < Re < 2 \times 10^3$. The equation can be expressed as:

$$C_L = \left(\frac{b_1}{Re} + \frac{b_2}{Re^{b_3}} + \frac{b_4}{Re^{b_5}}\right)[\sin(\alpha)]^{(1+b_6 Re^{b_7})}[\cos(\alpha)]^{(1+b_8 Re^{b_9})} \qquad \textit{(Eq. 2-39)}$$

In this equation, for the shape of rectangular-shaped plate-like objects, $b_1 = 4.485, b_2 = 1.325, b_3 = 0.123, b_4 = 0.001, b_5 = 0.001, b_6 = 0.016, b_7 = 0.287, b_8 = -0.011, b_9 = 0.333$.

By comparing the equation for coefficients of aerodynamic lift and aerodynamic drag, two key points can be obtained. First, the magnitude of the aerodynamic lift is usually

much smaller than the drag. Therefore, in some of the studies of firebrand transportation, the aerodynamic lift is neglected. However, in the objectives of this thesis, the relationship between the long-range spotting phenomenon and fire whirl will be established. Then, the aerodynamic lift could be one of the unneglectable factors. Another point is that compared with the coefficients of darg, the coefficient of aerodynamic lift is more sensitive to the angle of attack. Thus, when considering the aerodynamic lift effect on the motion of the firebrand, the impact of the angle of attack is necessary to be discussed in detail.

***Damping moment coefficient***

There is only limited publication that studies the damping moment of the rectangular-shaped plate-like object's motion in a flow field. However, as stated by Richards et al. [94], without some form of damping, the plates would continue to rotate without bound; therefore, a damping moment has been introduced to the motion of firebrand in a flow field.

Following Himoto's research [29], the moment acts in the direction that reduces the relative spin could be expressed as:

$$M_\alpha = -\frac{1}{2} C_M \cdot A_{ref} \cdot l_{ref} \cdot \rho |V_r|^2 \frac{\omega_R}{|\omega_R|} \qquad \text{(Eq. 2-40)}$$

In this equation, $M_\alpha$ is the damping moment. $C_M$ is the coefficient of the damping moment. $A_{ref}$ indicate the reference area. In the case of a rectangular-shaped plate, it is the cross-section area. $l_{ref}$ represent the reference length. In this case, it is the length of the plate. $\rho$ is the density of the ambient flow. $V_r$ is the object's relative

velocity with respect to the surrounding flow. $\omega_R$ is the objective's relative angular velocity with respect to the ambient flow. The coefficient of the damping moment can be expressed as [29]:

$$C_M = min\{0.35|\sin(\alpha)|, 0.14 - 0.23(|\sin(\alpha)| - 0.4)\} \qquad \text{(Eq. 2-41)}$$

## 2.4. The generator of a fire whirl

As mentioned in the previous paragraph, the main objective of this thesis is to investigate the lofting mechanism of long-distance spotting firebrands. From the literature review, it is pointed out that the fire whirl might be the reason for such a long-distance spotting phenomenon. Then, it is necessary to generate a fire whirl to study the firebrand's motion.

There are two main factors required to form a fire whirl. First, there needs to be the presence of an ambient swirl (circulation). The very beginning researcher, Emmons and Ying [17] stated that the available ambient vorticity caused by wind is the fundamental requirement to form a fire whirl. Another factor that needs to be mentioned is the heat source. The presence of heat induces a pressure minimum on the centre zone that sucks the air into the centre, which eventually creates an ambient vortex.

*Figure 2.28. A real photo of the fire whirl or fire tornado being generated in a real wildland fire [83].*

The most common place fire whirls have been observed is in nature. Larger fire whirls can sometimes be called fire tornadoes and can reach as high as 300 m in height and 1000 $^{\circ}$C in temperature [7]. In order to generate a fire whirl to study its effect on the firebrand's lofting mechanism, the literature review has been placed in the following paragraphs.

There are various approaches to generating a laboratory-scale fire whirl from the previous researchers' publications. Following the two main factors of forming a fire whirl, that method can be mainly classified by two rules.

First, the methods could be classified by their heat source. The laboratory-scale fire whirl generator can be divided into two ways, pool fire and burner. A pool fire consists of a 'pool' to contain the fuel, while a burner emits pressurized gas as fuel.
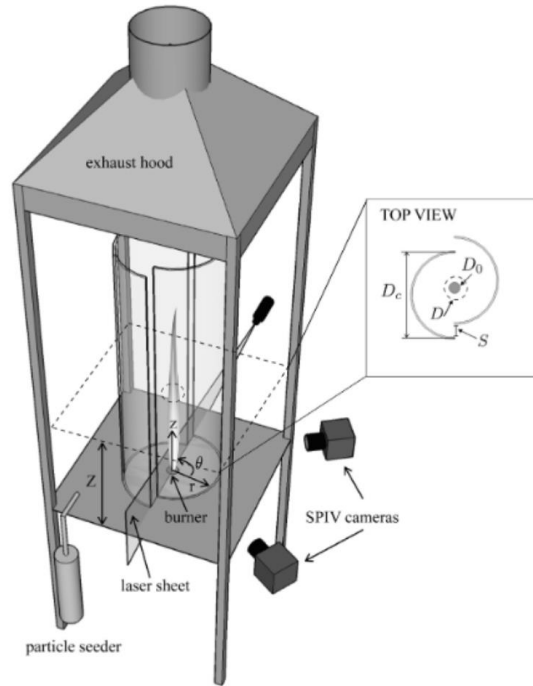
*Figure 2.29. A burner-based, on-source fire whirl generator with a Stereo PIV system to measure the flow field[24]. A Meker type burner has been utilized as the heat source, and two half-cylinder walls have been used as the on-source fire whirl generator.*

The experiments undertaken by K.A. Hartl and A.J. Smits in 2016 can be one example of the burner-generated fire whirl [25][28][26][27]. A Fisher Scientific 1201 Meker type burner, with an exit diameter of 38.1 mm, and a grid 10 mm thick made of holes 2mm square, has been used in this setup. The burner was sealed with epoxy to create a diffusion flame.

The advantage of using a burner to generate the fire whirl is obvious. Such as, the flow rate is controllable and can be kept constant during the experiment. So K.A. Hartl and A.J. Smits decided to use such a setup to study the relationship between the flame height to the ambient swirl and the magnitude of the heat release [26]. Thought there

are only limited studies about the burner-based fire whirl, some important investigations still pointed out that the velocity for a medium-scale burner-based fire whirl is one to two orders of magnitude stronger than that of pool fire-based ones.

The history of laboratory-scale fire whirl generated by pool fire could be traced back to the 1960s. The very first experimental set-up that uses a rotating screen to generate the fire whirl is based on a four-inch diameter pool fire.

The advantage of using a pool fire to generate the fire whirl is also obvious. Without the pressurized gas supplied for the burner, the safety improved significantly. Thus, the structure of the set-up that uses a pool fire will be apparently earlier than that of the burner-based set-up. The flame generated by the burner usually is higher than that from the pool-fire-based one. Therefore, the scale of the set-up is limited.



*Figure 2.30. A pool-fire-based off-source fire whirl generator[16].*

Classified by circulation, the laboratory-scale fire whirl generator can be mainly

65

separated into two types, manual circulation (off-source) and automatic circulation (on-source) [7]. The following table shows four typical approaches to introducing circulation. The first two can be assumed as manually, while the last two can be assumed as automatically.

*Table 2. The typical fire whirl generators in publication*

| Year | 1967 | 1979 | 2015 | 2018 |
|---|---|---|---|---|
| Author(s) | Emmons, H. & Ying, S [17] | Muraszew, [2][3]Fedele & Kuby [98] | Wang et. [99] | Wang et.[100][101] |
| Setup | Rotating Screen [16] | Blower to discharge air [17] | Two half-cylinder walls with a gap | Four rectangle walls |
| Sketch |  | | | |
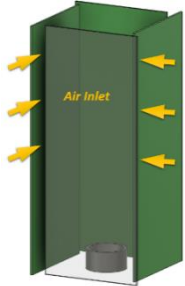
The advantage of manually circulating is straightforward by decoupling the rotation with the heat source. The magnitude of the circulation of the fire whirl is fully controllable. Such as, in the case of a rotating screen, the angular velocity of the screen

is linear related to the fire whirl's circulation, and in the case of a tangential blower, the fire whirl's circulation is also controlled by its air flow inlet.

The other type, automatic circulation, is defined as the fire whirl being formed directly over the heat source. The presence of heat-induced pressure decreased in the centre of the set-up, which pulls in air from the gap between each wall. Since the gap is designed to be asymmetrical, the air inlet to the centre zone is also asymmetrical. Eventually, the circulation forms.

Although most of the fire whirl generators are based on an on-source type, the disadvantage of such type of set-up is obvious, the heat source and the circulation are couped. It is true that changing the gap size can indirectly control circulation. But this kind of set-up is not accurate enough to study the physics of the fire whirl. However, the main objective of this thesis is to study the fire whirl's effect on the firebrand's lofting mechanism. The on-source fire whirl generator is also simulating the form of a fire whirl in real wildland fire. Such a type of set-up has been chosen in the following experiments.

From the previous introduction, the classification of a fire whirl generator can be demonstrated by the following table. There are four combinations in total. Each combination has its own advantage. In this thesis, the combination of pool fire with manual has been chosen for the purpose of simplicity.

*Table 3. The classification of the fire whirl generator*

| Heat source | Circulation type |
| --- | --- |

| Pool fire | Manual |
|:---:|:---:|
| Burner | Automatic |

Recent research shows that firebrands are responsible for more than 50% of the house losses in the wildland-urban interface area, which indicates the importance of studying their detailed physics of them. A huge number of researchers have worked on this topic during the past few decades. In general, those studies can be mainly divided into two aspects, theoretical and experimental. Therefore, in the investigation of this thesis, the firebrand's research is based on two aspects, experimental and theoretical modelling of firebrand research. The next chapter will be focused on the experimental investigation of the firebrand's lofting in the fire whirl.

# 3. Experimental for firebrand with a fire whirl

In the previous chapters, a literature review about the spotting phenomenon and how to generate a fire whirl has been introduced with detailed physics of the firebrands' motion in a flow field. During the literature review of the experimental study of the firebrand's spotting phenomenon, a contradiction was founded. Tohidi [80]pointed out that in his experiment, the 12 m/s jets could not loft a wooden sample of the firebrand, while Murazaw's fire whirl experiment succeeded in a similar size to the sample but at a low speed in the flow field. The existence of the fire whirl might be able to explain this phenomenon. Therefore, the experiment of investigating the impact of fire whirl on the firebrands' lofting mechanism developed in this thesis is going to be explained and discussed in this chapter.

The difficulty of doing experiments for firebrands with a fire whirl can be mainly divided into three parts. First, a suitable material should be chosen to build the sample of the firebrand. Then, a relatively strong fire whirl needs to be formed. Last, the profile of that fire whirl needs to be measured to make sure the experiment is repeatable. For the first task, multiple materials have been detected before the final decision is made. A relative strong fire whirl also requires some sort of parameter analysing. For the last task, the profile of that fire whirl was measured by the Particle image velocimetry (PIV) technique.

In this chapter, the experimental setup for investigating the fire whirl effect on the firebrand's lofting mechanism will be introduced firstly. The challenge of the set-up will be presented. Then the statistical approach to analysing the fire whirl's effect will

be introduced. In this part, a new dimensionless scale that quantifies the fire brand's performance is introduced. After that, analysing the data collected in the experiment will be presented together with the new scale. Finally, the conclusion of the experiment will be provided. Meanwhile, from the relationship between the phenomenon with the parameters in the experiment, a hypothesis will be given to provide a reasonable explanation about the extra impact of the existence of the fire whirl on the fire brand's lofting mechanism.

## 3.1. The set-up of fire whirl's effect

The goal of this experiment is to study the firebrand's lofting mechanism under the impact of a fire whirl. Therefore, the first step is to decide on the appropriate material as the sample of firebrands in this experiment. The ideal material should have two properties. First, it should be light enough that the laboratory-scale fire whirl's flow field is able to blow it up. Then, its density should not be too low that there is no apparent difference between the existence of fire whirl or not.

The original idea is to use a fully three-dimensional object to simulate the firebrand's lofting. However, the lightest possible combustible material, the balsa wood smoke filter, is still not able to be lofted by the generated fire whirl. Therefore, a compromising option, light paper, has been chosen for the experiment.

*Figure 3.1. The wooden smoke filter that being chosen as the sample of the firebrand.*
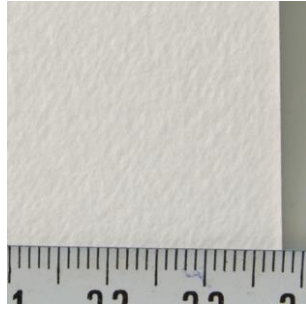


*Figure 3.2. The light paper that eventually being utilized to study the rectangular-*

*shaped plate-like firebrand's lofting mechanism.*

The aerial density of the light paper is $50$ $\boldsymbol{g/m^2}$. And three different aspect ratios of the sample have been utilized to undertake the experiment to study the shape's effect. $1cm \times 1cm$, $0.7\ cm \times 1.4\ cm$, and $0.6\ cm \times 1.7\ cm$ are the selected sizes. Three different sizes of the samples share the same cross-section area. The cross-section area is $1\ cm^2$. Apart from the investigation on the impact of aspect ratio, $1cm \times 2cm$ and $1cm \times 3cm$ are also selected to study the impact of cross-section area.
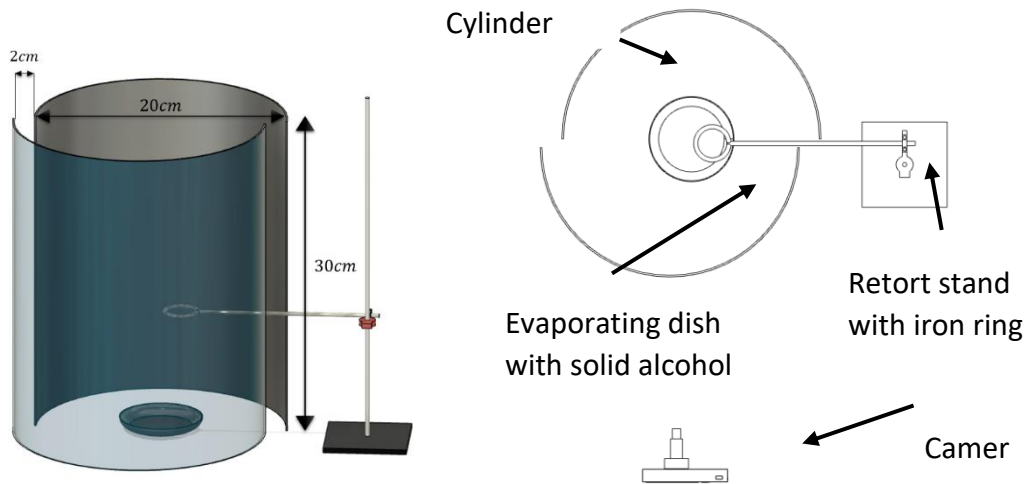
*Figure 3.3. The schematic of the experimental setup of the firebrand's lofting mechanism in fire whirl. The left-hand figure is the 3D model generated by Fusion 360. And the right-hand figure is the bird's view of the setup and the camera that was used to capture the data.*

As mentioned in the previous paragraphs, the fire whirl was generated by an on-source pool fire device. Two transparent half-cylinder walls, which are 30 cm in height, 20 cm in diameter, and 2mm in thickness, were arranged to generate the fire whirl. The material was chosen to be acrylic, which is considered the thermal stress breakage that occurs as a result of uneven heating. Since the objective of this experiment is qualitatively analyse the impact of the existence of the fire whirl on the lofting mechanism of the firebrand, the experiment just considers the impact of the existence of the fire whirl or not. For the group of fire whirls being generated, the asymmetrical gap between two half-cylinder walls was set to be 2 cm. And the asymmetrical gap for the control group was set to 0 cm.

*Figure 3.4. The fire whirl is generated by solid alcohol, which is replaced by a 98%*

*volume fraction of liquid alcohol in the following experiment.*

Originally, the fuel for the pool fire was solid alcohol, which is a type of gel that is mixed with liquid ethanol and other materials. However, due to the lack of research on solid alcohol with pool fire. Eventually, the fuel was replaced by 98% volume fraction ethanol. And the diameter of the can of pool fire is set to 5 cm.



*Figure 3.5. The fire whirl is generated by a 98% volume fraction of liquid alcohol in*

*the pool, of which the diameter is 50 mm.*

All the paper samples are released manually to the fire whirl. In order to keep the released position controllable, an adjustable holder and iron ring have been utilized in the experiment. For the purpose of obtaining a more general conclusion, five different

positions have been chosen to release the firebrands. The position is defined by the distance between the iron ring and the pool's edge. In this experiment, 3 cm, 5 cm, 7 cm, 9 cm, and 12 cm of the height to release are used to investigate the effect of the fire whirl on the firebrand lofting. At the same time, for other groups of cases that studied the impact of size and aspect ratio, the released height was kept the same to be 7 cm. At such height, the fire whirl's effect is neither too strong that other impacts were neglectable nor too weak that the fire whirl's effect is not apparent. Overall, two main test groups and 18 cases of experiments were undertaken in this experiment, and for each case, the test was repeated at least 50 times.
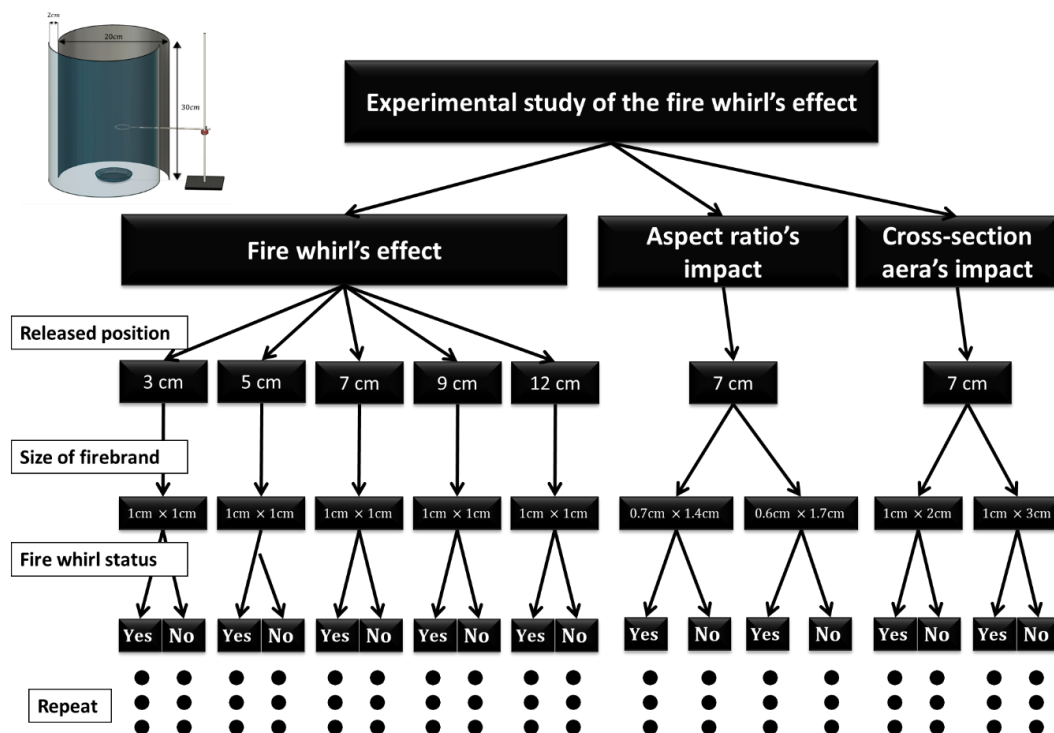


*Figure 3.6. The structure and logic of the experimental study of the fire whirl's effect on the firebrand's lofting mechanism.*

The overall setup for the experiments is shown in the Figure. A camera was set at the

front of the fire whirl generator to capture the performance of the firebrand in order to qualitative analyse the firebrand's lofting.
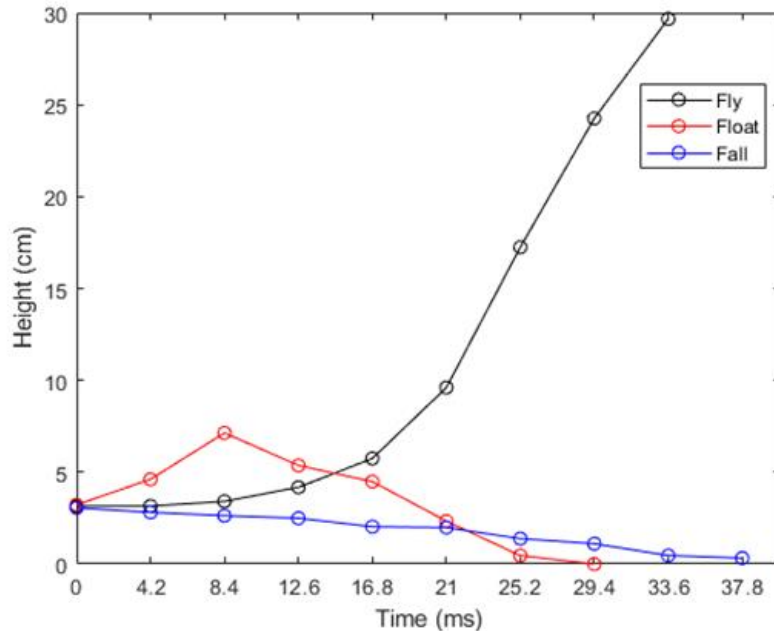


*Figure 3.7. The typical variation of height versus time for the three classifications about the firebrand's performance. In the figure, the black line shows the fly group of the firebrand, the red line shows the float group of the firebrand, and the blue line shows the fall group of the firebrand.*

However, as the fire whirl is not a quasi-steady state phenomenon, the firebrand's trajectory also varied significantly from one to the other. Therefore, the firebrand's lofting trajectory was classified into three types according to the outcome. Three classifications were named after their performance: fly, float, and fall. The flypaper samples indicated that it was being lifted significantly, which might be the hyper-long-distance firebrand in real wildland fire. The float paper samples indicated that it was being affected by the hot flow significantly. This type of paper sample tends to fly up at the beginning, but it won't last for a long time until fall. In a real fire, the float type

of firebrand might ignite the fuel at a short distance. Finally, the fall group described that the paper sample did not show any height increase during the transport, which means the hot flow didn't affect it significantly, which in real wildland fire, represented the majority of the ambers that were generated.



| Time / Class | 0 ms | 4.2 ms | 8.4 ms | 12.6 ms | 21 ms | 25.2 ms |
|---|---|---|---|---|---|---|
| Fly | | | | | | |
| Float | | | | | | |
| Fall | | | | | | |
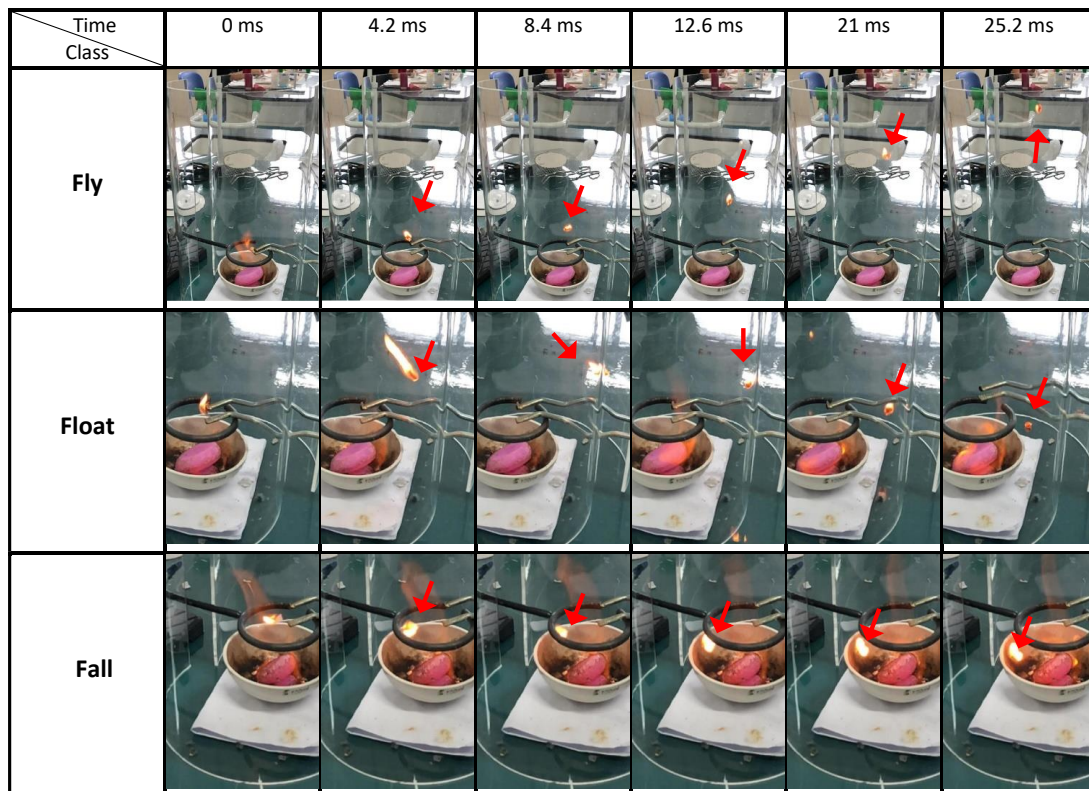
Figure 3.8. The snapshot of the video recorded about the firebrand's lofting in a fire whirl. In the video, the fire source is solid alcohol. However, in the real data collection procedure, 98% volume fraction liquid alcohol is used.

Classification for the performance of firebrand's lofting is not enough to study the fire whirl's effect. Then, based on the classification, a brand-new scale that corresponded firebrand's lofting trend with the certain scenario was introduced in this experiment. It is defined by the percentage ratio of the amount of fly and float cases in relation to the amount overall cases. The higher such ratio, the more apparent the lofting

tendency of the firebrand in such a condition. As mentioned in the previous paragraph, in the real wildland fire, the fly cases can seem like hyper-long-distance spotting, and the float group can be assumed as a short-range spotting phenomenon. The higher percentage of these two types occupied the overall cases, the more likely existence of the spotting in real wildland fire. By comparing this scale under different conditions, the conclusion about the fire whirl to the lofting mechanism of the firebrand could be made.

$$AR = \frac{Fly + Float}{Fly + Float + Fall} \qquad \text{(Eq. 3-1)}$$

In the equation, $Fly$ is the number of fly cases of the result in one of the conditions. $Float$ is the number of float cases of the result in one of the conditions. And $Fall$ is the number of rest cases of the result in one of the conditions.

Since the newly defined scale is the percentage of a certain ratio, it is named by the affected percentage or affected ratio.

## 3.2. Result of the experiment for the fire whirl's effect

### 3.2.1. Effect of the fire whirl on the lofting mechanism

In order to control the shape effect of firebrands, the initial paper samples were cut into 1cm×1cm squares. The Affected Percentage included both fly and float groups' results, which could be the real long-distance transport firebrand that will ignite the surrounding fuels in reality. This suggested that the higher the percentage, the higher possibility of a spot fire occurring. By analysing the tendency of the Affected Percentage while changing other variables, the relationship between these variables and spot fire was investigated.

Figure 3.9 shows the tendency of the Affected Percentage to vary with and without the fire whirl after releasing the firebrand at different distances to the heat source. Five positions of the release height were chosen to investigate this phenomenon.
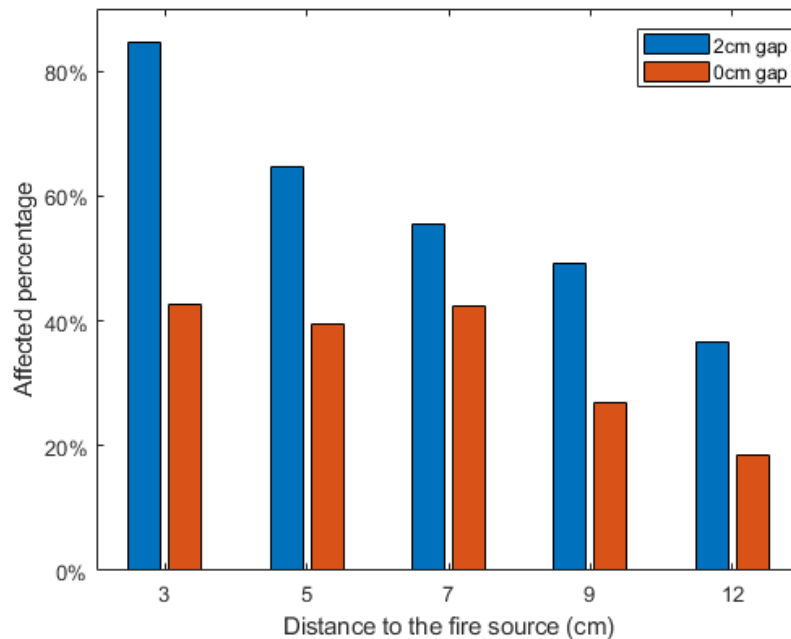


*Figure 3.9. Affect percentage of firebrands lofted from different release heights.*

As shown in Figure 3.9, when the release height is 3cm, 85% of the paper samples were affected by the fire whirl generator with a 2 cm gap, whereas when the 0 cm gap was applied to the Fire whirl generator (there is no fire whirl being generated), only 43% of the paper samples were affected. Thus, the fire whirl affected the behaviour of paper samples significantly. And this was also observed at different distances as well. For the release height of 5cm, the 0cm gap group only affected 40% of the whole released paper samples, while the 2cm gap group affected 65% of the samples. For the release height of 7cm, the 0cm gap group affected 42% of the samples, while the 2cm gap group affected 56% of the samples. In the 9cm distance of the heat sources, 49% of the samples were affected by the 2cm gap, while only 27% of the samples were

78

affected by the 0cm gap. By releasing the paper sample at a distance of 12cm, 37% of the samples were affected by the 2cm gap, while 19% of the samples were affected by the 0cm gap. The Affected Percentage of the fire whirl group is approximately two times higher than the non-fire whirl group.

## 3.2.2. Different shapes of firebrand's effect on the fire whirl

In this study, the release height was fixed in each group of experiments. The aspect ratio was varied to investigate the lofting mechanism of the fire whirl. In order to neglect the impact of irrelevant variables, in these experiments, all of the paper samples' cross-sectional area was to be $1\ cm^2$. Overall, in this study, the tested aspect ratios were 1:1, 1:2, and 1:3. Although a higher aspect ratio firebrand tends to have a higher affected percentage, they might also bend easily during transport, which affects the behaviour significantly. Therefore, the tested ratios were only chosen to be 1:1, 1:2, and 1:3.
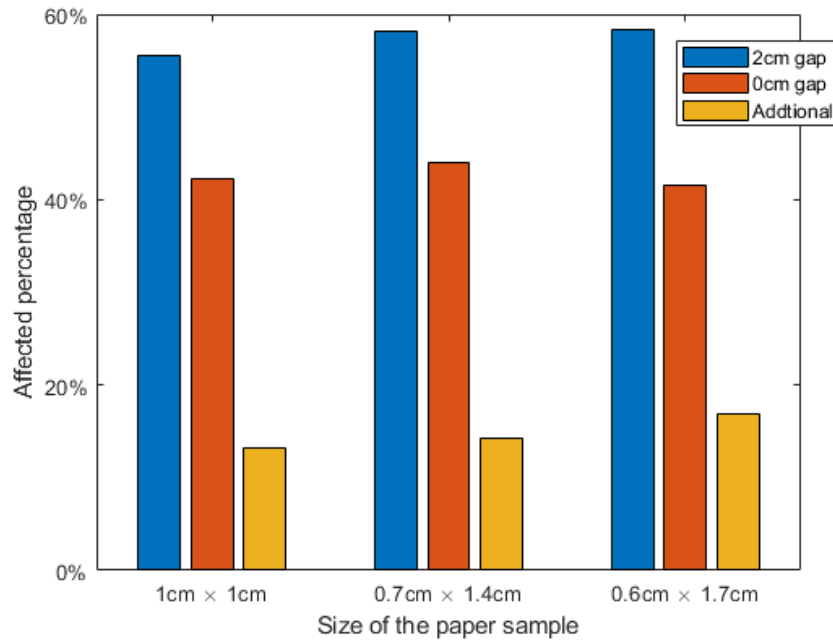
*Figure 3.10. The affected percentage of three shapes (1*1, 0.7*1.4, and 0.6*1.7) of the paper sample that released from 7 cm height lofted by 0cm gap and 2cm gap of the Fire whirl generator.*

As shown in Figure 3.10, the Affected Percentage was higher for those groups under the presence of the fire whirl in any aspect ratio. For the tests of the aspect ratio of 1:2, 58% of the paper samples were affected in the 2cm gap group, while only 44% of the paper samples were affected in the 0cm gap group. For the test with the aspect ratio of 1:3, 59% of the paper samples were affected in the 2cm gap group, while only 42% of the paper samples were affected in the 0cm gap group. Along with the increase of the aspect ratio, the affected percentage tended to increase for the tests of a 2cm gap, while the 0cm gap group did not experience such a phenomenon.

The magnitude of affected percentages itself might not have an obvious trend. However, when counting the difference between the fire whirl group's affected percentage to the no fire whirl group's affected percentage, an obvious ascending

tendency occurs. Such a difference was named after an additional percentage. With a higher aspect ratio of the paper sample, the additional percentage is increased in relation to the aspect ratio.

### 3.2.3. Effect of the cross-sectional area on the firebrand lofting.

This study focuses on the effect of the cross-sectional area of the firebrand when it is lofted by the fire whirl. In this study, the initial release position and aspect ratio of each pairing group of tests were fixed for consistency. For the aspect ratio of 1:2, $1\ cm^2$ and $2\ cm^2$ paper samples were tested, and for the aspect ratio of 1:3, $1\ cm^2$ and $3\ cm^2$ paper samples were tested. All of these firebrands were released from 7cm height above the edge of the evaporating dish.
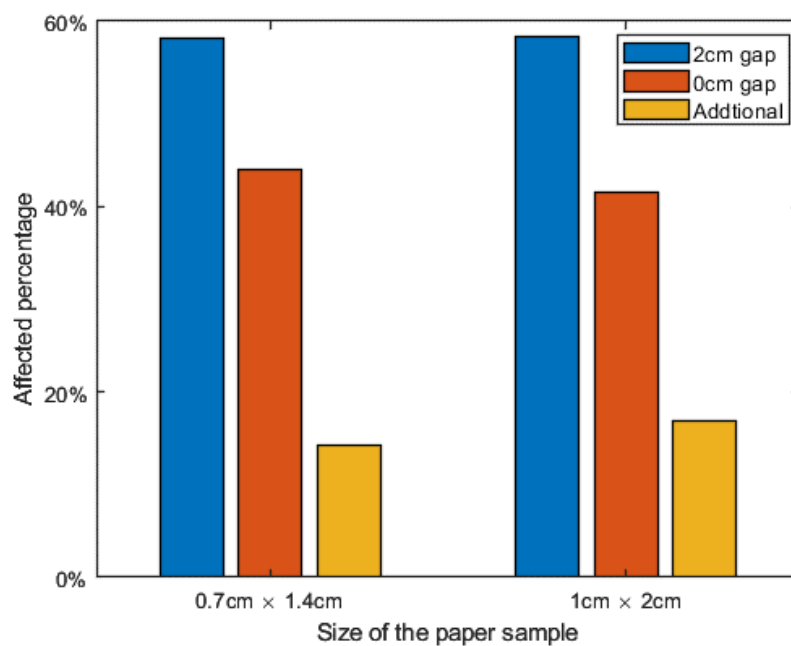
*Figure 3.11. The affected percentage of the same aspect ratio 1:2 but 1cm2 and 2cm2*

*cross-section area paper sample that released from 7cm height lofted by 0cm gap*

*and 2cm gap of the Fire whirl generator.*

As shown in Figure 3.11, the tendency of the Affected Percentage for the 2cm and 0cm gap experiment of the paper samples was different. The 2cm gap group's tests show a slight increase in the Affected Percentage relationship with the cross-sectional area, while the 0cm gap group's tests show the opposite behaviour. For the 2cm gap group, 58% of the paper samples were counted as being affected in $1\ cm^2$ paper samples group, while 60% of the paper samples were affected in $2\ cm^2$ paper group. For the 0cm gap group, 44% of the paper samples were affected in $1\ cm^2$ paper samples group, while 33% of the paper samples were affected in the $2\ cm^2$ paper group.

A possible reason for this phenomenon is that when the cross-sectional area increased, the weight of the paper sample also increased. In the group of 0cm gap tests, as there was no fire whirl effect, the paper samples were only lofted by the drag effect. However, in the group of 2cm gap tests, as there was fire whirl generated, the paper samples were lofted by both the drag effect and lift effect. Therefore, the tendency of the 0cm gap group and 2cm gap group were different from each other.

Similar to the experiment of the aspect ratio's effect, the affected percentage itself did not show an apparent trend. Since there are multiple factors that might affect the lofting performance of the firebrand, such as the firebrand's weight and the bending of the firebrand, it is essential to address the additional effect. Then, an additional calculation was made. By calculating the difference between the group with fire whirl

and without fire whirl, the fire whirl's additional effect was calculated. The additional effect is approximately linear to the cross-section area by observation.
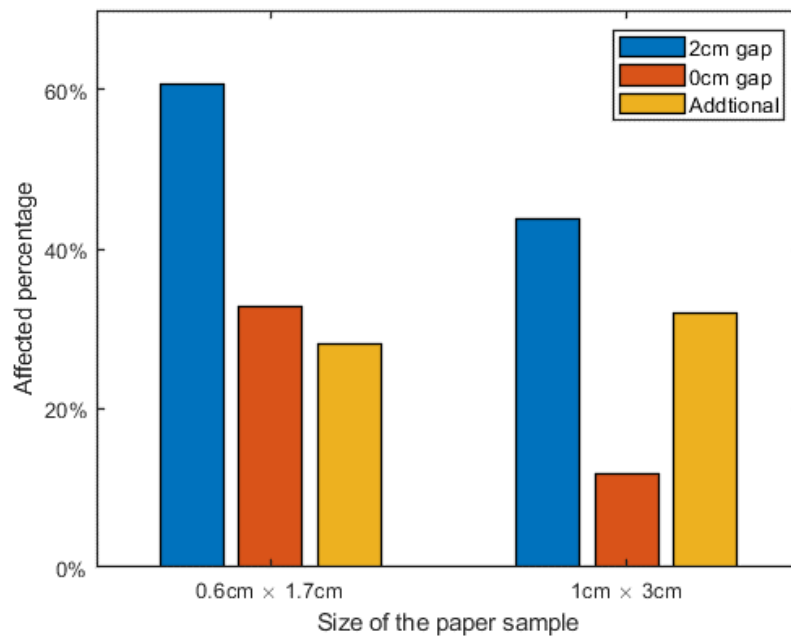


*Figure 3.12. The affected percentage of the same aspect ratio 1:3 but 1cm2 and 3cm2 cross-section area paper sample that released from 7cm height lofted by 0cm gap and 2cm gap of the Fire whirl generator.*

As shown in Figure 3.12, the tendency of the Affected Percentage for the 2cm and 0cm gap experiment of the paper samples was the same. Both tests show a negative relationship between the Affected Percentage and the cross-sectional area. For the 2cm gap group, 58% of the paper samples were counted as being affected in $1\ cm^2$ paper samples group, while 44% of the paper samples were affected in $3\ cm^2$ paper group. For the 0cm gap group, 42% of the paper samples were affected in $1\ cm^2$

paper samples group, while 12% of the paper samples were affected in the 3 $cm^2$ paper group.

When the cross-sectional area becomes large enough, the lift effect is no longer able to cover the negative impact of the increased weight. Both 2cm and 0cm gap groups of experiments showed a decreasing tendency of Affected Percentage along with the increase of cross-sectional area. Furthermore, the slopes of the relationships were different, which could be evidence of the lift effect relieving the negative impact of weight.

For the case of studying the cross-section area with an aspect ratio of 1:3, the 3 $cm^2$ group's simples were easier to be folded during the transition. Then, the affected percentages decreased significantly. However, the descending trend was not because of the fire whirl's effect. Therefore, similar to the previous group of cases, an additional calculation was made. Such additional effect also ascends in relation to the cross-section area.

## 3.3. Analyse the result of the experiment

From the previous sections' experiment, it is clear that the fire whirl contains an additional effect on the lofting mechanism of the firebrand. Such kind of additional effect is positively related to the aspect ratio. That is to say, for a higher aspect ratio, the additional effect from the fire whirl to the firebrand is stronger. The additional effect is also positively related to the cross-section area of the firebrand. The larger the cross-section area, the stronger the additional impact from the fire whirl on the firebrand.

84

Then, perhaps, such an additional effect is due to the force of aerodynamic lift. A detailed analysis will be provided in the following paragraph.

From the literature review of the firebrand's motion, it is clear that the aerodynamic forces from the ambient flow to the firebrand are the dominant effects of the firebrand's lofting. During firebrand transportation, there are mainly two aerodynamic forces, which are the aerodynamic drag and aerodynamic lift.

The aerodynamic drag force is defined as the aerodynamic effect from the ambient flow to the object that is opposite to the relative motion of the object to the ambient flow.

The aerodynamic lift force is defined as the aerodynamic effect from the ambient flow to the object that is perpendicular to the relative motion of the object to the ambient flow.

To explain this phenomenon easily, assume the firebrand is fixed in a swirl flow and a vertical flow. Then, all the analyse is undertaken in a two-dimensional coordinate.

Then, the major forces that applied to the firebrand could be expressed as:

$$m\frac{d\overrightarrow{V_a}}{dt} = \overrightarrow{F_G} + \overrightarrow{F_l} + \overrightarrow{F_d} \qquad \text{(Eq. 3-2)}$$

In this equation, the aerodynamic drag is $F_d$, the aerodynamic lift is $F_l$, and the force due to gravity is $F_G$.

Both aerodynamic lift and drag could be decomposed into two groups of vectors that parallel the x and y-axis.

85

$$F_l \propto \left(\overrightarrow{V_{rx}} + \overrightarrow{V_{ry}}\right)^2 \qquad\qquad \text{(Eq. 3-3)}$$

$$F_d \propto \left(\overrightarrow{V_{rx}} + \overrightarrow{V_{ry}}\right)^2 \qquad\qquad \text{(Eq. 3-4)}$$

As

$$\overrightarrow{V_{rx}} \cdot \overrightarrow{V_{ry}} = 0 \qquad\qquad \text{(Eq. 3-5)}$$

The equation could be expressed as:

$$F_l \propto \overrightarrow{V_{rx}}^2 + \overrightarrow{V_{ry}}^2 \qquad\qquad \text{(Eq. 3-6)}$$

$$F_d \propto \overrightarrow{V_{rx}}^2 + \overrightarrow{V_{ry}}^2 \qquad\qquad \text{(Eq. 3-7)}$$

Then after decomposing the swirl flow's velocity into axial and tangential parts, the following analysis could be given.
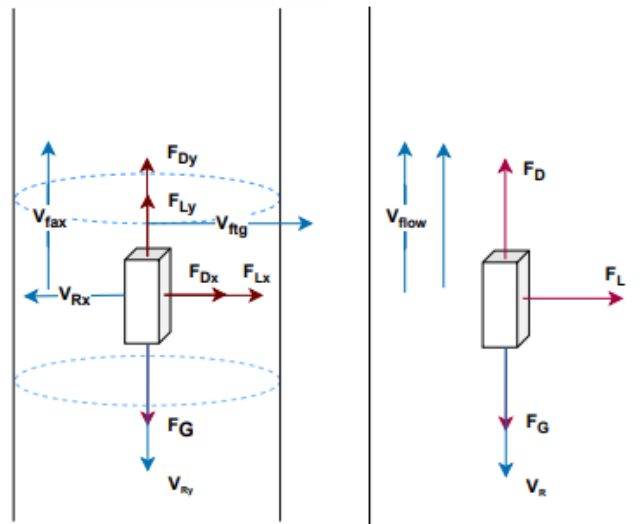


Figure 3.13. The schematic is about the forces that are exerted on a fixed object in a swirling flow field (left-hand) and a vertical flow field (right hand).

The left-hand condition for Figure 3.13 indicates the scenario that there is a fire whirl being generated. While the right-hand shows, no fire whirls were generated. In the

left-hand's situation, the tangential parts of the swirl flow will generate a vertical lift force's effect on the firebrand. While the right-hand situation, the lift force is totally horizontal and has zero effect on the lofting. The additional lift effect in the vertical direction generated from the swirl flow is an additional force compared with the other situation. Meanwhile, the aerodynamic lift is also positively related to the objects' cross-sectional area and the aspect ratio. Then the aerodynamic effect might be the additional impact on the firebrand lofting mechanism from the fire whirl.

In the next section, a detailed investigation of the generated fire whirl might be some additional proof that the additional impact from the fire whirl on the firebrand is its aerodynamic lift effect.

## 3.4. Flow field experiment for the fire whirl

### 3.4.1. Introduction of PIV

Particle Image Velocimetry (PIV) is defined as a non-intrusive method for velocity measurements under various conditions [18]. This technique uses a number of suspended particles spreading in the fluid in order to measure the flow filed. The whole system can be mainly divided into three functional parts:

- Particles that are being used to trace.

The fundamental mechanism of the PIV system is to use the particle to visualize the flow. Therefore, a type of certain properties' particles should be applied. Ideal particles should have the following properties. First, the particle should be tiny enough in size so that it won't affect the flow or change the properties of the fluid medium. Then, it should have a similar density to the fluid, as it will make the particle follow

the flow smoothly and be suspended for a longer period of time.

- Illumination.

From the previous requirement, the tracing particle should also be very different to visualize. Then, a certain light source should be provided to make the particle visible and also able to be traced by a visual recording device like a high-speed camera. The illumination of the particle is usually conducted via a thin laser sheet. The reflection of the laser from the particle allows better visualisation of the particle in such a thin laser sheet.

- Visual recording.

The PIV is not only visualized but also measures the flow field for the fluid. Thus, high-speed cameras and video recorders are necessary for further analysis of the flow.
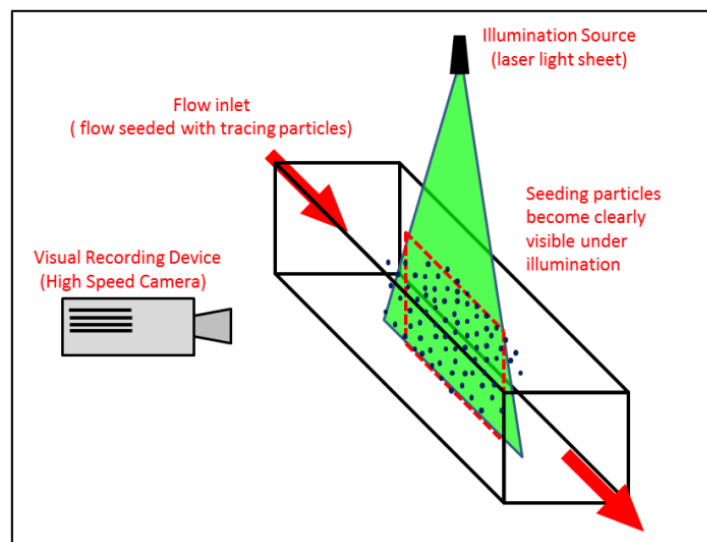


*Figure 3.14. The schematic of the PIV system [58].*

The outcome of the PIV system is to compute the flow field velocities, which measure the tracer particles' displacement from the flow recording during different time

instances. Multiple techniques can be used to get the outcome. One of the most commonly used techniques in PIV systems is the double frame. The double frame requires that the camera shutter be opened twice with a very short interval between two frames for each recorded time step. The synchronization of the shutter and the laser pulse is also required to be accomplished in the PIV system.
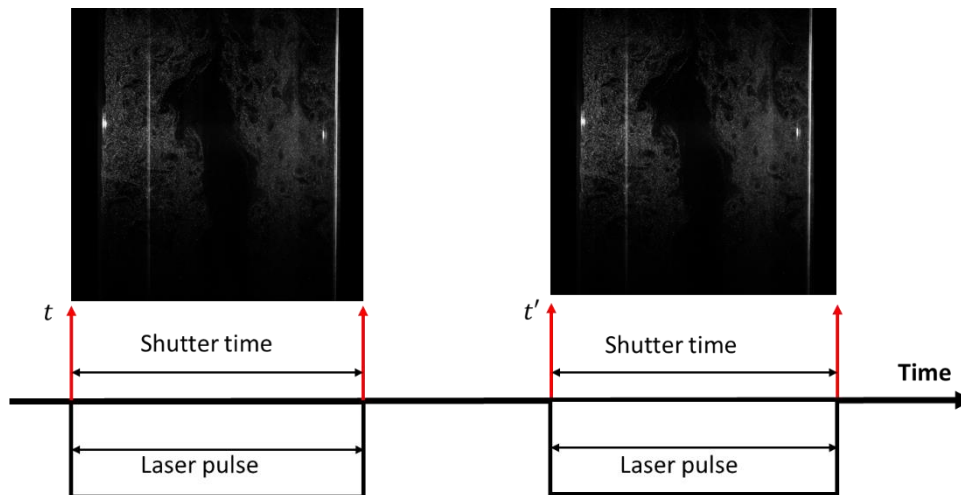


*Figure 3.15. The relationship between the camera's shutter time and the laser pulse duration. The captured photo is utilized to demonstrate the theory of the flow field.*

## 3.4.2. Set-up of the PIV experiment

Figure 3.16 shows a schematic of the fire whirl generator, PIV system, and particle seeding device. Two transparent cylindrical walls, 300 mm in height, 200 mm in diameter, and 2 mm in thickness, were arranged to generate the fire whirl. The gap between each half-cylinder wall controlled the intensity of the fire. Wall gaps of 0 mm and 20 mm were chosen to be tested. A circular pool of ethanol fuel with a diameter of 50 mm was set at the centre of the cylindrical walls. The laser sheet passed through the walls to create a measurement plane located 130 mm above the pool.

The PIV system consists of an Nd: YAG double-pulsed laser (532 nm) and a dual-frame CCD camera. DANTECT DYNAMICS software was used to evaluate and display the data. A 532 nm bandpass filter was used with the CCD camera to focus on the particle reflection in the laser sheet. The imaging frame rate was set to 10 Hz, and the interval between a pair of images was set to 1000 µs. Cross-correlation with a 64 × 64 pixel kernel was applied as an interrogation area to estimate the velocity vector field.

Various seeding particles were tested in this experiment, such as the $SiO_2$ powder and $Al_2O_3$ powder. However, these particles' density prevented them from being suspended in the fire whirl for a long period of time. Therefore, the flow around the fire whirl was seeded with hollow glass spheres by a particle seeding device. The average diameter of the glass particles was 15 µm, and 90% of the particles had a diameter below 20 µm.
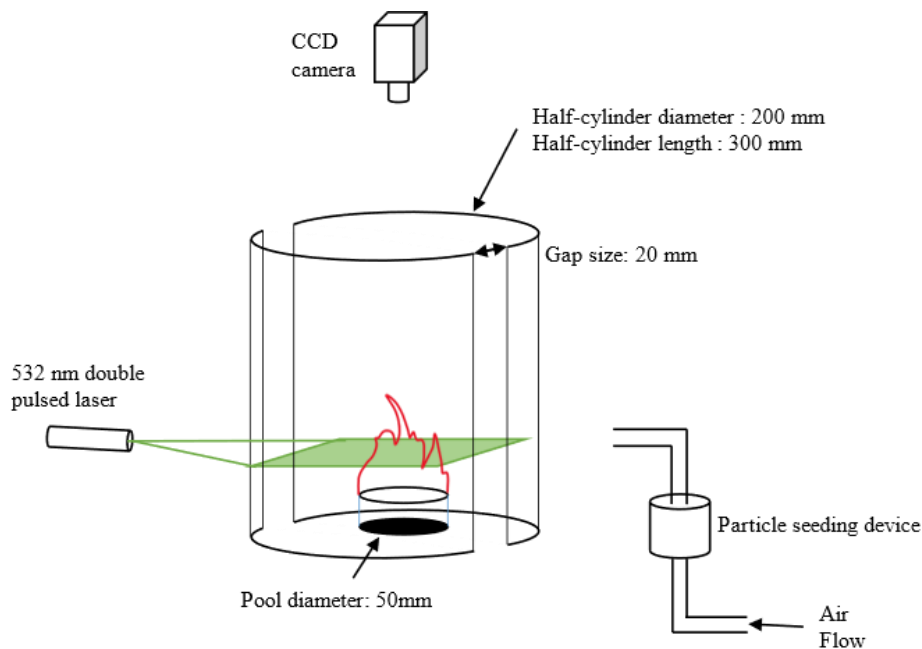


*Figure 3.16. The vertical view position captures the PIV system.*

As the objective of this experiment is to measure the flow field of the fire whirl for

further analysis and validation, various tests were undertaken under different conditions and even different positions. Some of the test cases were even different scenarios compared with the following fire whirl test. However, such experiment results could be used for further analysis.
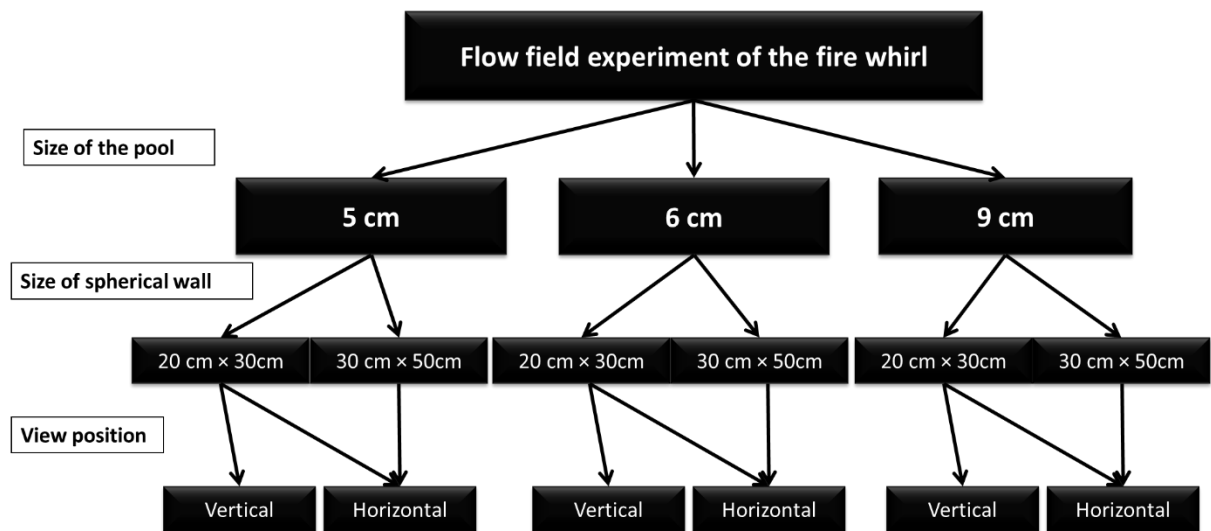


*Figure 3.17. The structure and logic of the PIV test on the flow field for the different parameters' fire whirl generator.*

The vertical view position could own observe the circulation generated from the fire whirl, while the horizontal view position could calculate the upward effect generated from the fire whirl. Although due to the strong upward lift effect from the fire whirl, the central zone lacks sufficient particles to calculate a reliable velocity. It still provided a symmetrical study of the fire whirl's flow field.

The PIV field is a result of a pair of frames processed by DANTECT DYNAMIC software. Previously, the vertical view position's schematic was given, which could only be utilized to measure the horizontal circulation. In order to measure the vertical flow

field, a horizontal view position should also be undertaken in the PIV experiment. The laser sheet goes through the gap so that a thin layer above the pool fire's flow field can be visualized by the PIV system as the fire whirl's vertical velocity is significantly larger than its circulation. Then a shorter interval between a pair of images was chosen. By testing, the time interval was set to 120 μs.
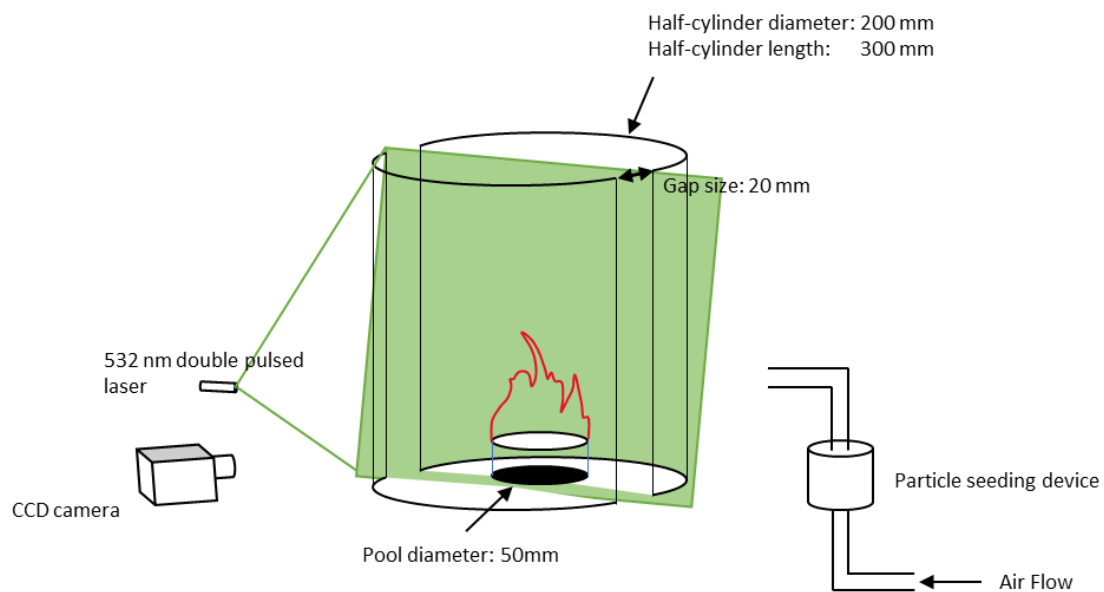


*Figure 3.18. The horizontal view captures the PIV system.*

## 3.4.3. Fire whirl's Flow field from vertical view position

The first case is measuring the flow field of a fire whirl generator 20 cm in diameter and 30 cm in length, and the diameter of the pool is 5 cm. For such a case, it is clear that circulation is generated in the main zone, which is clockwise. Due to the strong vertical lofting from the fire whirl, the tracing particle in the central zone is rare. Therefore, the calculated velocity in the centre zone is not smooth. However, in the other era of the test zone, the vector of velocity is continuous and obvious. At the boundary era of the central zone, the flow's horizontal velocity is around 1.2 m/s and

is related to the distance to the central point of the fire whirl, and the velocity decreased sharply to 0.75 m/s and even 0.45 m/s.
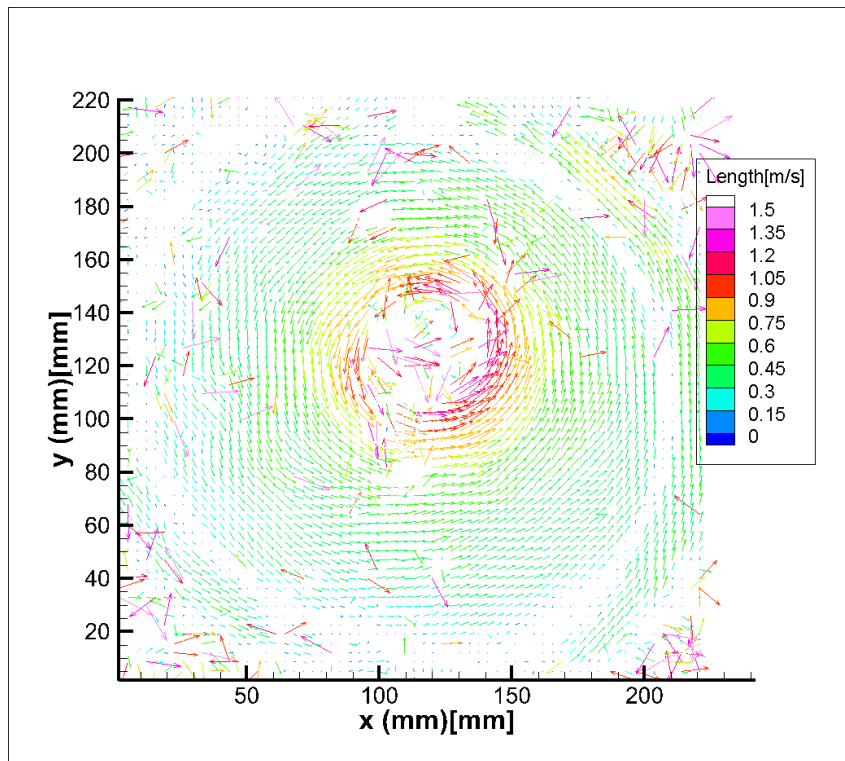


*Figure 3.19. The vertical view position's flow field of the 5 cm pool size and 20 cm ** 30 cm fire whirl generator.*

The first case's condition is just like that being utilized in other tests of firebrand's lofting mechanism. Therefore, the calculated velocity field could be used as qualitatively analyse the fire whirl's velocity field. Two conclusions could be given directly. For the first one, the circulation generated from the fire whirl covers the whole test zone. That is to say, the tangential flow that affects the firebrand is not only in the central zone but also in the whole test zone. For the second one, the highest horizontal velocity appears at the centre zone of the fire whirl, and also, the diameter of the centre zone of the fire whirl is slightly larger than the diameter of the pool.

The second case is measuring the flow field of a fire whirl generator 20 cm in diameter and 30 cm in length. The size of the pool is 6 cm. The direction of the circulation for the flow is also clockwise. Similar to the last case, the high vertical upward effect decreased the density of the tracing particle. Therefore, the central zone is not that smooth. However, the rest area of the fire whirl's velocity is clear and smooth. At the boundary area of the central zone, the horizontal velocity is around 1.4 m/s, which is slightly higher than that of the last case. However, the rest velocity is almost similar to the last cases.
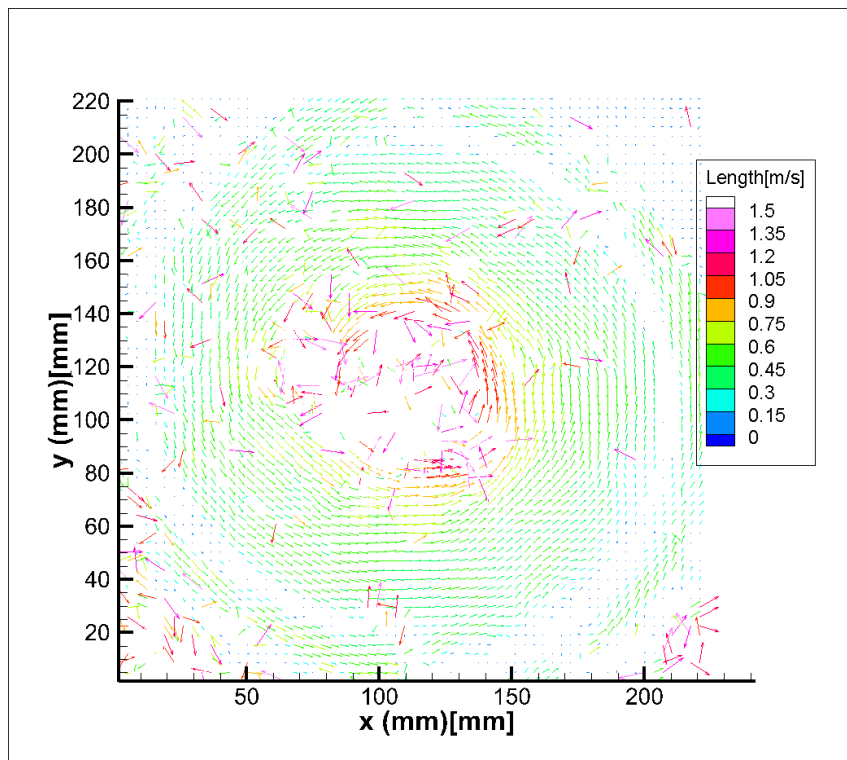


*Figure 3.20. The vertical view position's flow field of the 6 cm pool size and 20 cm \* 30 cm fire whirl generator.*

The second case's condition is almost the same as the experiment of the firebrand's lofting mechanism. The only modification of the condition is the pool fire's size. A

larger pool fire increased the velocity at and around the central zone, and the rest area's velocity didn't vary significantly. Since the central zone is slightly larger than the size of the pool, the second case's central zone is larger than the first case's central zone.

The second case is measuring the flow field of a fire whirl generator 20 cm in diameter and 30 cm in length. The size of the pool is 9 cm. A clockwise circulation is generated in this setup. The outer zone's velocity is around 0.45 m/s and almost the same as the previous few cases. However, the central zone's horizontal velocity is larger than in the previous cases due to the larger pool size. The horizontal velocity of the boundary of the central zone is around 1.5 m/s. Moreover, the thickness of the boundary is also thicker than in the last two cases.

Compared with the three cases, a larger pool size generates a stronger horizontal velocity. However, the magnitude of the increase in the horizontal velocity is limited. The boundary's velocity's value varied from 1.2 m/s and 1.4 m/s to 1.5 m/s.
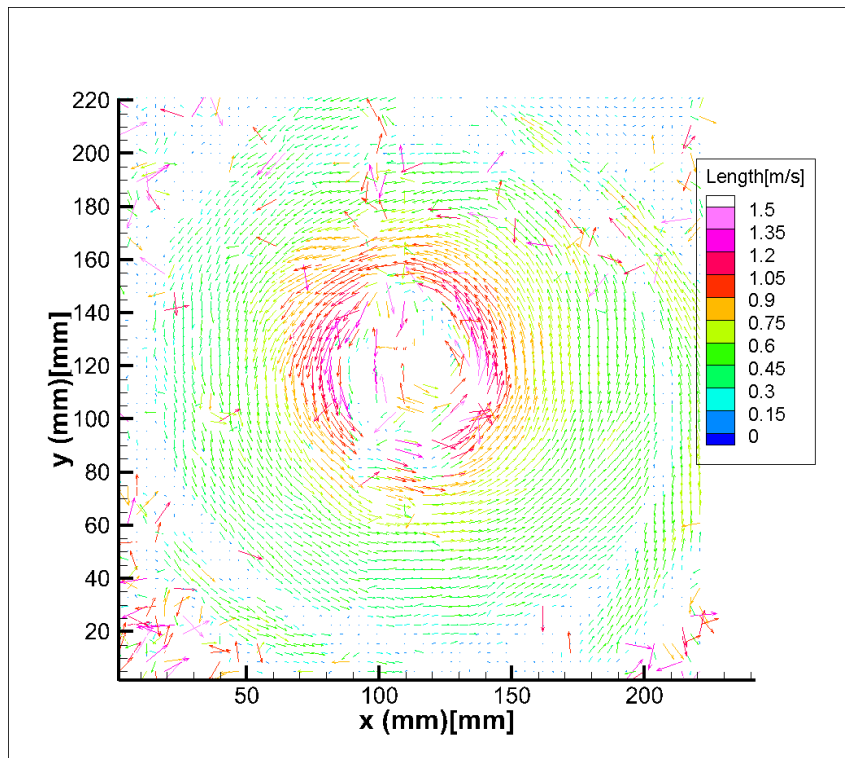
*Figure 3.21. The vertical view position's flow field of the 9 cm pool size and 20 cm ***

*30 cm fire whirl generator.*

## 3.4.4. Fire whirl's Flow field from a horizontal view

## position

The horizontal view position of the fire whirl's flow field is tested in six different

scenarios.
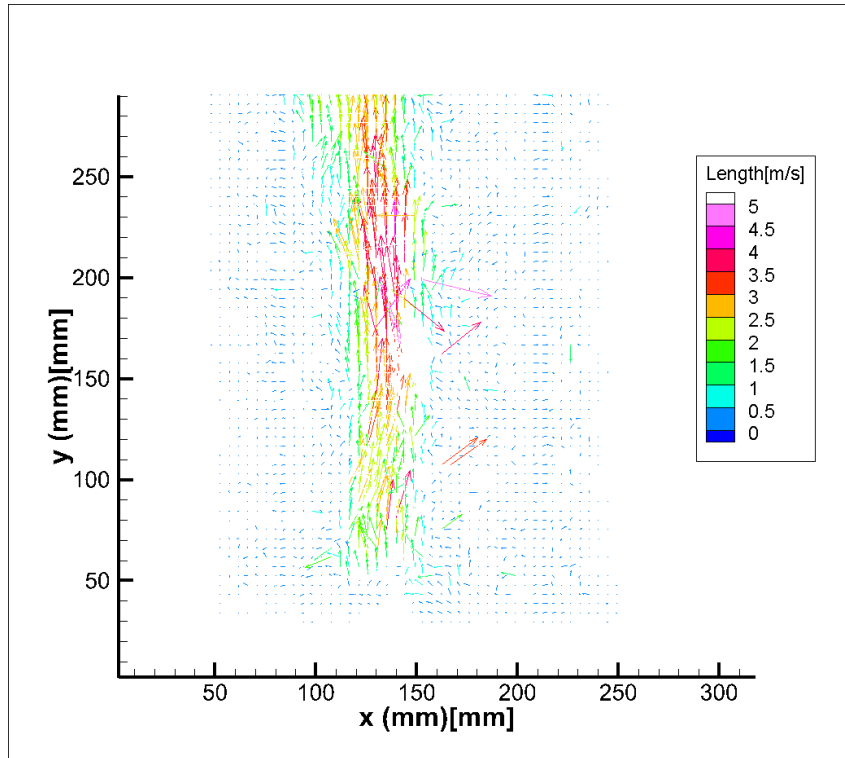
*Figure 3.22. The horizontal view position's flow field of the 5 cm pool size and 20 cm ** 30 cm fire whirl generator.*

For the first case, the vertical velocity of the flow field is measured with the fire whirl generator 20 cm in diameter and 30 cm in length, and the diameter of the pool is 5 cm. With the help of a shorter 120 μs of time interval to capture the pair of images, the central zone of the vertical velocity is able to be captured. The central zone of the fire whirl's vertical velocity is significantly larger than the outer region, in which the central velocity is as high as 3.5 m/s, while the outer region is around 0.5 m/s. Therefore, a property of the central zone's velocity is obvious. For the horizontal velocity generated from the fire whirl, it is the same magnitude as the central zone and the outer zone. However, in the cases of vertical velocity, the central zone's vertical velocity is significantly larger than the outer zone than one magnitude. Whatsmore, the value of the horizontal velocity is apparently less than that of the

vertical direction. The central line's velocity is increased at the beginning along the distance to the fire pool. Till it reaches its maximum velocity at 200 mm above the ground for about 3.5 m/s, that velocity tends to be decreasing.

The first case's condition is the same as the one being utilized in the experiment testing the firebrand's lofting mechanism. Therefore, the velocity field could be used to qualitatively analyse the fire whirl's effect on the fire brand lofting mechanism. A strong vertical plume is the dominant mechanism of the firebrand as the scenario with the fire plume, which is the same as the statistic analyse experiment that firebrand releases at different heights.
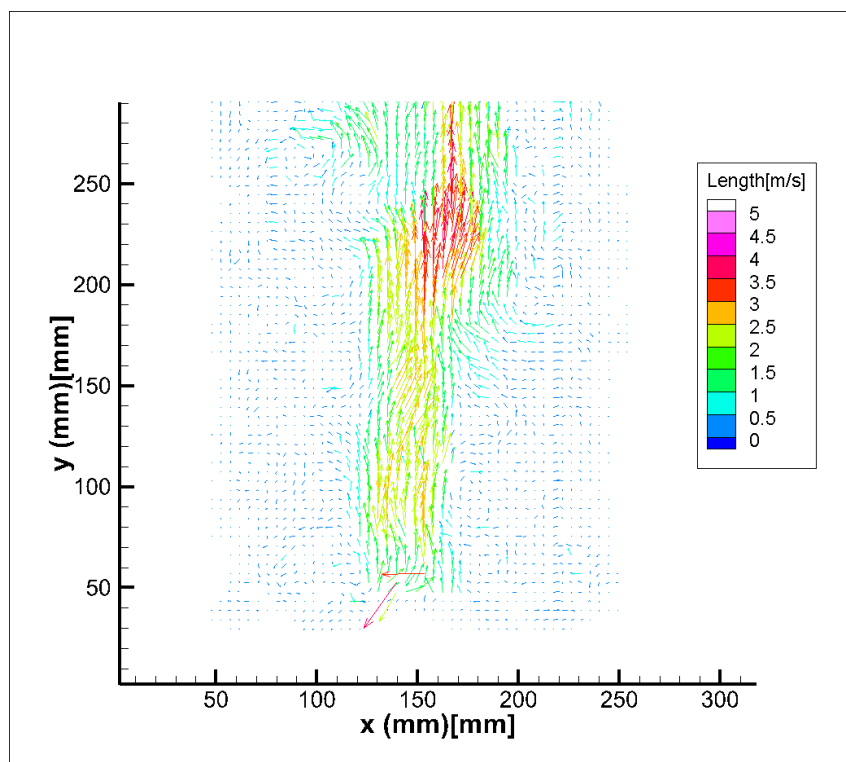


*Figure 3.23. The horizontal view position's flow field of the 6 cm pool size and 20 cm * 30 cm fire whirl generator.*

98

The second case's condition is measuring the flow field of the fire whirl generator with 20 cm in diameter and 30 cm in length, which the diameter of the pool is 6 cm. By comparing with the first case, it is clear that the central zone of the fire whirl's vertical velocity is significantly higher than that of the 5 cm pool fire's fire whirl. At 150 mm above the ground, the vertical velocity reaches around 4 m/s. In the other region that is far from the central line, the vertical velocity is as low as 0.5 m/s, which is similar to that of the previous case. Since the central zone is slightly wider than the pool size, the second case's central zone is slightly thicker than that of the first case.
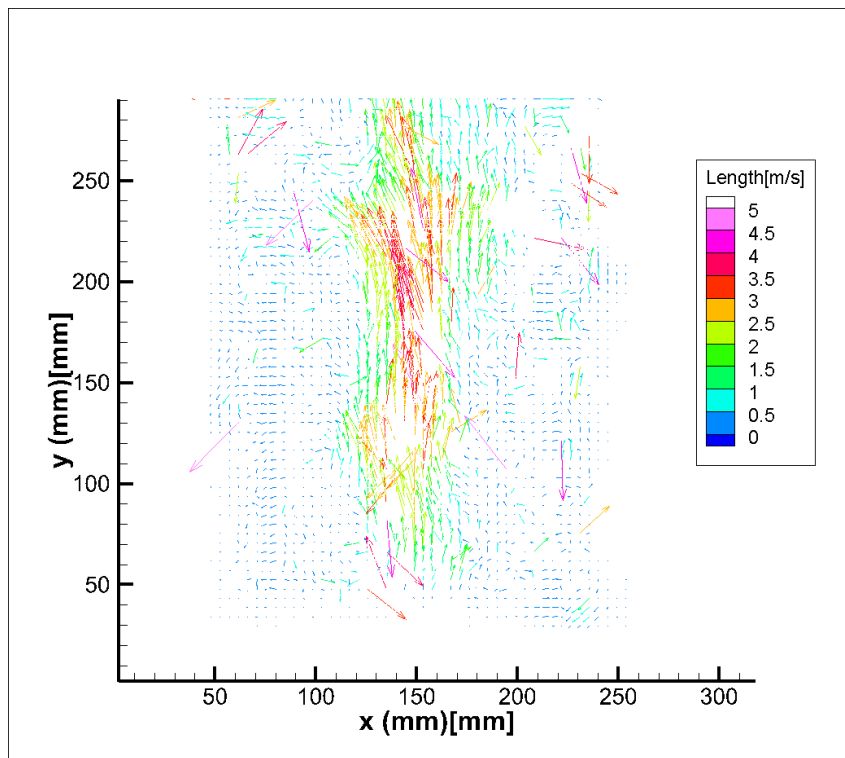


*Figure 3.24. The horizontal view position's flow field of the 9 cm pool size and 20 cm * 30 cm fire whirl generator.*

The second case only slightly modified the condition that was being utilized in the firebrand's lofting mechanism experiment. A slightly larger pool fire generates a slightly stronger fire whirl. However, the improvement of the vertical velocity is

99

apparently sharper than the horizontal circulation velocity. The maximum velocity is located at a low position. One thing needs to be pointed out such maximum velocity is limited by the size of the fire whirl generator in comparison to a larger half-cylinder wall.

The second case's condition is measuring the flow field of the fire whirl generator with 20 cm in diameter and 30 cm in length, which the diameter of the pool is 9 cm. The largest pool fire generated the strongest fire whirl. The vertical velocity of the flow at 80 mm above the ground has already reached 4 m/s. While at the same time, the out region's vertical velocity was not varied significantly, which is at around 0.5 m/s.

By comparing the first three cases of the vertical velocity field, it is clear that the vertical velocity along the central line of the pool fire is much more sensitive to the pool size compared to that of the horizontal velocity.

The fourth case's condition is measuring the flow field of the fire whirl generator with 30 cm in diameter and 50 cm in length, which the diameter of the pool is 5 cm. A sever fire whirl is generated in the smallest pool fire in the largest fire whirl generator. The vertical velocity of the flow at 80 mm above the ground has already reached 3.5 m/s. For a higher position, like 200 mm above the ground, the vertical velocity even reaches 5 m/s. While at the same time, the out region's vertical velocity was not varied significantly, which is at around 0.5 m/s.
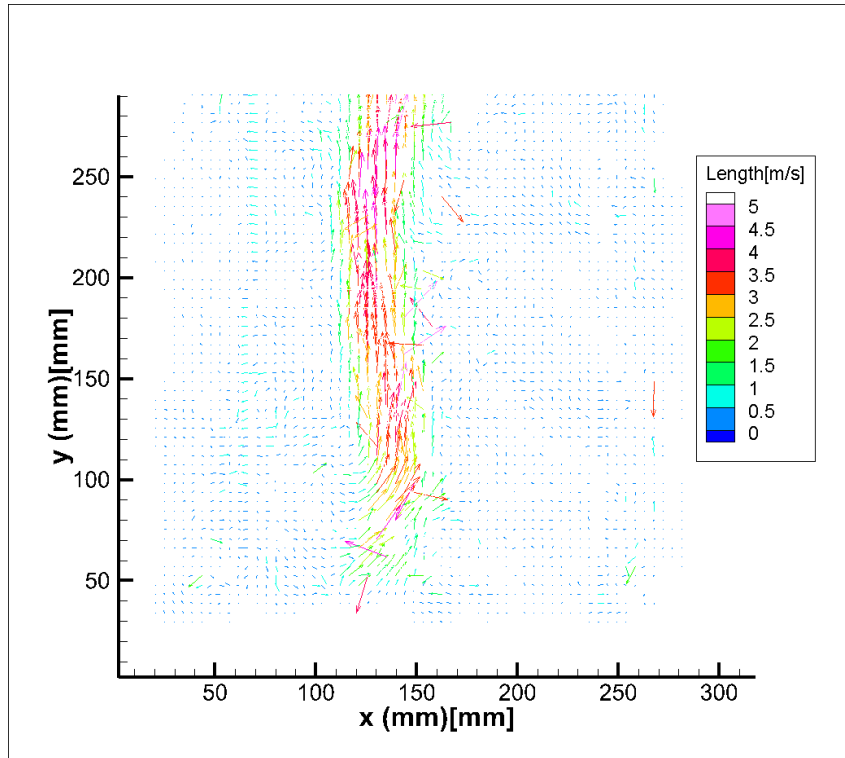
*Figure 3.25. The horizontal view position's flow field of the 5 cm pool size and 30 cm ** 50 cm fire whirl generator.*

The fourth case is trying to study the fire whirl generator's impact on the flow field. It is clear that the fire whirl generator's impact is way more significant than that of the pool size. A larger fire whirl generator with the smallest fire whirl could generate a stronger fire whirl than a smaller fire whirl generator with the largest fire whirl. Due to the strength of the fire whirl being very high, the central zone of the fire whirl is straighter than the fire whirl generated in a smaller half-cylinder wall.

The fifth case measures the flow field with the half-cylinder wall 30 cm in diameter and 50 cm in length. The diameter of the pool is 6 cm. In such conditions, with a larger pool size, the high velocity appears more approach the ground more. At around 100 mm, the vertical velocity reached 4 m/s. At 150mm above the ground, the vertical velocity was as high as 5 m/s and even higher.

101

The sixth case's condition is similar to the fifth one, but the size of the pool increased

to 9 cm. However, apart from the size of the central zone being larger than that of the

6 cm pool fire, the flow field in 9 cm pool fire cases didn't vary a lot. At around 100

mm, the vertical velocity reached 4 m/s. At 150mm above the ground, the vertical

velocity was as high as 5 m/s and even higher.
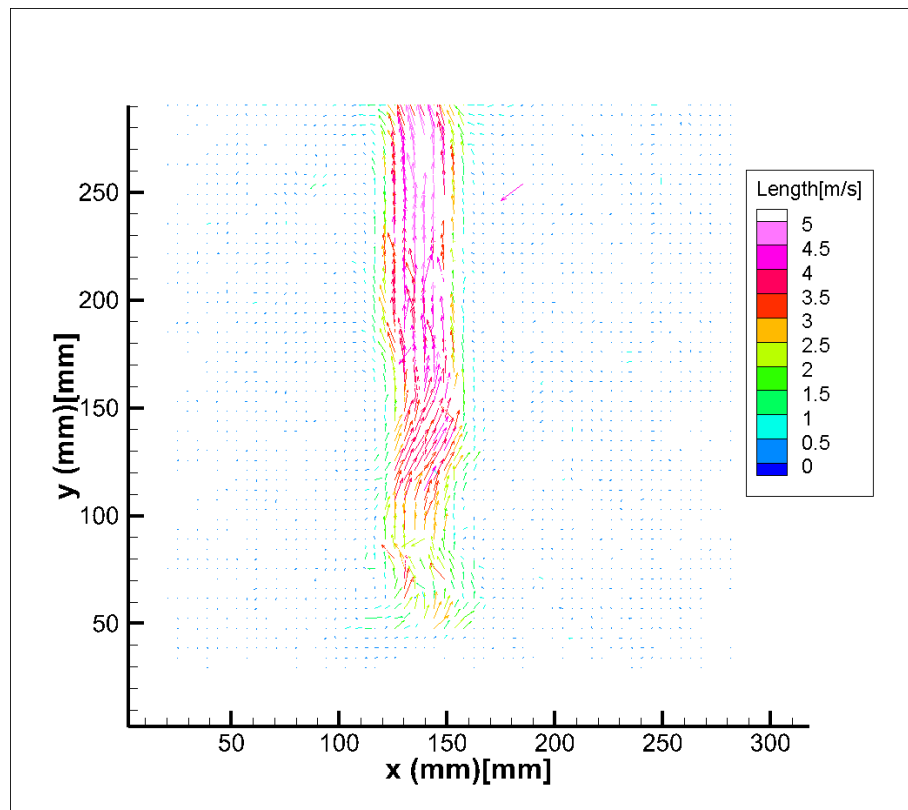


*Figure 3.26. The horizontal view position's flow field of the 5 cm pool size and 30 cm ***

*50 cm fire whirl generator.*
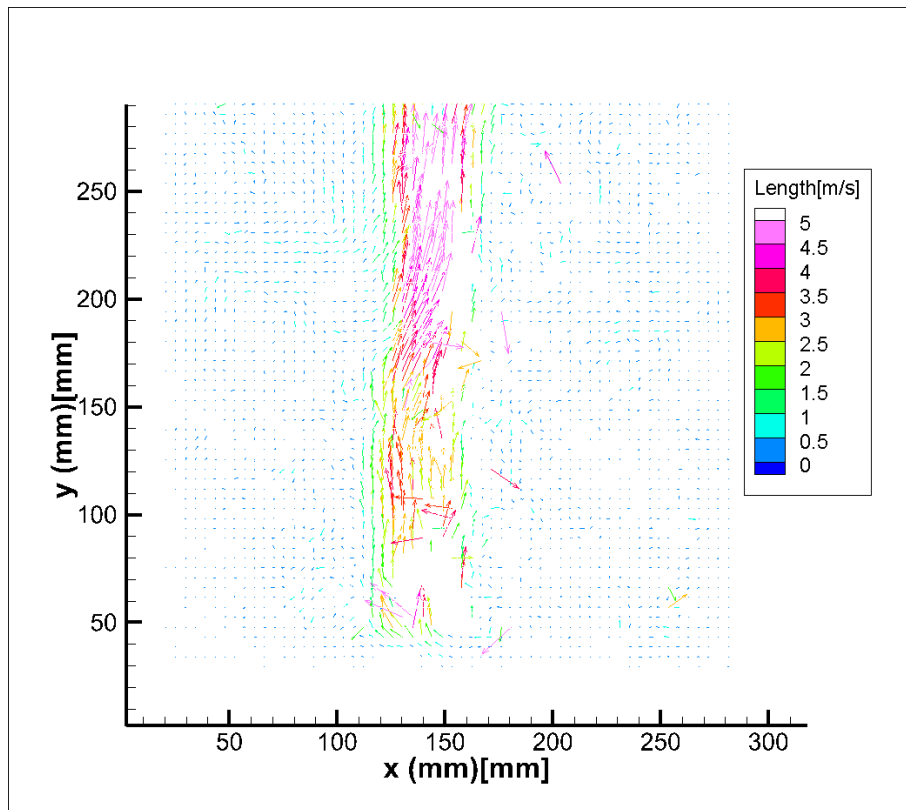
*Figure 3.27. The horizontal view position's flow field of the 9 cm pool size and 30 cm \* 50 cm fire whirl generator.*

## 3.4.5. Conclusion of the fire whirl flow field test

The flow field for the fire whirl is not the major objective of this thesis. However, in order to understand the fire whirl's effect on the firebrand's lofting mechanism, Studying the basic structure of the fire whirl is quite necessary.

The conclusion for the fire whirl flow field test can be separated into three aspects:

- Comparing the horizontal and vertical velocity of the fire whirl's flow field.

The laser sheet that is being utilized in the horizontal velocity field passes through the walls to create a measurement plane located 130 mm above the pool, which is 150 mm above the ground. 150 mm is high enough for most of the cases that the vertical

velocity reaches a high velocity at around 3.5 m/s. It is true that the horizontal velocity could only reach around 1 m/s, which is not as high as the vertical one. However, these velocities were of the same magnitude. Therefore, neglecting the horizontal velocity for the fire whirl's effect on the firebrand's lofting mechanism is apparently unacceptable.

- Comparing the test in horizontal and vertical velocity of the fire whirl's flow field.

Another obvious conclusion could be made that the horizontal velocity of the fire whirl covers the whole test zone. The inner region's velocity is around 1.2 m/s, while the outer region is around 0.6 m/s. However, the vertical velocity seems only to appear in the zone close to the central zone. In the central zone, the vertical velocity could reach as hight as 5m/s. At the same time, the outer region's velocity is lower than 0.5m/s.

- Comparing the different pool sizes and half-cylinder wall size

For the test case about the horizontal velocity of the fire whirl, the increase in the pool size only obtained a limited effect on the result. The inner region's velocity increased from 1.2 m/s to 1.5 m/s. From the test case in vertical velocity. The increase in the pool size also only gained a limited improvement to the result. The position for 3 m/s vertical velocities along the central line decreased from 180 mm to 120 mm.

However, the impact of a larger half-cylinder wall size is relatively more apparent. A larger fire whirl generator with the smallest fire whirl could generate a stronger fire whirl than a smaller fire whirl generator with the largest fire whirl. However, for a larger fire whirl generator, the impact of pool fire's size is even able to be neglected.

The purpose of using the PIV to measure to flow field of a fire whirl is more than just validating the simulated result, it also enhances the understanding of the properties of the fire whirl itself.

# 4. Modelling the firebrand's lofting

The previous chapter introduces the experimental investigation of the firebrand's lofting with the impact of a fire whirl. Some of the brief parameter investigations about the fire whirl generator have been undertaken. Some of the properties of the fire whirl were also given directly. However, investigating the firebrand's lofting mechanism is more than just doing an experiment. Some sort of physical-based model has also been introduced to study the detailed physics of the fire whirl's lofting mechanism to the firebrand. In order to study the firebrand's lofting mechanism with a physical-based mathematical model, such type of model should be built for further investigation.

In this chapter, the concepts of the models built for further investigation will be introduced. The structure of the model is presented in detail. The model modelling of the fire brand's lofting mechanism is introduced from several aspects: the aerodynamic forces of the firebrand lofting mechanism, methods to solve the equation of the motion, and some basic burning effects on the firebrand. The aerodynamic forces can be separate into three aspects, the darg, the lift, and the tumbling effect. The direction of the aerodynamic lift effect will be introduced in detail as in the three-dimensional motion. The basic definition of That is perpendicular to the relative motion of the adjacent flow is not accurate enough. Two methods will be compared in solving the second-order derivative governing equation of the firebrand's motion. Eventually, as the period of time for a firebrand being lofted is relatively short, only the simplest combustion model that the firebrand's weight varies during

transportation has been discussed and utilized in this model. In the last, the assumptions of the models are highlighted to explain the current limitation for modelling the firebrand's lofting.

## 4.1. Aerodynamic forces

In this section, the fundamental aspects of transporting model of firebrands are introduced. The aerodynamic forces exerted on the firebrand during the lofting period are investigated, and the aerodynamic lift on the firebrand is highlighted. As this model calculates the firebrand's motion in a 3D domain, the vector calculation covering all angles of attack with the inclined angel is also discussed in detail. Furthermore, other than the aerodynamic forces, the momentum of tumbling also being introduced in this section to provide a physics-based model.
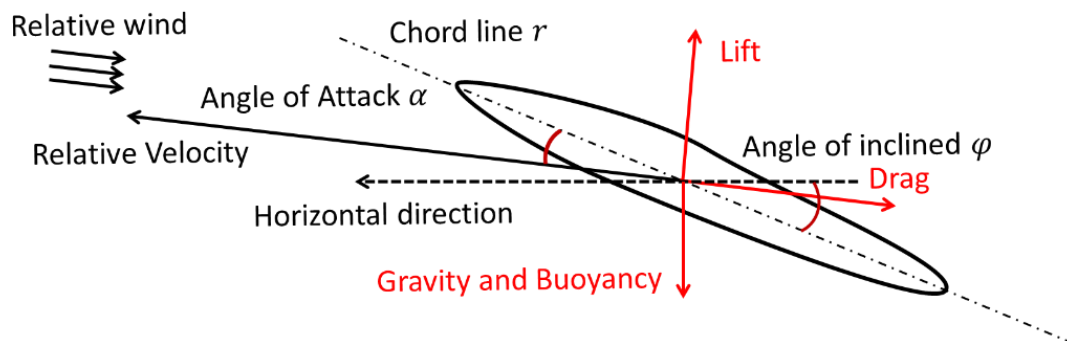


*Figure 4.1. The schematic is about the forces exerted on the firebrand that is*

*travelling within a flow field.*

As Figure 4.1 showed, the forces being applied to the firebrand while transporting in a flow field could mainly be summarized as four forces, which are aerodynamic lift $F_L$, aerodynamic drag $F_D$, buoyancy $F_B$, and gravity $F_G$ [35]. Since the gravity and buoyancy only obtain the impact in the vertical direction, these two forces' impacts

are combined with each other in the calculation. Therefore, the net force on a firebrand when it is transporting through a flow field can be expressed as:

$$F = F_D + F_L + F_G - F_B$$

Another two very important reference angles are highlighted in the figure, which are the angle of attaching $\alpha$ and the inclined angle $\phi$. $\alpha$ is defined as the angle between the chord of the firebrand r and its direction of relative velocity $V_r$ and with respect to the surrounding flow. Moreover, the other is the angle between the firebrand's chord line and the horizontal direction.
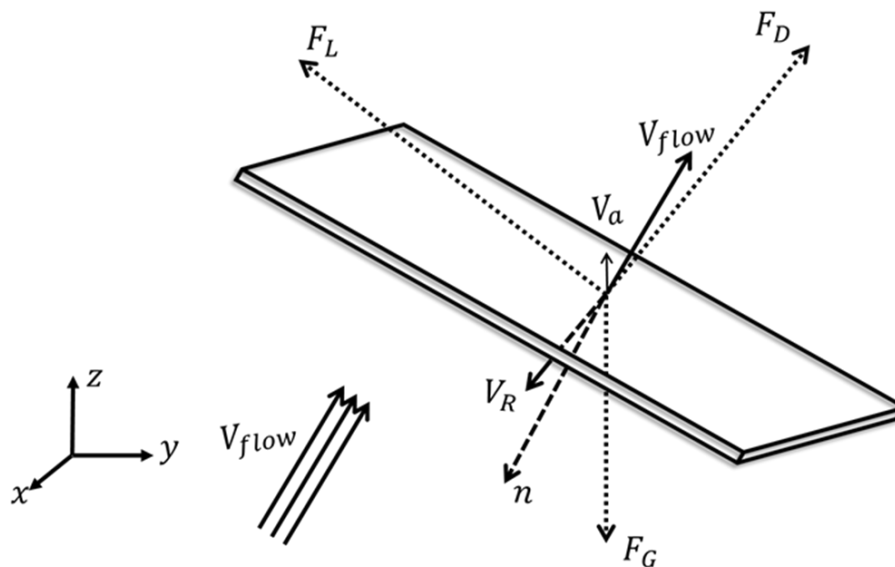


*Figure 4.2. The three-dimensional schematic of the forces exerted on a rectangular-shaped plate-like object in a flow field.*

In the following few sections, the forces that are being exerted on the firebrand while transporting in a flow field will be introduced.

## 4.1.1. Aerodynamic drag

Aerodynamic drag is defined as a force that is opposite to the solid object's moving

direction. Thus, determining the direction of drag is relatively simple. Once the relative

motion's direction is determined, the drag force is just opposite to it.
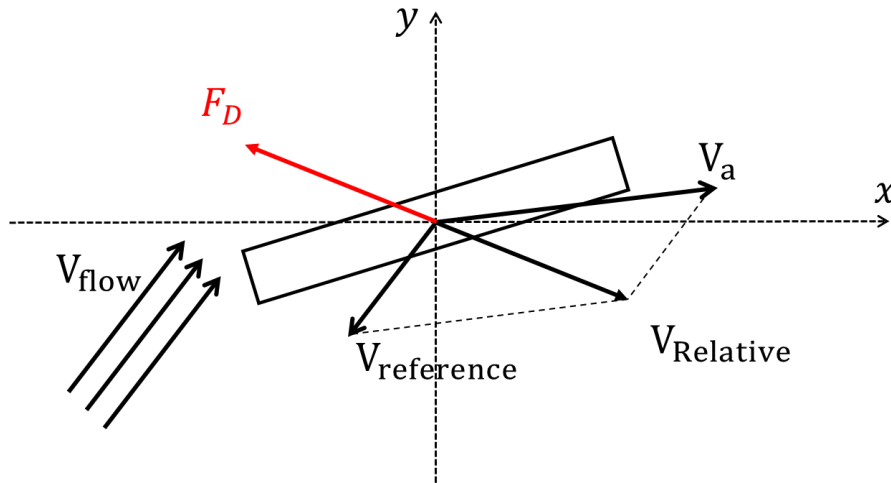


*Figure 4.3. The schematic about the direction of the aerodynamic drag for an object*

*moving in a flow field.*

From the knowledge of rigid body motion, the direction of relative velocity could be

calculated with the body's absolute velocity with the flow field's velocity by the

following equation:

$$\overrightarrow{V_{Relative}} = \overrightarrow{V_a} - \overrightarrow{V_{flow}}$$ (Eq. 4-2)

The direction of the drag force $F_D$ will be the opposite of the relative velocity of the

firebrand in relation to the surrounding flow field $\overrightarrow{V_{Relative}}$. Further, in regular

conditions, the drag force is found to be proportional to the square of the relative

velocity. Then mathematically, the equation of drag force can be written as:

$$F_D = \frac{1}{2} C_d \cdot \rho \cdot V_r^2 \cdot A_c$$ (Eq. 4-3)

In this equation, $F_D$ is the aerodynamic drag. $C_d$ represents the drag coefficient, which depends on the shape of the object and the Reynolds number of the system. $V_r$ is the relative velocity of the firebrand to the surrounding flow. $A_c$ is the firebrand's cross-sectional area.

In the literature review of previous research related to the firebrand transporting model, a huge amount of study had been untaken to measure the drag coefficient experimentally. In this thesis, the firebrand is assumed to be rectangular-plate-like. Therefore, the suitable equation to determine the drag coefficient will be Zastawny and Ortiz's [88], which is presented as:

$$C_D = \frac{5.82}{Re^{0.44}} + \frac{15.56}{Re^{1.068}}$$
$$+ \left( \frac{35.41}{Re^{0.96}} + \frac{3.63}{Re^{0.05}} - \frac{5.82}{Re^{0.44}} \right.$$
$$\left. + \frac{15.56}{Re^{1.068}} \right) [\sin(\alpha)]^{1.96}, Re \leq 10^3 \qquad \text{(Eq. 4-4)}$$

In this equation, $Re$ defined as the Reynolds number. And $\alpha$ is the angle of attack of the firebrand during the transportation. And the Reynolds number for a firebrand is defined as:

$$Re = \frac{\rho_a V_f l}{\mu} \qquad \text{(Eq. 4-5)}$$

In the equation, $\rho_a$ and $\mu$ indicate the density and the dynamic viscosity of the ambient fluid of the firebrand, $V_f$ and $c$ represent the relative velocity and characteristic length (length) of the firebrand. Due to the small size of the firebrand

and relatively high velocity of the firebrand, the firebrand's Reynolds number is varied

around 1000. Then, for the scenario when the Reynolds number is larger than 1000.

Another equation for the drag coefficient is given below:

$$C_D = -0.0283 \left(\frac{\alpha - 45}{26.41}\right)^3 - 0.0407 \left(\frac{\alpha - 45}{26.41}\right)$$
$$+ 0.3717 \left(\frac{\alpha - 45}{26.41}\right) + 0.6886$$

*(Eq. 4-6)*

Figure 4.4 demonstrates the variation of the drag coefficient in relation to the

Reynolds number under a certain angle of attack. It is clear that the larger the angle

of attack, the higher coefficient, which eventually provides a higher aerodynamic drag

force.

It needs to be mentioned that the Figure 4.4 shows a sudden change at the $Re = 1000$.

Physically, $Re = 1000$ could be assumed as the boundary of the turbulence flow,

therefore, the inconsistence of the coefficient is reasonable. Moreover, the figure is

plotted by using two different models. Two of the models are measured the

coefficients separately, which also bring the discontinues to the coefficient. An

interpolation is introduced to weaken the discontinues.
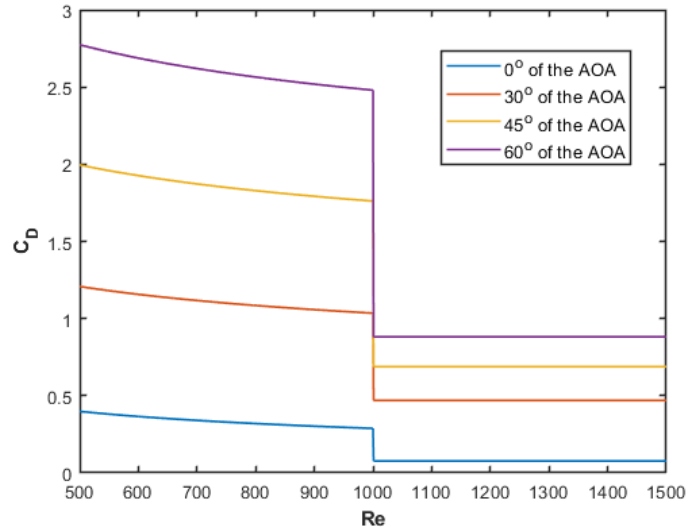
*Figure 4.4. The drag model is being utilized in the calculation. The value of the drag*

*coefficient in relation to the Reynolds number with a certain angle of attack.*

## 4.1.2. Aerodynamic lift

Aerodynamic lift is defined as the force that is perpendicular to the direction of

relative motion. Thus, it is relatively difficult to determine the direction of the

aerodynamic lift. In the two-dimension domain, there will be two possible directions

for any scenario of an object's motion through the flow field.
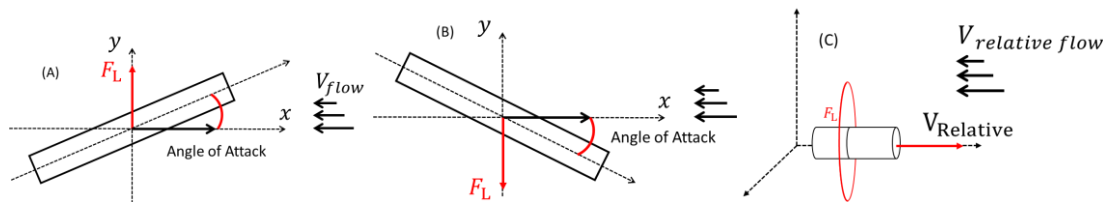


*Figure 4.5. The schematic about the direction of the aerodynamic lift for an object*

*that is moving in a flow field. (A) and (B) represent two conditions. (C) represents in*

*the three-dimensional domain, the aerodynamic lift could point to a plate that is*

*vertical to relative velocity.*

And in a 3D domain, for a certain scenario, the object's aerodynamic lift force's direction could assemble a plate. Therefore, the first step to calculating the aerodynamic lift effect is to determine its direction of it.

To determine the direction of lift force, the normal vector $\vec{n}$ of the firebrand in the plate built by the firebrand's chord $\vec{r}$ and firebrand's relative velocity $\vec{V_r}$ needs to be defined firstly. By using the right-hand rule of cross-production, the normal vector $\vec{n}$ can be given directly as:

$$\vec{n} = \frac{\left(\vec{r} \times \left(\vec{V_r} \times \vec{r}\right)\right)}{\left|\left(\vec{r} \times \left(\vec{V_r} \times \vec{r}\right)\right)\right|} \qquad (Eq.\ 4\text{-}7)$$

And based on the normal vector, an indirect way of measuring the direction of aerodynamic lift will be delivered in the following paragraph.

As mentioned in the previous paragraph, the normal vector is found at the plate built by the firebrand's chord and its relative velocity. Then, the normal vector, chord, and relative velocity are coplanar. It is clear that the force of aerodynamic lift is also on this plate, which is always perpendicular to the relative velocity. Then two potential directions for the aerodynamic lift could be expressed:

$$\vec{n_{F_l}} = \pm \frac{\left(\vec{V_r} \times \left(\vec{V_r} \times \vec{r}\right)\right)}{\left|\left(\vec{V_r} \times \left(\vec{V_r} \times \vec{r}\right)\right)\right|} \qquad (Eq.\ 4\text{-}8)$$

A reference vector is defined as:

$$\overrightarrow{n_{ref}} = \frac{\left(\vec{n} \times (\overrightarrow{V_r} \times \vec{n})\right)}{\left|\left(\vec{n} \times (\overrightarrow{V_r} \times \vec{n})\right)\right|} \qquad \text{(Eq. 4-9)}$$

No matter where the normal vector is pointed, the reference vector will always be at an acute angle with the aerodynamic force's direction. That is to say, by calculating the dot product of the reference vector and potential directions of the aerodynamic lift, the one that makes the dot production's result to be positive will be the correct direction. This indirect method is correct for most situations. A few tests will be provided in the following paragraph.

Since all the vectors are coplanar, the 3D condition could be simplified into 2D calculations. Then A and B in Figure 4.5 covered the majority of the situation. Based on the direction of the normal vector, each situation can be divided into two different scenarios.

The first scenario for situation A will be the normal vector pointing upward. Then the reference vector will be shown in the figure below. Apparently, the angle between the reference vector and aerodynamic lift is acute.
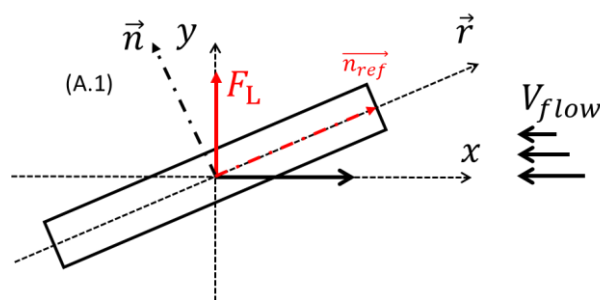


*Figure 4.6. Condition one of the normal vector's directions, of which the lift force is pointed upward. Then calculating the direction of the reference vector.*

The second scenario for situation A will be the normal vector pointing downward.

Then the reference vector will be shown in the figure below. Although the normal vector point in a different direction, the reference vector still point in the same direction. Therefore, the angle between the reference vector and aerodynamic lift is acute.
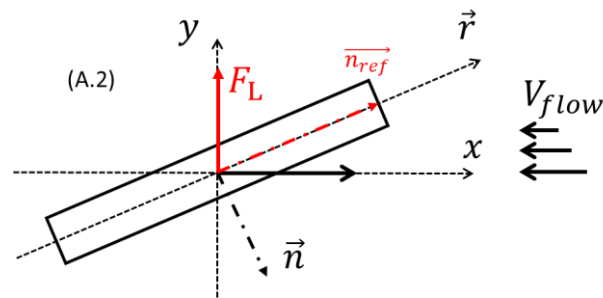


*Figure 4.7. Condition two of the normal vector's directions, of which the lift force is pointed upward. Then calculating the direction of the reference vector.*

Then, for condition B, based on the direction of the normal vector, there are also two scenarios to test this method. The first scenario for condition B is that the normal vector is pointed upward. Then the reference vector will be shown in the figure below. It is clear that the result of dot production with the aerodynamic lift force with the reference vectors will be positive.
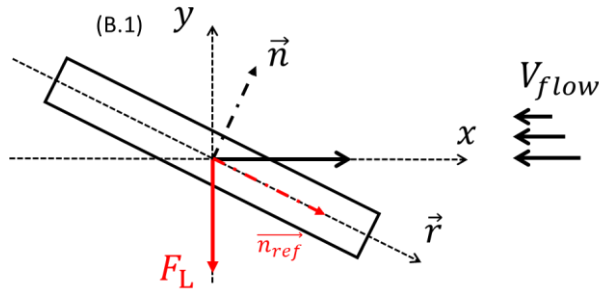
*Figure 4.8. Condition one of the normal vector's directions, of which the lift force is pointed downward. Then calculating the direction of the reference vector.*

For the last scenario, the normal vector is pointing downward. At the same time, the reference vector will be shown in the figure below. Although the normal vector point in a different direction, the reference vector still points in the same direction. Therefore, the angle between the reference vector and aerodynamic lift is acute.
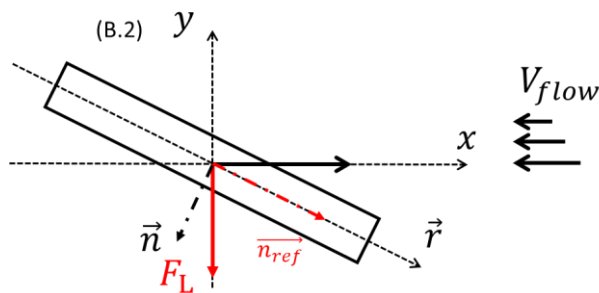


*Figure 4.9. Condition two of the normal vector's directions, of which the lift force is pointed downward. Then calculating the direction of the reference vector.*

There will be two special conditions that cannot be calculated through this method. For the first one is that the relative velocity and firebrand's chord are parallel with each other, of which the angle of attack in such a condition is zero. In that situation, the aerodynamic lift effect could be pointed anywhere that is perpendicular to the relative velocity, and in the experiment, the magnitude of the lift force is quite small.

116

Then in the calculation, the aerodynamic lift is neglected in that condition. For the second condition, the relative velocity and firebrand's chord are perpendicular to each other. Eventually, the reference vector will be perpendicular to all of the potential directions of the lift force. Such a condition is quite similar to the zero angles of attack. Then in the calculation, the aerodynamic lift is neglected in that condition.

The equation for aerodynamic lift is defined by imitating that of the aerodynamic drag [35], then it can be expressed as:

$$F_L = \frac{1}{2} C_l \cdot \rho \cdot V_r^2 \cdot A \qquad \textit{(Eq. 4-10)}$$

In this equation, $F_L$ represents the aerodynamic lift. $C_l$ represents the lift coefficient, which is related to the firebrand's shape, inclination, and flow condition. $V_r$ is the relative velocity of the firebrand to the surrounding flow. $A$ represents the firebrand's area.

It should be pointed out that in the literature review of previous research related to the firebrand transporting model, although there is not as much investigation of the coefficient of lift as that of the drag coefficient, there are still quantities study measuring the drag coefficient experimentally. In this thesis, the firebrand is assumed to be rectangular-plate-like. Therefore, the suitable equation to determine the lift coefficient will be Zastawny[87] and Ortiz's [56], which is presented as:

$$C_L = \left( \frac{b_1}{Re^{b_2}} + \frac{b_3}{Re^{b_4}} \right) [\sin(\alpha)]^{b_5 + b_6 Re^{b_7}} [\cos(\alpha)]^{b_8 - b_9 Re^{b_{10}}} \qquad \textit{(Eq. 4-11)}$$

In this equation, for the shape of rectangular-shaped plate-like objects, $b_1 = 12.112, b_2 = 1.035, b_3 = 3.887, b_4 = 0.109, b_5 = 0.811, b_6 = 0.248, b_7 =$

$-0.198, b_8 = 5.822, b_9 = -4.718, b_{10} = 0.0007.$

Similar to that for the coefficient of aerodynamic drag, the firebrand's Reynolds number is varied around 1000. Then, for the scenario when the Reynolds number is larger than 1000. The relationship of the lift coefficient to the Reynolds number is given below:
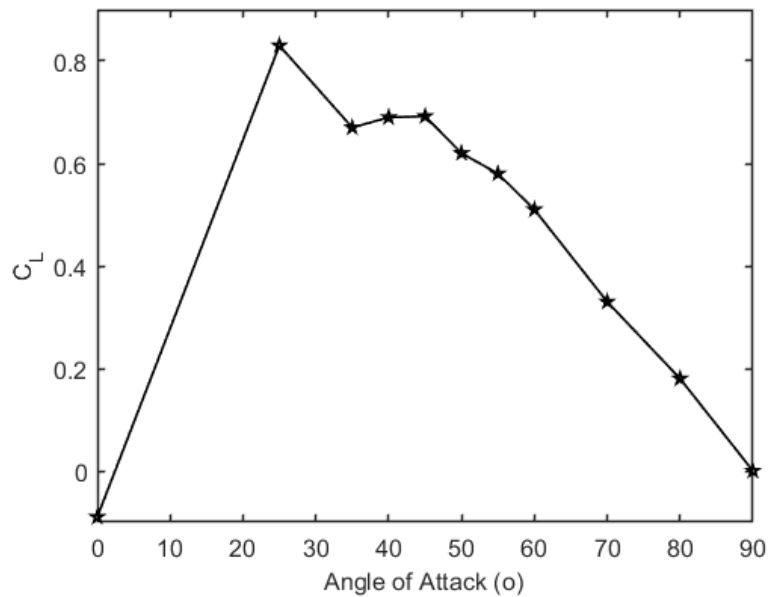


*Figure 4.10. The data about the coefficient of the lift was collected in Zastawny[87]*

*and Ortiz's [56] experiment.*

A second-order interpolation has been applied to the experiment data of the coefficient of aerodynamic lift with respect to the angle of attack. The interpolation will provide a smoother and more detail lift coefficient to calculate the trajectory of the firebrand.
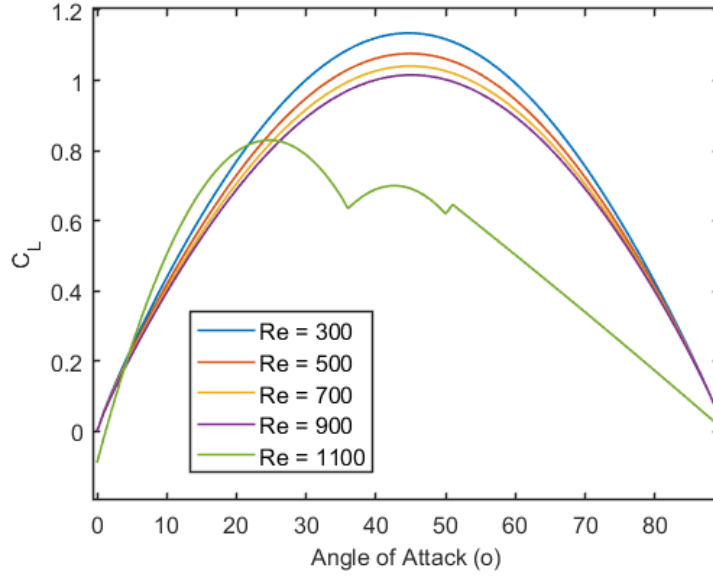
*Figure 4.11. The second-order interpolation of the experimental data was collected from Figure 4.10. This process will provide a much smooth variation in the change in the angle of attack.*

### 4.1.3. Aerodynamic moment for tumbling

Following Himoto's research [29], the moment $M_\alpha$ is defined as the reduction effect from the surrounding flow to the relative spin $\omega_R$. As firebrand cannot rotating forever during transportation. And the moment $M_\alpha$ can be expressed after defining a coefficient of momentum $C_M$ as:

$$M_\alpha = -\frac{1}{2} C_M \cdot A_{ref} \cdot l_{ref} \cdot \rho |V_r|^2 \frac{\omega_R}{|\omega_R|} \qquad \text{(Eq. 4-12)}$$

In this equation, $M_\alpha$ represents the aerodynamic moment. $C_M$ represents the moment coefficient, which is related to the firebrand's shape, inclination, and some flow conditions. $V_r$ is the relative velocity of the firebrand to the surrounding flow. $A_{ref}$ represents the firebrand's reference area, which is the cross-sectional area for

the thesis cases. $\rho$ is the density of the surrounding flow. $\omega_R$ represents the relative rotation with respect to the surrounding flow.

For the real case of firebrand lofting, the size of the firebrand is smaller than the size of the fire whirl in more than one magnitude. Then, for any instant of motion, the rotation of the ambient flow to the firebrand's motion is neglectable. Therefore, the relative angular velocity for the firebrand is the actual angular velocity of the firebrand during transportation.

The moment coefficient is given directly in the publication, which $C_M$ is

$$C_M = min\{0.35|\sin(\alpha)|, 0.14 - 0.23(|\sin(\alpha)| - 0.4)\} \qquad \text{(Eq. 4-13)}$$

## 4.2. Equation of the motion

In the previous section, the aerodynamic forces that are being applied to the firebrand have been introduced in detail. The net forces of firebrand while travelling through a flow field have been given directly. In this section, a detailed discussion about the governing equations of firebrand's trajectories will be provided. Then, a specified semi-theoretical method to solve the differential equations for firebrand's motion will be intruded compared with the numerical method of Runge–Kutta methods.

### 4.2.1. Governing equations about firebrand trajectories

The trajectory of the firebrand in this study is calculated from the deferential equation based on Newton's second law of motion. From the previous section's introduction, the net forces that applied on the firebrand while travelling in a flow field can be written as:

$$F = F_D + F_L + F_G + F_B \qquad \text{(Eq. 4-14)}$$

In the equation, $F_L$ represents aerodynamic lift. Aerodynamic drag is represented by $F_D$, buoyancy is $F_B$, and $F_G$ indicated the gravity that is being applied to the firebrand. Based on Newton's second law of motion, the motion of the firebrand in the calculation can be given as:

$$M \cdot \frac{dV}{dt} = F_D + F_L + F_G + F_B \qquad \text{(Eq. 4-15)}$$

In this equation, $M$ represents the mass of firebrands. And $V$ is the absolute velocity of the firebrand during transportation.

Previously, major forces shown in the motion of firebrand's equation have been introduced. Gravity, together with buoyancy, only contains the vertical impact. Thus, by decomposing the vectors into x, y, and z directions, the previous equation could convert into:

$$M \cdot \frac{dV_x}{dt} = \underbrace{\frac{1}{2} C_d \cdot \rho \cdot A_{ref} \cdot V_r \cdot V_{rx}}_{Drag}$$
$$+ \underbrace{\frac{1}{2} C_l \cdot \rho \cdot V_r^2 \cdot A_{ref} \cdot \left( n_{F_L} \cdot n_x \right)}_{Lift}$$
\qquad \text{(Eq. 4-16)}

$$M \cdot \frac{dV_y}{dt} = \underbrace{\frac{1}{2} C_d \cdot \rho \cdot A_{ref} \cdot V_r \cdot V_{ry}}_{Drag}$$
$$+ \underbrace{\frac{1}{2} C_l \cdot \rho \cdot V_r^2 \cdot A_{ref} \cdot \left( n_{F_L} \cdot n_y \right)}_{Lift}$$
\qquad \text{(Eq. 4-17)}

$$M \cdot \frac{dV_z}{dt} = \underbrace{\frac{1}{2} C_d \cdot \rho \cdot A_{ref} \cdot V_r \cdot V_{rz}}_{Drag}$$

$$+ \underbrace{\frac{1}{2} C_l \cdot \rho \cdot V_r^2 \cdot A_{ref} \cdot (n_{F_L} \cdot n_z)}_{Lift} \quad \text{(Eq. 4-18)}$$

$$+ \underbrace{(\rho_f - \rho_a) \cdot V \cdot g}_{Gravity\ and\ Bouyancy}$$

Since the direction of gravity and buoyancy is vertical only, the x and y direction's equations of motion do not have that term. However, the drag and lift effects are three-dimensional at the same time. Thus, in all three directions of the equations of motion, drag and lift has their own projection. In the following paragraph, the details of the previous decomposition will be demonstrated.

It is known that the equation of magnitude of the drag is given below:

$$F_D = \frac{1}{2} C_d \cdot \rho \cdot V_r^2 \cdot A_c \quad \text{(Eq. 4-19)}$$

In this equation, $F_D$ is the aerodynamic drag. $C_d$ represents the drag coefficient, which depends on the shape of the object and the Reynolds number of the system. $V_r$ is the relative velocity of the firebrand to the surrounding flow. $A_c$ is the firebrand's cross-sectional area.

The drag force is defined as the opposite direction to the relative motion, then the equation of vector force of drag can be written as:

$$\vec{F_D} = -\frac{1}{2} C_d \cdot \rho \cdot V_r^2 \cdot A_c \cdot \frac{\vec{V_r}}{|\vec{V_r}|} \quad \text{(Eq. 4-20)}$$

In the three-dimensional domain, the vector of relative velocity can be expressed by its three axes projection $(V_{rx}, V_{ry}, V_{rz})$. At the same time, the projection of force of

drag could be simplified and expressed as the relative velocity's three axes projection.

$$F_{Dx} = -\frac{1}{2}C_d \cdot \rho \cdot V_r \cdot A_c \cdot V_{rx} \qquad \text{(Eq. 4-21)}$$

$$F_{Dy} = -\frac{1}{2}C_d \cdot \rho \cdot V_r \cdot A_c \cdot V_{ry} \qquad \text{(Eq. 4-22)}$$

$$F_{Dz} = -\frac{1}{2}C_d \cdot \rho \cdot V_r \cdot A_c \cdot V_{rz} \qquad \text{(Eq. 4-23)}$$

And the magnitude of aerodynamic lift is also known as the following equation:

$$F_L = \frac{1}{2}C_l \cdot \rho \cdot V_r^2 \cdot A \qquad \text{(Eq. 4-24)}$$

In this equation, $F_L$ represents the aerodynamic lift. $C_l$ represents the lift coefficient, which is related to the firebrand's shape, inclination, and some flow conditions. $V_r$ is the relative velocity of the firebrand to the surrounding flow. $A$ represents the firebrand's area.

An indirect method for measuring the direction of the aerodynamic lift force is introduced in the previous section, and then the $\overrightarrow{n_{F_l}}$ is calculatable based on the firebrand's chord and relative velocity. The direction of lift force can be written as the three components of its projection to the three axes $(n_{F_{lx}}, n_{F_{ly}}, n_{F_{lz}})$.

The equation of vector aerodynamic lift force can be written as:

$$\overrightarrow{F_L} = \frac{1}{2}C_l \cdot \rho \cdot V_r^2 \cdot A \cdot \overrightarrow{n_{F_l}} \qquad \text{(Eq. 4-25)}$$

And three axes projection of the lift force can be expressed as:

$$F_{Lx} = \frac{1}{2}C_l \cdot \rho \cdot V_r^2 \cdot A \cdot n_{F_{lx}} \qquad \text{(Eq. 4-26)}$$

$$F_{Ly} = \frac{1}{2}C_l \cdot \rho \cdot V_r^2 \cdot A \cdot n_{F_{ly}} \qquad \text{(Eq. 4-27)}$$

$$F_{Ly} = \frac{1}{2}C_l \cdot \rho \cdot V_r^2 \cdot A \cdot n_{F_{ly}}$$

Eventually, the governing equations of firebrand travelling through a flow field could be given.

## 4.2.2. Methods for solving the governing equations

In the previous section, the details of the governing equations have been discussed. By solving the governing equations, the relationship between the relative velocity to the acceleration of the firebrand should be cited clearly from the knowledge of the relative motion of rigid body motion.

$$\overrightarrow{V_{Relative}} = \overrightarrow{V_a} - \overrightarrow{V_{flow}}$$

Then the absolute velocity of the firebrand could be expressed as:

$$\overrightarrow{V_a} = \overrightarrow{V_{Relative}} + \overrightarrow{V_{flow}}$$

And the relationship between a particle's absolute velocity to its acceleration is obvious. Therefore, the solvable governing equation is written as:

$$M \cdot \frac{dV_{ax}}{dt} = \underbrace{\frac{1}{2}C_d \cdot \rho \cdot A_{ref} \cdot \left|\overrightarrow{V_a} - \overrightarrow{V_{flow}}\right| \cdot (V_{ax} - V_{flowx})}_{Drag}$$

$$+ \underbrace{\frac{1}{2}C_l \cdot \rho \cdot (V_a - V_{flow})^2 \cdot A_{ref} \cdot (\overrightarrow{n_{F_L}} \cdot \overrightarrow{n_x})}_{Lift}$$

$$M \cdot \frac{dV_{ay}}{dt} = \underbrace{\frac{1}{2}C_d \cdot \rho \cdot A_{ref} \cdot \left|\overrightarrow{V_a} - \overrightarrow{V_{flow}}\right| \cdot (V_{ay} - V_{flowy})}_{Drag}$$

$$+ \underbrace{\frac{1}{2}C_l \cdot \rho \cdot (V_a - V_{flow})^2 \cdot A_{ref} \cdot (\overrightarrow{n_{F_L}} \cdot \overrightarrow{n_y})}_{Lift}$$

$$M \cdot \frac{dV_{az}}{dt} = \underbrace{\frac{1}{2} C_d \cdot \rho \cdot A_{ref} \cdot \left| \overrightarrow{V_a} - \overrightarrow{V_{flow}} \right| \cdot \left( V_{az} - V_{flowz} \right)}_{Drag} \qquad \text{(Eq. 4-33)}$$

$$+ \underbrace{\frac{1}{2} C_l \cdot \rho \cdot \left( V_a - V_{flow} \right)^2 A_{ref} \cdot \left( \overrightarrow{n_{F_L}} \cdot \overrightarrow{n_z} \right)}_{Lift}$$

$$+ \underbrace{\left( \rho_f - \rho_a \right) \cdot V \cdot g}_{Gravity \ and \ Bouyancy}$$

The governing equations are not able to find the theoretical solution. Then the Runge–Kutta method is the simplest and most basic approach to solve it. In MATLAB, there is already a commercial function called 'ODE45' to solve the differential equation by the four[th] and fif[th] order of the Runge-Kutta method.

However, a semi-theoretical approach could also be utilized to solve this type of equation. This method converts the non-linear differential governing equations into a linear differential equation. In this semi-theoretical approach, an approximation is introduced that the term $\left| \overrightarrow{V_a} - \overrightarrow{V_{flow}} \right|$ is not changing during a short period of time. The axis direction vector $(n_x, n_y, n_z)$ needs an additional transformation to simplify the equation, which is being expressed as:

$$(n_x, n_y, n_z) = \left( \frac{\overrightarrow{V_{rx}}}{\left| \overrightarrow{V_{rx}} \right|}, \frac{\overrightarrow{V_{ry}}}{\left| \overrightarrow{V_{ry}} \right|}, \frac{\overrightarrow{V_{rz}}}{\left| \overrightarrow{V_{rz}} \right|} \right) \qquad \text{(Eq. 4-34)}$$

Then the lift effect's equation could be expressed as:

$$F_{Lx} = \frac{1}{2} C_l \cdot \rho \cdot \left( \left| \overrightarrow{V_a} - \overrightarrow{V_{flow}} \right| \right)^2 \cdot A_{ref} \cdot \left( \overrightarrow{n_{F_L}} \cdot \frac{\overrightarrow{V_{rx}}}{\left| \overrightarrow{V_{rx}} \right|} \right) \qquad \text{(Eq. 4-35)}$$

$$F_{Ly} = \frac{1}{2} C_l \cdot \rho \cdot \left( \left| \overrightarrow{V_a} - \overrightarrow{V_{flow}} \right| \right)^2 \cdot A_{ref} \cdot \left( \overrightarrow{n_{F_L}} \cdot \frac{\overrightarrow{V_{ry}}}{\left| \overrightarrow{V_{ry}} \right|} \right) \qquad \text{(Eq. 4-36)}$$

$$F_{Lz} = \frac{1}{2} C_l \cdot \rho \cdot \left( \left| \vec{V_a} - \vec{V_{flow}} \right| \right)^2 \cdot A_{ref} \cdot \left( \vec{n_{F_L}} \cdot \frac{\vec{V_{rz}}}{\left| \vec{V_{rz}} \right|} \right) \qquad \text{(Eq. 4-37)}$$

Then the governing equations could be transformed into the linearized form, which could be expressed as:

$$M \cdot \frac{dV_{ax}}{dt} = \alpha \left( V_{ax} - V_{flowx} \right) + \beta_x \cdot \left( V_{ax} - V_{flowx} \right) \qquad \text{(Eq. 4-38)}$$

$$M \cdot \frac{dV_{ay}}{dt} = \alpha \left( V_{ay} - V_{flowy} \right) + \beta_y \cdot \left( V_{ay} - V_{flowy} \right) \qquad \text{(Eq. 4-39)}$$

$$M \cdot \frac{dV_{az}}{dt} = \alpha \left( V_{az} - V_{flowz} \right) + \beta_z \cdot \left( V_{az} - V_{flowz} \right) \qquad \text{(Eq. 4-40)}$$

$$+ \underbrace{\left( \rho_f - \rho_a \right) \cdot V \cdot g}_{\textbf{\textit{Gravity and Bouyancy}}}$$

$$\alpha = \frac{1}{2} C_d \cdot \rho \cdot A_{ref} \cdot \left| \vec{V_a} - \vec{V_{flow}} \right| \qquad \text{(Eq. 4-41)}$$

$$\beta_x = \frac{1}{2} C_l \cdot \rho \cdot \left( \left| \vec{V_a} - \vec{V_{flow}} \right| \right)^2 \cdot A_{ref} \cdot \frac{\vec{n_{F_L}}}{\left| \vec{V_{rx}} \right|} \cdot \vec{n_x} \qquad \text{(Eq. 4-42)}$$

$$\beta_y = \frac{1}{2} C_l \cdot \rho \cdot \left( \left| \vec{V_a} - \vec{V_{flow}} \right| \right)^2 \cdot A_{ref} \cdot \frac{\vec{n_{F_L}}}{\left| \vec{V_{ry}} \right|} \cdot \vec{n_y} \qquad \text{(Eq. 4-43)}$$

$$\beta_z = \frac{1}{2} C_l \cdot \rho \cdot \left( \left| \vec{V_a} - \vec{V_{flow}} \right| \right)^2 \cdot A_{ref} \cdot \frac{\vec{n_{F_L}}}{\left| \vec{V_{rz}} \right|} \cdot \vec{n_z} \qquad \text{(Eq. 4-44)}$$

Assuming the flow field's velocity is not changing over a short duration, the theoretical solution of x direction of transformed equations could be given directly as:

$$M \cdot \frac{dV_{ax}}{dt} = \left( \alpha + \beta_x \right) \left( V_{ax} - V_{flowx} \right) \qquad \text{(Eq. 4-45)}$$

$$\frac{dV_{ax}}{\left( V_{ax} - V_{flowx} \right)} = \frac{\alpha + \beta_x}{M} \qquad \text{(Eq. 4-46)}$$

$$V_{ax} = V_{flowx} + Ce^{\frac{\alpha + \beta_x}{M} t} \qquad \text{(Eq. 4-47)}$$

When $t = 0$, the initial condition should be

$$C = \left(V_{ax0} - V_{flowx}\right) \qquad\qquad \text{(Eq. 4-48)}$$

And similarly, for the Y direction and the Z direction

$$V_{ay} = V_{flowy} + \left(V_{ay0} - V_{flowy}\right)e^{\frac{\alpha + \beta_y}{M}t} \qquad\qquad \text{(Eq. 4-49)}$$

$$V_{az} = V_{flowz} + \frac{\left(\rho_f - \rho_a\right) \cdot V \cdot g}{(\alpha + \beta_z) \cdot M}$$

$$+ \left(V_{az0} - V_{flowz}\right. \qquad\qquad \text{(Eq. 4-50)}$$

$$\left. - \frac{\left(\rho_f - \rho_a\right) \cdot V \cdot g}{(\alpha + \beta_z) \cdot M}\right) e^{\frac{\alpha + \beta_z}{M}t}$$

Both these two methods are solvable for firebrand's direction. However, for a continued flow field, the second method will be better. In contrast, the simplest ODE45 method is more suitable for discrete flow fields.

A simplest 2D scenario test case has been utilized to compare the two methods' performance. The flow field is set to be 2 m/s horizontal wind, and the firebrand is released at 50 m above the ground with 1 m/s vertical velocity downward.
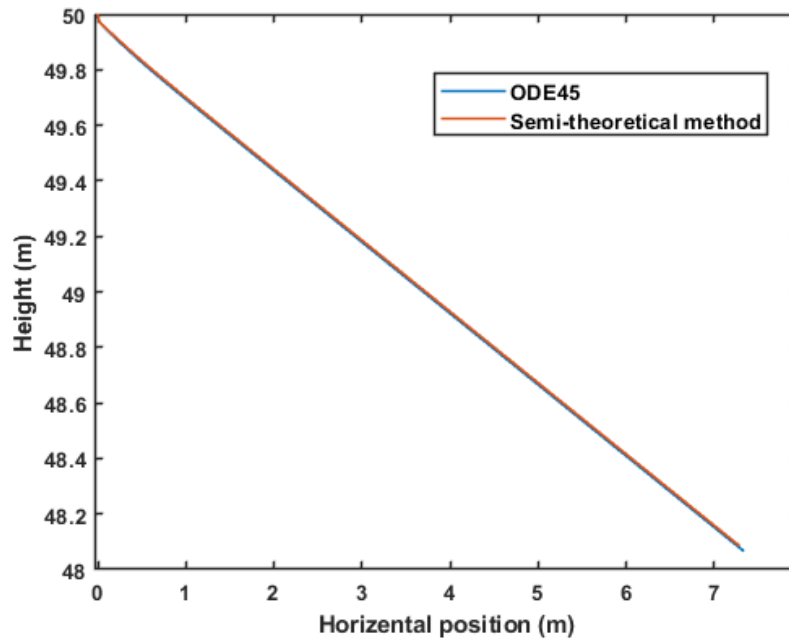
*Figure 4.12. The comparison of the solution of the test case was obtained from the traditional ODE 45 numerical method and the brand-new semi-theoretical method. It is clear that the results of these two methods are quite similar to each other.*

In the comparison of the two methods, it is clear that both of the methods could solve the governing equations and provide a reliable prediction about the firebrand's trajectory. However, each method got its own advantage. In the case that the fluid field varies significantly, the approximation applied to the semi-theoretical approach might not fit the real situation. Then, the fully numerical method will be the only option. However, for other cases, the semi-theoretical method obtains a higher efficiency. Therefore, deciding the method that is being utilized to solve the equation should be determined case by case.

## 4.3. Equation of the burning effect

In the previous few sections, the aerodynamic details of firebrand transporting in the

flow field have been introduced. The dominant flow field's effect and aerodynamic forces that are exerted on a firebrand have been focused on. After that, a brand new semi-theoretical method of solving the firebrand's governing equations was introduced. Its performance against the traditional numerical ODE method has been compared directly. However, one of the key factors for a firebrand has been neglected, which is its combustion effect. For long-distance horizontal travelling modelling about firebrands, the previous researcher built various types of models to quantify the impact of the combustion on the firebrand's motion. Some of the models are focused on the weight loss effect, while others investigate the relationship between the shape change with the combustion procedure.

The main objective of this thesis is to study the lofting mechanism of a firebrand. It is clear that the lofting stage's period is relatively short compared with its horizontal transportation. In such a short lofting time, the firebrand's shape won't change significantly. Therefore, only the weight loss effect has been considered in this thesis. The most general burning model from Tarifa [11] was applied o the modelling of the firebrand's lofting mechanism. This model is also known as the d-squared law. And the mass loss can be written as:

$$\frac{d(D_{eff}^2)}{dt} = -\beta \qquad \text{(Eq. 4-51)}$$

where the $\beta$ is the dimensionless coefficient of burning and $D_{eff}^2$ is the square of the effective mass diameter of firebrands.

The effective mass diameter of the firebrand for Tarifa's experiment could be expressed as follows：

$$D_{eff} = \left(\frac{6m_p}{\rho_{p,0}\,\pi}\right)^{1/3} \qquad \textit{(Eq. 4-52)}$$

Later research approximated $\beta$ by the modified burning constant as a function of the

Reynolds number and Prandtl number.

$$\beta = \beta_0 \cdot \left(1 + 0.276 \cdot Re^{\frac{1}{2}} \cdot Pr^{\frac{1}{3}}\right) \qquad \textit{(Eq. 4-53)}$$

where the $\beta_0$ was found to be 1.8×10-7.

And the Prandtl number is defined as the ratio of momentum diffusivity to thermal

diffusivity, which is given by:

$$Pr = \frac{\upsilon}{\alpha} = \frac{c_p \mu}{k} \qquad \textit{(Eq. 4-54)}$$

In this equation, $\upsilon$ indicates the momentum diffusivity. Thermal diffusivity is

expressed by $\alpha$. $c_p$ is the specific heat capacity. $\mu$ represents the dynamic viscosity.

And $k$ is the thermal conductivity.

Following the d-squared law, a combustion model for disk-shaped wooden particles

developed by Anthenien [8] was developed in 2006, which can be expressed as:

$$\frac{dm}{dt} = -\frac{\pi}{4} \cdot \tau \cdot \beta_0 \cdot \rho \cdot \left(1 + 0.276 \cdot Re^{\frac{1}{2}} \cdot Pr^{\frac{1}{3}}\right) \qquad \textit{(Eq. 4-55)}$$

$\tau$ represents the thickness of a rectangular-shaped firebrand.

And this model has been utilized in the model investigating the firebrand's lofting

mechanism within the flow field.

The Prandtl number for air is around 0.71. Assuming the Reynolds number is 1000,

Then the d-squared law can be expressed as

$$\frac{dm}{dt} = 5.136 \times 10^{-4}$$

(Eq. 4-56)

And for various thicknesses of the rectangular-shaped firebrand with respect to different Reynolds numbers.
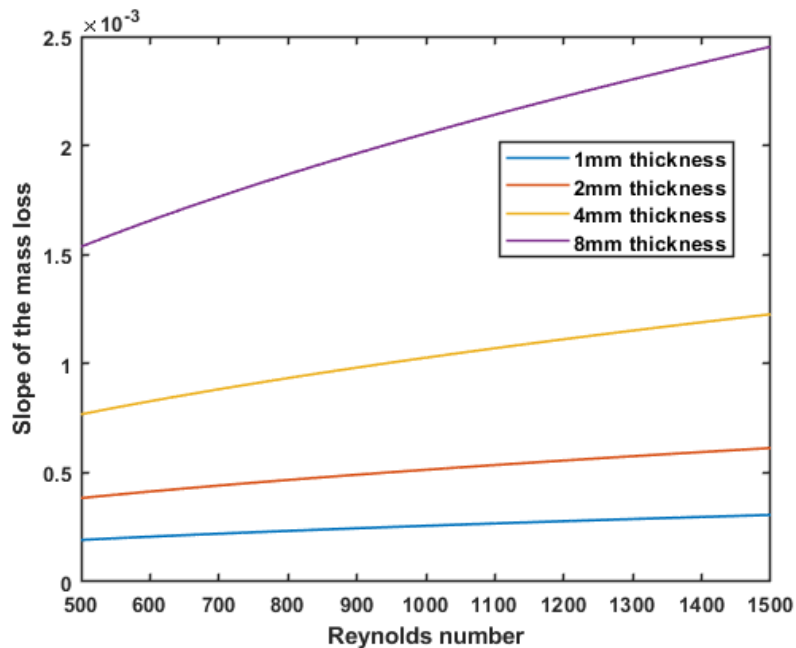


*Figure 4.13. The mass loss rate for different Reynolds numbers with different thicknesses about the rectangular-shaped firebrand during the combustion.*

The Figure shows that the mass loss rate is positively related to the thickness of the disk-shaped firebrand and also positively relative to the Reynolds number. Whatsmore, the thicker the firebrand, the more sensitive the Reynolds number affects the mass loss rate. No matter which combination, the mass loss rate with respect to time is still very low, which the magnitude of it is around $1 \times 10^{-3}$.

In this chapter, the modelling of firebrands' trajectory has been introduced in detail. The aerodynamic forces that are being applied to firebrand during its transportation

were first discussed. A brand-new indirect method of measuring the direction of aerodynamic lift has been introduced. Then, the governing equations for firebrand have been provided together with its transformation from the original Newton's Second law. After that, a brand new semi-theoretical method was introduced. Moreover, the comparison between the new method and the traditional Runge–Kutta method has been listed. Finally, the mass loss model that is being applied to the model has been introduced. In the next chapter, the physical-based firebrand transportation model has been utilized to predict the lofting of a firebrand within a simulated fire whirl. In addition, a brief validation has been placed between the simulated fire whirl to the LES result introduced in the previous chapter.

# 5. Firebrand behaviour in a simulated 3D fire whirl

In the previous chapter, a detail introduction about the physics of firebrand's transportation in a flow has been placed. Further, the governing equation generated from the physics has been derived directly, including several modifications so that the previous equations are solvable numerically and semi-theoretically.

Thus, based on the model introduced in the previous chapter, the comparisons of various models will be placed in this chapter to study the impact of each aerodynamic force. The numerical calculations about the firebrand trajectory are based on a simulated fire whirl. The difference between various models' trajectories about the firebrand indicated that some of the aerodynamic forces are quite important to the lofting mechanism, while some of the impacts are neglectable.

The first section will introduce an open-sourced software of Fire Dynamic Simulator (FDS), which is being utilized to calculate the flow field of a fire whirl.

## 5.1. Introduction about the simulated 3D fire whirl

In this section, the basic features of FDS and the existing studying of using FDS to simulate the fire whirl will be discussed.

FDS is a computational fluid dynamics model of fire-driven fluid flow [43][10]. In such modelling, the motion of a fluid can be described by a set of partial differential equations, which are called Navier-Stokes equations. Such equations consist of three parts, which are the conservation of mass, conservation of momentum and conservation of energy.

The equation of conservation of mass is also called continuity equations, which could be written as:

$$\frac{\partial \rho}{\partial t} + \frac{\partial \rho u}{\partial x} + \frac{\partial \rho v}{\partial y} + \frac{\partial \rho w}{\partial z} = 0 \qquad \text{(Eq. 5-1)}$$

In the equation, $\rho$ is the density of the equation, $u, v, w$ are the three axes' projections of the fluid's velocity.

The equation of conservation of momentum could be written as [54] :

$$\rho \frac{Du}{Dt} = \nabla \cdot \sigma + \rho f \qquad \text{(Eq. 5-2)}$$

In the equation, $u$ is the flow velocity vector. $\sigma$ is the stress tenor. $f$ is the vector considering the body forces. The general form of the stress tenor could be written as:

$$\sigma = \begin{bmatrix} \sigma_{xx} & \tau_{xy} & t_{xz} \\ t_{yx} & \sigma_{yy} & t_{yz} \\ t_{zx} & t_{zy} & \sigma_{zz} \end{bmatrix} \qquad \text{(Eq. 5-3)}$$

The conservation of energy is also required to be considered to make the Navier-Stokes equations solvable.

There are also important approximations that FDS applied to the original form of Navier-Stokes equations, which are low speed and low Mach number approximation.

That approximation decomposed the pressure $p$ into a background pressure $\bar{p}(z,t)$, plus a perturbation pressure $\tilde{p}(x,y,z,t)$.  And the background pressure is calculated by the ideal gas law [54], as:

$$\bar{p} = \rho TR \sum_{\alpha} \frac{z_{\alpha}}{W_{\alpha}} \qquad \text{(Eq. 5-4)}$$

In this equation, $z_{\alpha}$ is the mass fraction of a certain reaction species in the calculation.

$W_\alpha$ is the molar mass of that species.

The purpose of such a low Mach number approximation is that the temperature and density are inversely proportional to each other. It also has a few consequences. For the first consequence, the sound waves are filtered out, as the sound waves are travelled much faster than the fire's flow field. Another consequence is that the number of dependent variables in the system is reduced by one.

For the turbulence model, both Large Eddy Simulation (LES) and Direct Numerical Simulation (DNS) are used in FDS. The DNS method calculates instances, for instance, of all the physical processes of turbulence [54]. As the turbulence are not steady and chaotic, it usually takes a larger computing capacity and requires a finer mesh. The LES is a technique that only simulates the big scale's turbulence and uses the model to evaluate the effect of small scales on the big scales.

The LES method is carried out in four conceptual steps:

1. Defined a filter operator $G$. It filtered out the small scales of the velocity from big scales velocity by the following integration.

$$\tilde{u}(x,y) = G[u(x,y)] = \iint u(\tau,\varphi)G(x-\tau,y-\varphi)d\tau d\varphi \qquad \text{(Eq. 5-5)}$$

In the equation, $u$ is the original velocity of the fluid, $\tilde{u}$ is the filtered velocity of the fluid, and $G$ is the filter convolution kernel.

2. Applied the filter operation to the Navier-Stoke equations and obtained the filtered equations.

3. Modelling the Sub-Grid-Stress.

4. Solving the equation numerically.

135

For FDS, the convolution kernel is a box filter, which could calculate the quantities

means in a box.

$$\tilde{u}(x,y) = G[u(x,y)] = \int\int_{x-\frac{\delta x}{2},y-\frac{\delta x}{2}}^{x+\frac{\delta x}{2},y+\frac{\delta x}{2}} u(\tau,\varphi)d\tau d\varphi \qquad \text{(Eq. 5-6)}$$

Then the Navier-Stoke equations could be written as:

$$\frac{D\widetilde{\rho u}}{Dt} = \nabla \cdot \tilde{\sigma} + \widetilde{\rho f} \qquad \text{(Eq. 5-7)}$$

And the sub-grid scale stress is defined as:

$$\tau_{ij}^{sgs} = \rho(\widetilde{u_i u_j} - \widetilde{u_i}\widetilde{u_j}) \qquad \text{(Eq. 5-8)}$$

Therefore, the sub-grid scale stress tensor is:

$$\sigma^{sgs} = \begin{bmatrix} \rho(\widetilde{uu} - \tilde{u}\tilde{u}) & \rho(\widetilde{uv} - \tilde{u}\tilde{v}) & \rho(\widetilde{uw} - \tilde{u}\tilde{w}) \\ \rho(\widetilde{vu} - \tilde{v}\tilde{u}) & \rho(\widetilde{vv} - \tilde{v}\tilde{v}) & \rho(\widetilde{vw} - \tilde{v}\tilde{w}) \\ \rho(\widetilde{wu} - \tilde{w}\tilde{u}) & \rho(\widetilde{wv} - \tilde{w}\tilde{v}) & \rho(\widetilde{ww} - \tilde{w}\tilde{w}) \end{bmatrix} \qquad \text{(Eq. 5-9)}$$

Then the equation of conservation of momentum could be written as:

$$\frac{D\widetilde{\rho u}}{Dt} = \nabla \cdot \tilde{\sigma} + \nabla \cdot \sigma^{sgs} + \widetilde{\rho f} \qquad \text{(Eq. 5-10)}$$

Based on Newton's law of viscosity, the stress tensor could be written as:

$$\sigma = \begin{bmatrix} -2\mu\left(\frac{du}{dx}\right)+\frac{2}{3}\mu\nabla\cdot u & -\mu\left(\frac{dv}{dx}+\frac{du}{dy}\right) & -\mu\left(\frac{dw}{dx}+\frac{du}{dz}\right) \\ -\mu\left(\frac{dv}{dx}+\frac{du}{dy}\right) & -2\mu\left(\frac{dv}{dy}\right)+\frac{2}{3}\mu\nabla\cdot u & -\mu\left(\frac{dw}{dy}+\frac{dv}{dz}\right) \\ -\mu\left(\frac{dw}{dx}+\frac{du}{dz}\right) & -\mu\left(\frac{dw}{dy}+\frac{dv}{dz}\right) & -2\mu\left(\frac{dw}{dz}\right)+\frac{2}{3}\mu\nabla\cdot u \end{bmatrix} \qquad \text{(Eq. 5-11)}$$

The sub-grid-scale stress should also follow Newton's law of viscosity, and then the

overall stress tensor $\sigma^{oa}$ should be the same form as the stress tensor $\sigma$.

And then the original conservation of momentum will transform into:

$$\frac{D\widetilde{\rho}\widetilde{u}}{Dt} = \nabla \cdot \sigma^{oa} + \widetilde{\rho f} \qquad \text{(Eq. 5-12)}$$

A few sub-gride-scale turbulence models have been applied in FDS, such as the constant coefficient Smagorinsky model [66], the Dynamic Smagorinsky model [55], and Deardorff's model [15]. The default model is Deardorff's model, which is also the one that is being utilized in the fire whirl's flow field simulation.

Deardorff's model [15] assumes that

$$\mu_{sgs} = \rho C_V \Delta \sqrt{k_{sgs}} \qquad \text{(Eq. 5-13)}$$

$$k_{sgs} = \frac{1}{2}\left(\left(\overline{u} - \widehat{\overline{u}}\right)^2 + \left(\overline{v} - \widehat{\overline{v}}\right)^2 + \left(\overline{w} - \widehat{\overline{w}}\right)^2\right) \qquad \text{(Eq. 5-14)}$$

In the equation, $C_V = 0.1$. $\overline{u}$ is the average value of $u$ at the grid cell centre, in which $u$ represents the filtered velocity). $\widehat{\overline{u}}$ is a weighted average of $u$ at the grid cell centre as:

$$\overline{u_{ijk}} = \frac{u_{ijk} + u_{i-1jk}}{2} \ , \widehat{\overline{u_{ijk}}} = \frac{\overline{u_{ijk}}}{2} + \frac{\overline{u_{i-1jk}} + \overline{u_{i+1jk}}}{4} \qquad \text{(Eq. 5-15)}$$

There are two combustion models in FDS, which are the mixture fraction model and the finite-rate approach. In the finite-rate approach, FDS calculate each process of reaction individually. Thus, it will require a large amount of computational time. As the only required output from FDS is the flow field from a fire whirl, the mixture fraction model, as the default method, is utilized in the simulation.

The mixture faction method is based on the lumped species, which is a group of primitive species from the simple reaction. Take the methane as an example then the mass fraction of lumped species vector should be written as:

$$Y = \left[Y_{CH_4}, Y_{O_2}, Y_{N_2}, Y_{CO_2}, Y_{H_2o}\right]^T \qquad \text{(Eq. 5-16)}$$

$Y$ indicated the mass fraction of a certain species.

And in the reaction, the change in fuel is calculated based on the limiting reactant:

$$\Delta Y = -\min\left(Y_F, Y_\alpha \frac{v_F W_F}{v_\alpha W_\alpha}\right) \qquad \text{(Eq. 5-17)}$$

Other models, such as the radiation model also included in the FDS. However, as the main objective of this thesis is to study the firebrand's lofting mechanism, the other details about FDS are just neglected.

## 5.2. The Flow field of a Simulated fire whirl

There is a long history of using FDS to simulate a wildland fire. The first version of FDS was published in February 2000. Since then, FDS has been utilized as a tool to calculate the flow field in a huge amount of publications related to wildland and urban fire.

Therefore, in this thesis, the FDS will be utilized to calculate the flow field of a fire whirl. The scale of the simulated fire whirl is set to be the same as the one being utilized in the third chapter's experiment. Two transparent half-cylinder walls, which are 30 cm in height, 20 cm in diameter, and 2mm in thickness, were arranged to generate the fire whirl. The domain size was 0.275m ×0.275m ×0.8m with a grid resolution of 60 ×60 ×150 in x, y, and z directions. Moreover, the fuel pool is set to be 50 mm in diameter, which is also the same as the one that is being utilized in the PIV experiment. The built-in liquid ethanol was utilized in the experiment. All in all, the setup in the simulation is absolutely the same as that of the experimental.

The LES simulation results are transient, which is suitable for the experimental

observation that the phenomenon of fire whirl is not a static state.
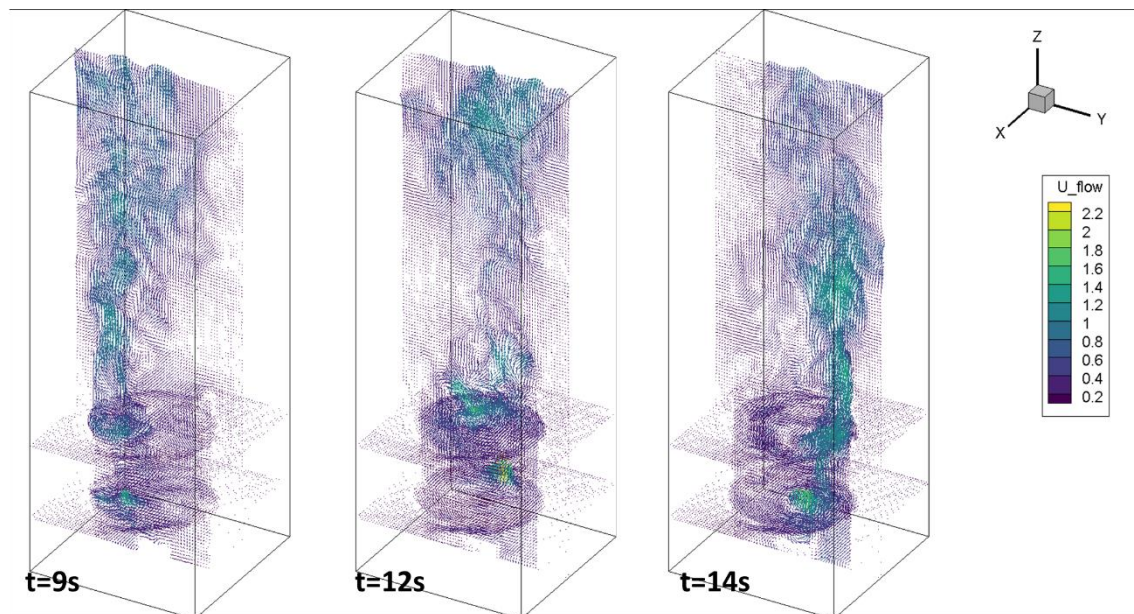


*Figure 5.1. The time slice about the flow field was calculated by Fire Dynamic Simulator for t=9s, 12s, and 14s. The centre of the fire whirl keeps rotating during the combustion.*

From the Figure, it is clear that the core of the fire whirl keeps rotating during the calculation. Based on the PIV result, the highest velocity only occurs around the centre zone of the fire whirl, while the vertical velocities for the result area of the fire whirls are able to be neglected. Then a compromise has to be made that we only take an instant flow field of the fire whirl to calculate the fire whirl. It is true that this compromise will ignore the fire whirls varying over time. However, such a compromise will significantly improve the speed of calculation for firebrand's trajectory. Since multiple models and multiple parameters will be investigated in this numerical study, improving the speed of calculation will increase the efficiency of the studying significantly.

Then a brief comparison between the PIV results and the FDS simulated velocity field. As the central core of the fire whirl is to keep rotation from both experimental PIV results and FDS simulation velocity field, a manually pairing process was undertaken to find the group of the result that could be utilized to make the comparison.
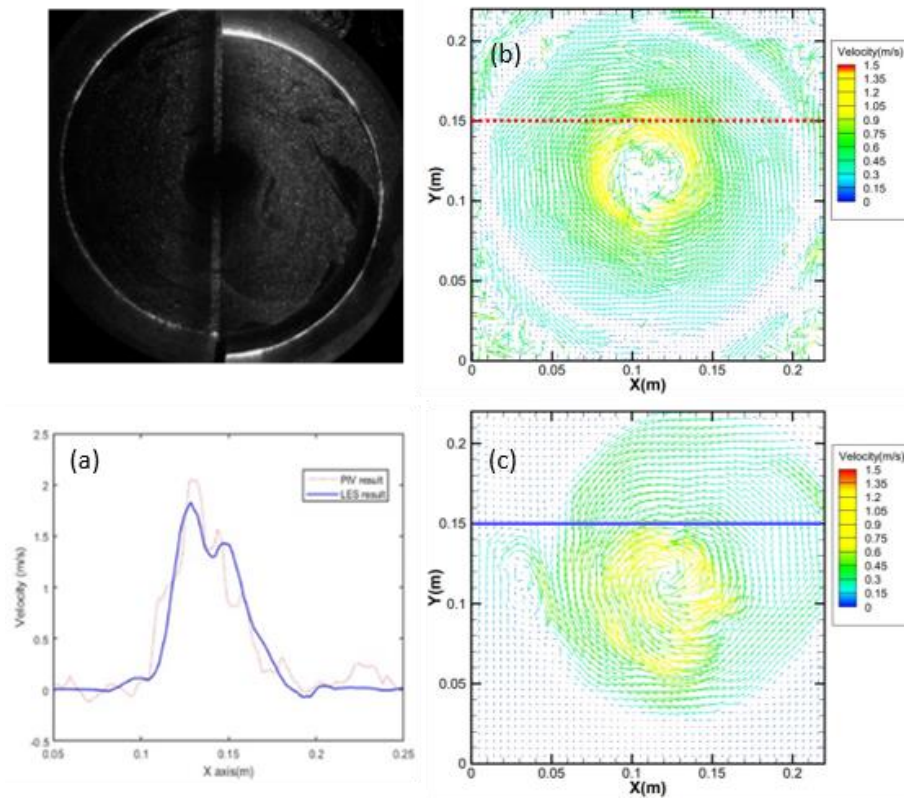


*Figure 5.2. (a) The comparison of a line of the data above the centre zone of the fire whirl between the PIV collected data (b) and numerical solution flow filed (c).*

As the horizontal view position of the PIV experiment's laser sheet is above the pool 130 mm, the data slice for the simulated velocity field was also taken 130mm above the fire pool. Considering the central core's velocity for the PIV result is unreliable due to the limited number of the tracing particle suspended in that region, the comparison data should be manually picked. For the two-dimension data slices from PIV and FDS results, the line of data just above the central was chosen. In that line of data, the

central's velocity is relative hight, whereas the boundary's velocity is approaching zero.

And the result shows a great similarity with each other, which could be evidence that the flow field simulated by FDS could be utilized in the investigation of a firebrand's lofting mechanism in a fire whirl.

In this section, the transient flow field for the fire whirl has been calculated. However, as the main objective of this thesis is to study the firebrand's lofting mechanism, the change of the fire whirl's core will significantly affect the simulated solution. In the following chapter, only one instant of the flow field will be utilized to calculate the trajectory of the firebrand.

In the following few sections, a number of models and parameters will be provided to study the detailed physics of the firebrand's lofting mechanism in a simulated fire whirl.

## 5.3. Investigation of the firebrand's lofting mechanism

In the previous section, a validated fire whirl's flow field was introduced. Then in this section, a series of studies of the firebrand's lofting mechanism will be placed by using the simulated flow field. The instance velocity field that contains the maximum vertical velocity will be utilized to calculate the trajectory of the firebrand.

The series study contains the study of aerodynamic forces' impact on the firebrand's lofting mechanism, the burning model to the impact of the firebrand's lofting behaviour, and the free tumbling's effect on the firebrand's lofting. For each of the studying groups, a series of the initial angle of inclined will be studied to get a more general conclusion.
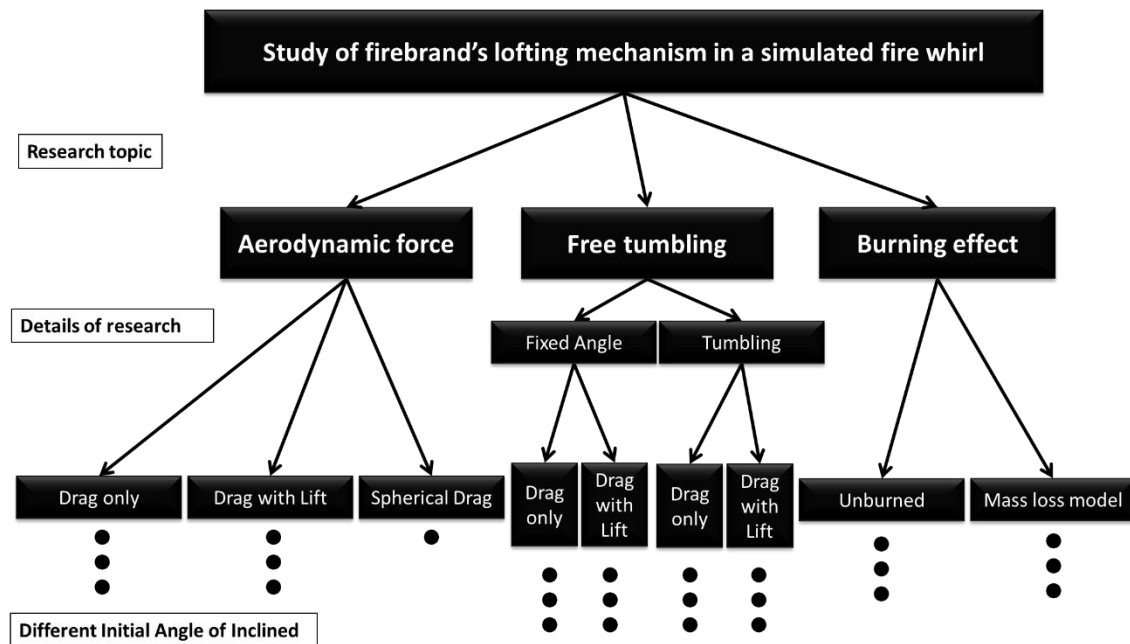
*Figure 5.3. the structure and logic of the parametric investigation of the firebrand's lofting mechanism with a different model that included different details.*

The first study topic for the lofting mechanism for the firebrand in a fire whirl will be the aerodynamic forces exerted on it.

## 5.3.1. Aerodynamic forces

From the Fourth chapter's introduction, the main forces that apply to the firebrand's motion in a flow field are aerodynamic drag and aerodynamic lift. From the analysis of the flow field for the fire whirl, another conclusion could be given clearly, that the aerodynamic drag force is the dominant effect to the lofting of the firebrand, as the vertical velocity in the core zone of the firebrand is significantly larger than the horizontal velocity. The definition of the aerodynamic drag force is always opposite to the relative velocity, while the aerodynamic lift force is always perpendicular to the relative velocity. Then if a firebrand would like to be lofted by a flow field, the drag force will be related to its ambient flow's vertical velocity, and the lift force will be

related to the ambient flow's horizontal velocity. Thus, drag should be the dominant effect of the lofting.

In this section, a detailed analysis of the aerodynamic forces' impact on a firebrand's lofting performance under a simulated fire whirl's flow field will be placed. From the analysis of the magnitude of forces, two models for firebrand's lofting will be introduced, which are drag only model and the lift and drag model.

For the drag-only model, the net force for a firebrand going through a flow field could be summarized as:

$$F = F_D + F_G + F_B \qquad \text{(Eq. 5-18)}$$

And the drag with life effect model, the net force could be given as:

$$F = F_D + F_L + F_G + F_B \qquad \text{(Eq. 5-19)}$$

All the details about the included forces are introduced in the previous chapter of this thesis. A brief comparison between the two models has been provided below. The instant flow field simulated from the FDS that contains the maximum vertical velocity was chosen to calculate the lofting of the firebrand, as a strong vertical velocity usually connects to a strong trend of being lofted. The initial position of the firebrand is also set at the maximum vertical velocity position for the same reason.
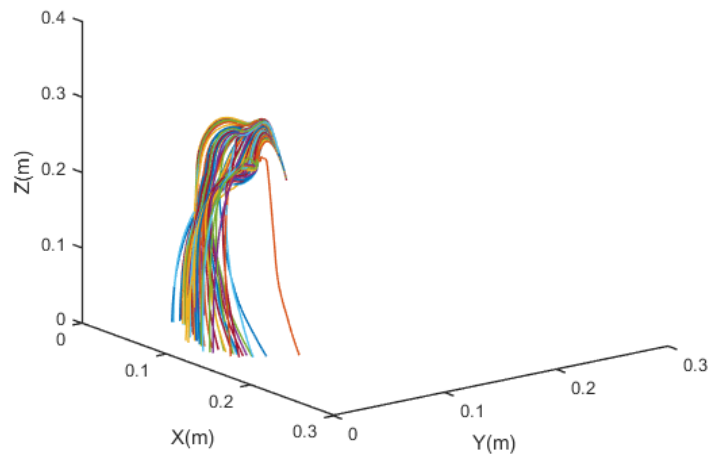
*Figure 5.4. The trajectory of the firebrand's motion in the fire whirl only considers the*

*aerodynamic drag effect.*

Figure 5.4 shows the result of the firebrand's trajectories of the drag-only model. And each line in that figure shows the trajectory of a fixed initial inclined angle. Further analysis of the relationship between the initial angle of the inclined and the trajectory will be provided in the following paragraphs. Currently, a qualitative comparison between the two models will be placed.
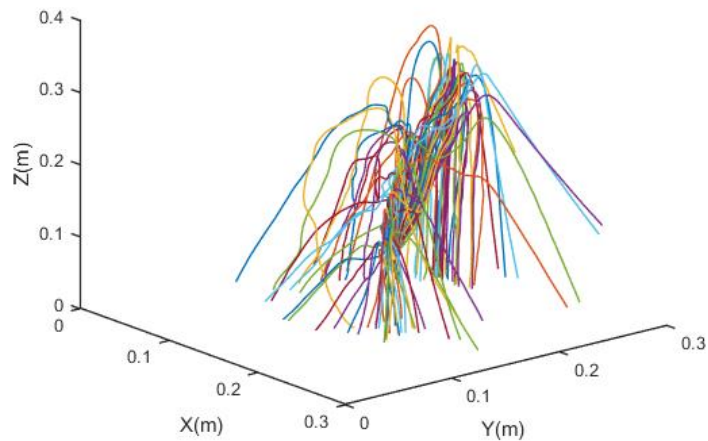
*Figure 5.5. The trajectory of the firebrand's motion in the flow field considers the*

*aerodynamic drag and lift effect.*

Figure 5.5 shows the result of the firebrand's trajectories of the drag-with-lift model. Each line shown in the figure represented the trajectory of a certain initial angle of inclination. By direct comparison between the two model's performance, the two models' result of firebrand's lofting within a certain flow field varied significantly in many aspects. The maximum lofting heights and landing positions from the two model's results are totally different. The sensitivity of the angle of incline for these two models is also not quite similar to each other.
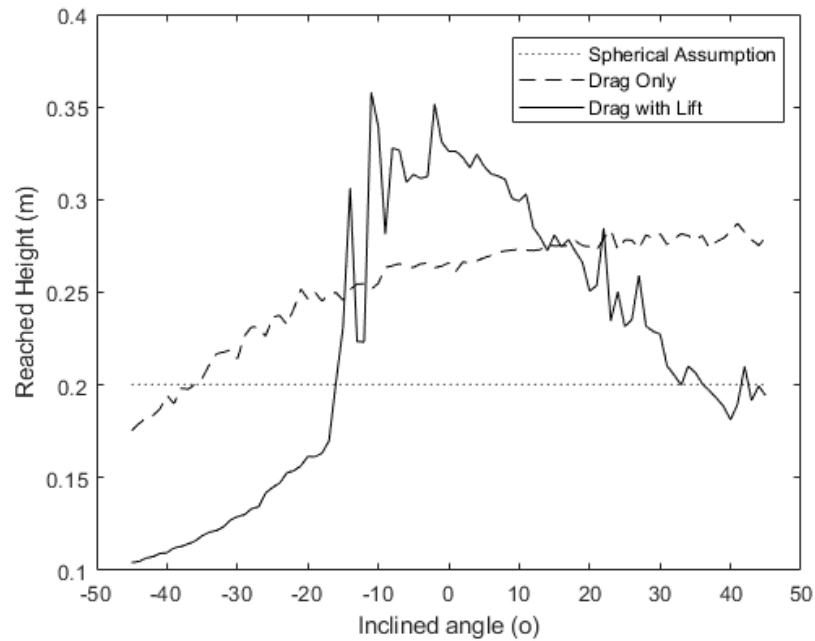
*Figure 5.6. The maximum reachable height for the drag-only model, drag with-lift*

*model, and spherical assumption model with different inclined angles.*

The main objective of this thesis is to study the lofting mechanism of the firebrand in fire whirls. Therefore, studying the firebrand's maximum lofting height will be one of the aspects of studying the firebrand's lofting mechanism. Then, by collecting each line of the firebrand's trajectory's maximum reachable height, the Figure could be plotted. By qualitatively analysing the firebrand's lofting model in a certain fire whirl's flow field, it is clear that the two model's performances are quite different. In order to study the performance of the lofting mechanism, the model with the spherical assumption is also introduced to benchmark the two other two models.

In the spherical assumption, the lift force of the firebrand is neglected. Therefore, the drag force for the firebrand going through a flow field could be written as:

$$F_D = \frac{1}{2} C_d \cdot \rho \cdot V_r^2 \cdot A_c$$

146

In this equation, $F_D$ is the aerodynamic drag. $C_d$ represents the drag coefficient, which is assumed to be 1.4 in any condition during the firebrand's transportation. $V_r$ is the relative velocity of the firebrand to the surrounding flow. $A_c$ is the firebrand's cross-sectional area.

Comparing the maximum reachable height for drag only model and the spherical assumption model, then it is known that the rectangular plate-like assumption will increase the trend of lofting in most of the scenarios. For a relatively large negative angle of inclination, the maximum lofting height might be decreased.

Comparing the maximum reachable height for drag with the lift model and drag-only model, then it is known that the aerodynamic force of lift is not always a positive factor for the lofting performance of the firebrand. Within a relatively narrow range of inclined angles, from -10º to 10º, the maximum reachable height for drag with lift model will be larger than that of the drag-only model. While at the other situation, the aerodynamic lift effect will be a negative factor in the lofting of the firebrand.
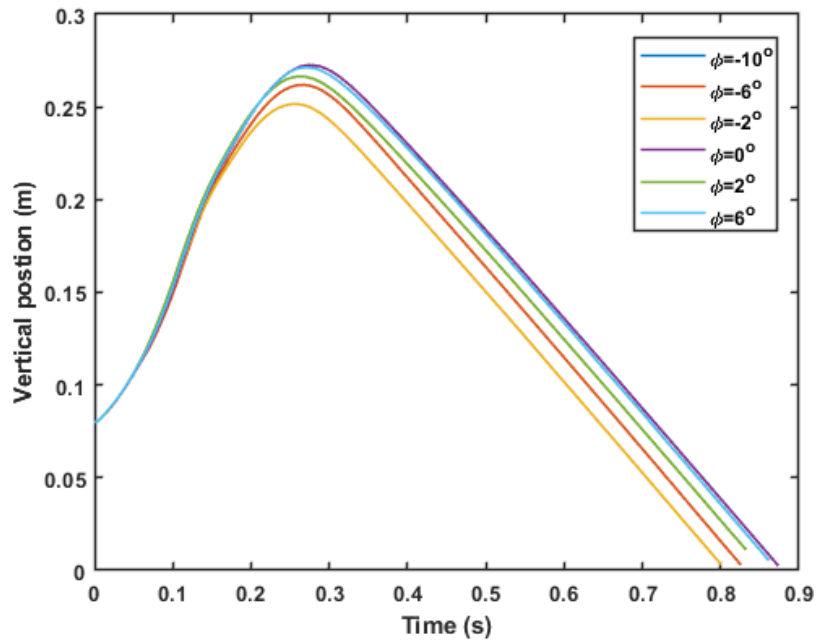
*Figure 5.7. A detail presentation about the firebrand's vertical position's change with respect to the time in the flow field for the drag-only model.*

Figure 5.7 shows the firebrand's vertical position's variation with respect to time during the firebrand's transportation for the drag-only model. Each line represents a specific inclined angle for the firebrand. It is clear that the variation between the line to lines is relatively small. There are only limited changes in the firebrand's vertical position's motion with respect to time from the angle of inclination of -10° to 6°. Considering that after 0.3 seconds' motion, the firebrand is already moved out of the core zone of the fire whirl. The firebrand's lofting is only sensitive to the change of angle of inclined limitedly.

148
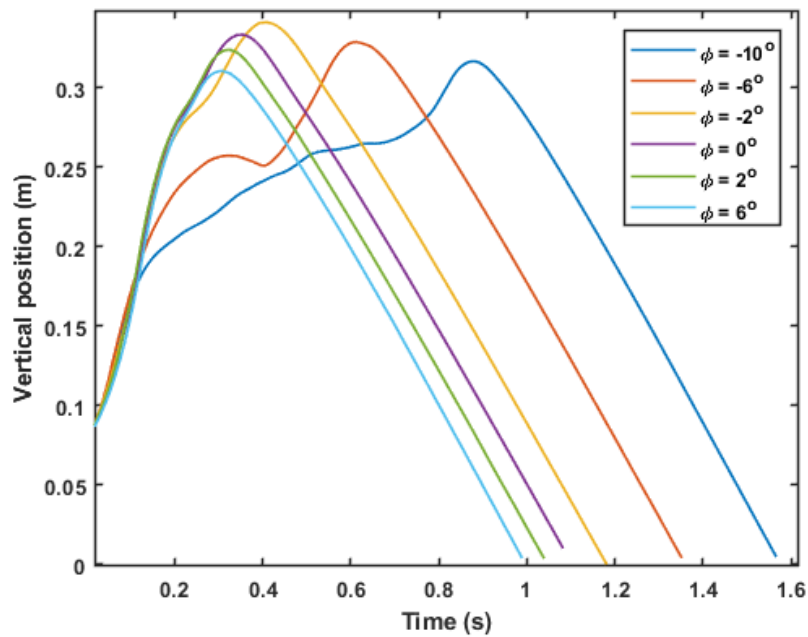
*Figure 5.8. A detail presentation about the firebrand's vertical position's change with respect to the time in the flow field for the drag with lift model.*

Figure 5.8 shows the firebrand's vertical position's variation with respect to time during the firebrand's transportation for the drag with lift model. Each line in the figure indicates a specific angle of inclination for the firebrand. From the observation, in the falling stage for the transpiration, which indicates after the firebrand reach around 0.35m, the performances of the firebrands are quite similar to each other as the firebrand moves out of the core zone of the fire whirl. In the lofting stage, which indicates that before the firebrand reaches its highest position, the firebrand's performance for the drag with lift model is relatively sensitive to the variation of the angle of inclination compared with the darg-only model.

In the previous paragraph, the comparison of drag only model with the drag and lift

149

model proves that it is impossible to neglect the impact of the aerodynamic lift effect while studying the lofting mechanism for the firebrand in a fire whirl. Then, in the following chapter, the magnitude of the aerodynamic lift will be investigated qualitatively.
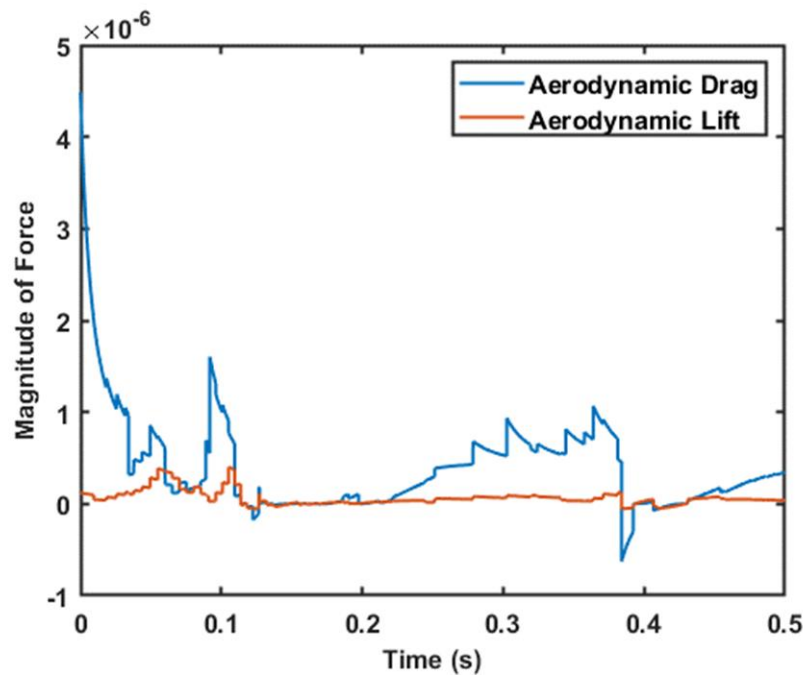


*Figure 5.9. The variation in the magnitude of aerodynamic drag and aerodynamic lift during the transportation of the firebrand with the* $-4°$ *of the initial angle of inclination.*

The figure shows the comparison of the magnitude of aerodynamic drag and aerodynamic lift during the transportation of the firebrand with the $-4°$ of the initial angle of inclination. It is clear that in most of the conditions, the magnitude of aerodynamic drag is larger than that of the aerodynamic lift. However, in order to compare the magnitude of these two forces, A logarithmic scale figure needs to be plotted.
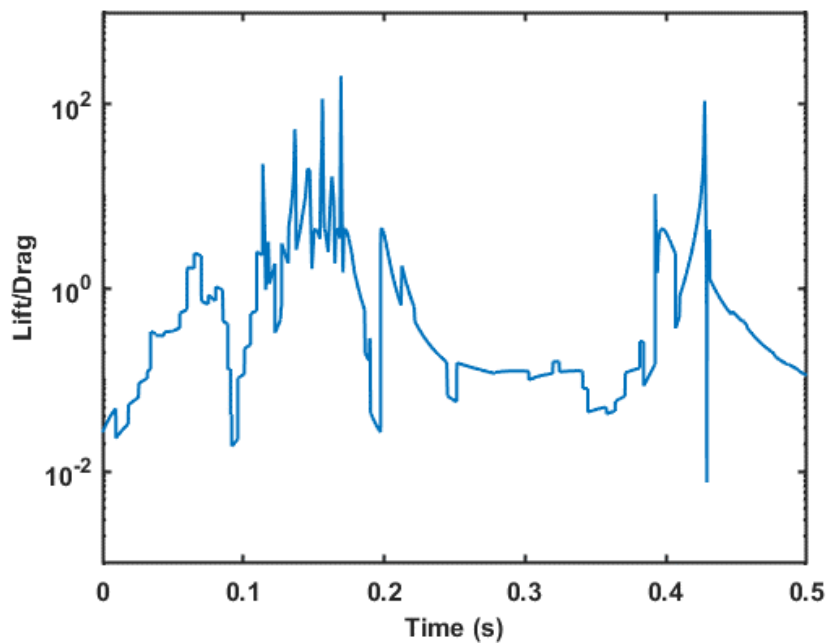
*Figure 5.10. The ratio of the magnitude of aerodynamic drag to aerodynamic lift during the transportation of the firebrand with the $-4°$ of the initial angle of inclination.*

In this figure, it is clear that the lift-to-drag ratio is mostly round 1. That is to say, the magnitude of drag to the lift in the lofting of a firebrand in a fire whirl is similar to each other, which proves the point that it is not able to neglect the aerodynamic lift while calculating the firebrand lofting in a fire whirl.

## 5.3.2. Tumbling effect

In the previous chapter, the aerodynamic forces that affect the firebrand's lofting have been analysed. However, due to the analyse of the firebrand's transporting model, the aerodynamic forces are not the only effect of the ambient flow on the firebrand's motion. The aerodynamic momentum should also be studied. Therefore, in this

section, the aerodynamic momentum, which is related to the firebrand's tumbling, will be introduced and studied in detail with the two models that being introduced in the previous section, which are the model that considered both aerodynamic lift and drag and the model only consider the aerodynamic darg.

One thing for the tumbling effect in the current model is quite limited, and qualitative observation of the difference between the model that considers the tumbling effect that neglect the tumbling effect is non-sense. The variation of the trajectories is almost able to be neglected. Then, in this section, only the quantitative comparison between the model neglecting the tumbling effect with the model that considers the tumbling effect will be undertaken.

Two groups of comparison will be made. For the first one, the model that considers the drag-with-lift effect will be utilized to study the impact of the tumbling effect.
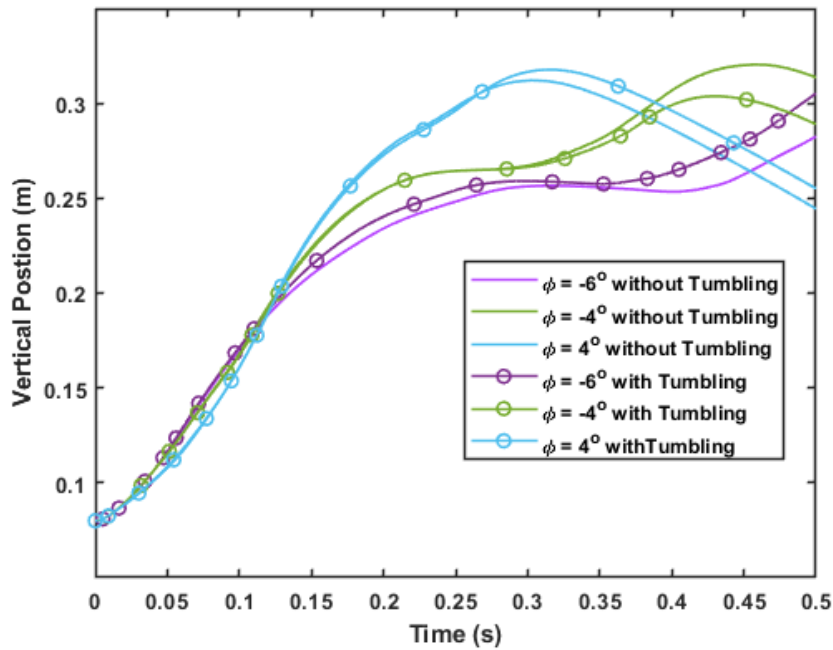
*Figure 5.11. A detail presentation about the firebrand's vertical position's change with respect to the time in the flow field for the existence of the tumbling effect based on the drag with lift model.*

The figure shows that although the tumbling effect does affect the performance of the lofting model that considers the aerodynamic drag and lift, the variation of the trajectory between the one considering the tumbling with those neglecting the tumbling is limited. The main reason is that the current model for the aerodynamic moment is not that accurate. As the Figure shows, the angle of inclination is only varied and limited. Therefore, the force will only vary limited, which eventually proves that the trajectory will not change sharply while taking the current tumbling model into account.
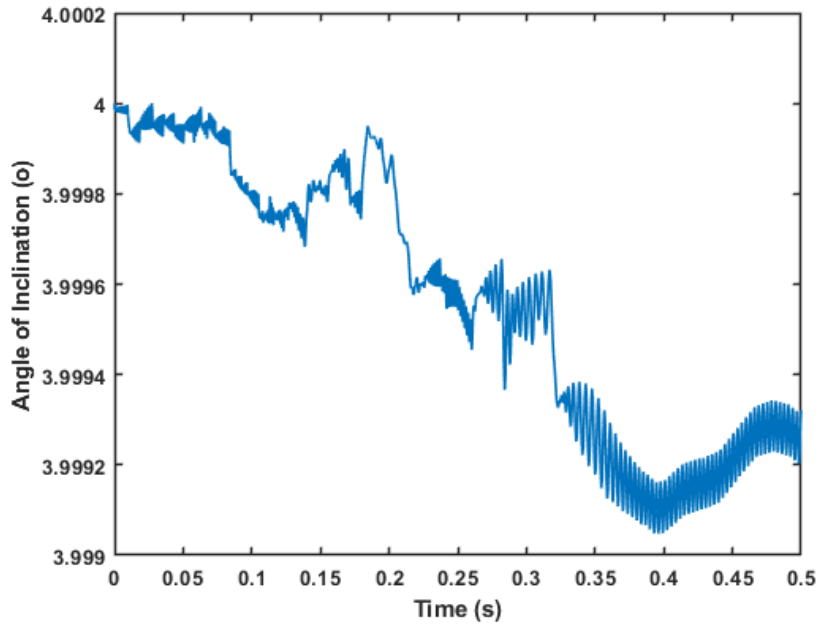
*Figure 5.12. The variation about the angle of inclination with respect to time for the*

*firebrand with an initial angle of 4⁰ based on drag with lift model.*

The Figure shows that with the $4^o$ of the initial inclined angle, during the transportation, the change of the angle of inclination is with in 1 per mill. It is true that such variation affects the lofting of the firebrand to some extent. However, such impact is relatively small compared to the impact of introducing the lift effect to the drag-only model demonstrated in the previous section.
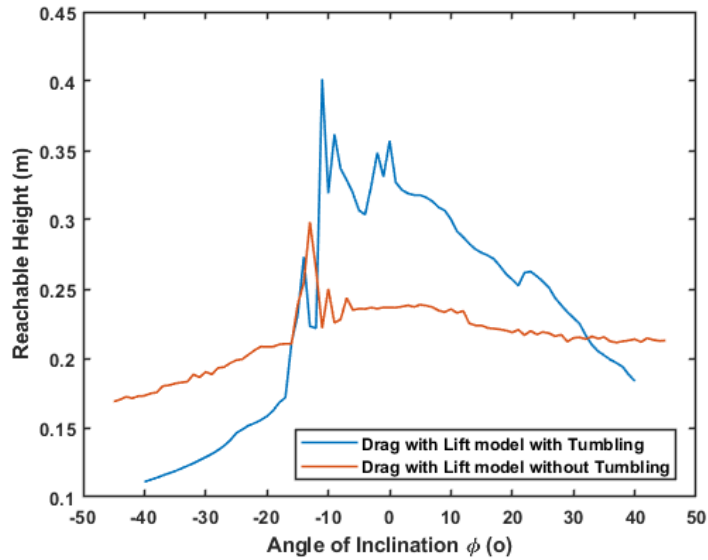
*Figure 5.13. The comparison of the maximum reachable height with different initial angles of inclination for drag with lift model with and without tumbling effect.*

By collecting all of the initial angles of inclination for the calculation in the drag-with-lift model with the paring group that considers the tumbling effect, the Figure could be given. From this Figure 5.13, the impact of the tumbling effect is obvious. However, the basic shape of the trend is not varied. The tumbling effect is not always a positive factor. In the range of the angle of inclination from -10° to 40°, the tumbling model's maximum reachable height is higher than that without the tumbling effect. While for other cases, the tumbling model might take a negative effect.

The second comparison will be applied to the model that only considers the drag effect. From the first comparison being applied to the model that considers drag with lift, it is clear that the current tumbling model will only affect the lofting in a limited magnitude. The second comparison is going to focus on the aerodynamic lift effect to the tumbling effect of firebrand's lofting in a fire whirl's flow field.

155
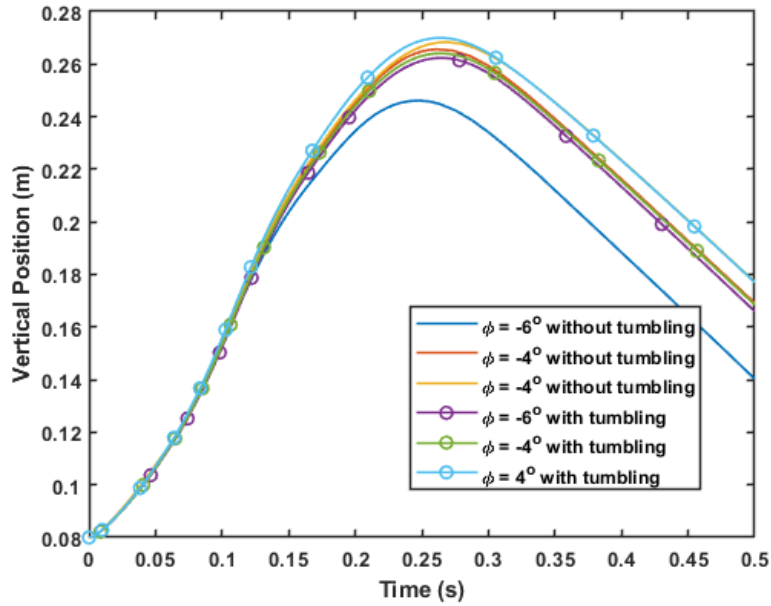
*Figure 5.14. A detail presentation about the firebrand's vertical position's change*

*with respect to the time in the flow field for the existence of the tumbling effect*

*based on the drag-only model.*

The figure's result indicates that for the model that only considers the drag, the impact of taking tumbling into account will be relatively weaker compared to that of the model of drag with lift. This could be explained by the magnitude of the sensitivity of drag and lift to the angle difference. The aerodynamic lift is more sensitive to the angle than the aerodynamic drag. Therefore, the model that only considers the drag will be less sensitive to the tumbling effect.
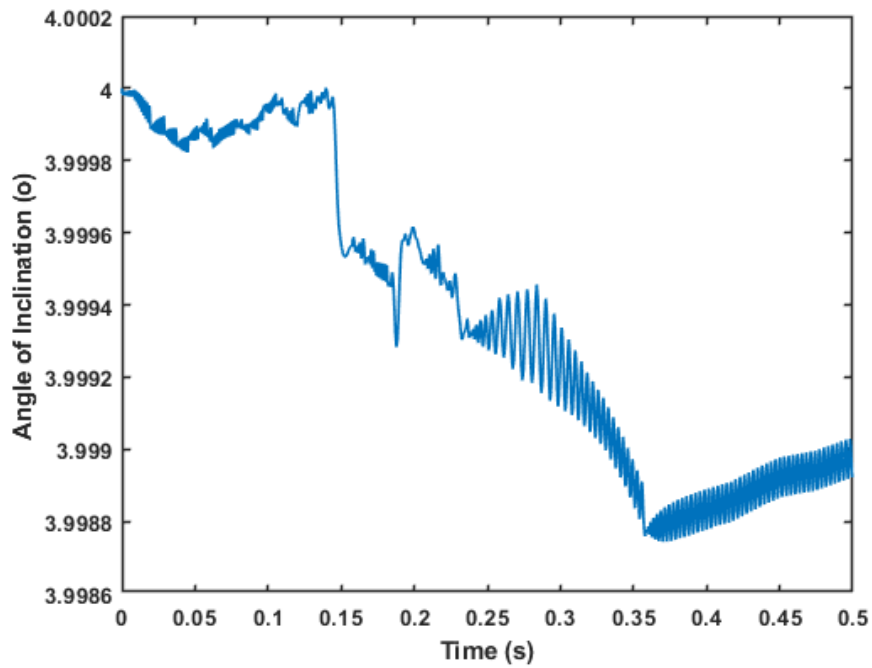
*Figure 5.15. The variation in the angle of inclination with respect to time for the firebrand with an initial angle of $4^O$ is based on drag only a model.*

Figure 5.15 shows that the variation of the angle of inclination for the model that only considers the drag effect is similar to that of the model considering both drag and lift effect, which indicates that the change of angle is not related to which model it calculated with.
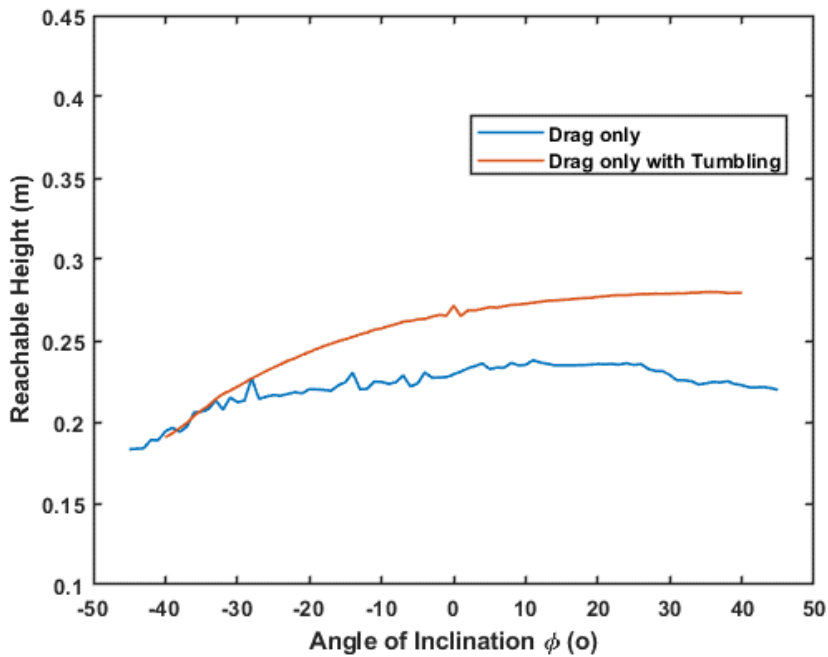
*Figure 5.16. The comparison of the maximum reachable height with different initial angles of inclination for the drag-only model with and without the tumbling effect.*

By collecting all of the initial angles of inclination for the calculation in the drag-only model with the paring group that considers the tumbling effect, Figure 5.16 could be given. From this figure, the trend of drag only model with the tumbling effect's maximum reachable height is linear related to the angle of inclination. The larger the angle of inclination, the higher the maximum reachable height becomes, compared to the result that not considering the tumbling effect.

## 5.3.3. Mass losing effect

From the analysis in the fourth chapter, it is known that the impact of mass loss effect on the short period of time firebrand's transportation, such as firebrand's lofting, is limited. Then in this section, only the details study of the mass losing effect on the firebrand's lofting will undertake.

158

From Newton's Second law, it is known that the acceleration will be inversed proportional to the mass for a fixed net force. Then the impact of the mass loss effect will not relate to any aerodynamic forces. Only the governing equations themselves were affected by the loss of mass. Thus, there is no need to study the multiple models with respect to the mass loss effect. Therefore, only the model that considered both aerodynamic drag and aerodynamic lift would be utilized to study the mass loss effect.
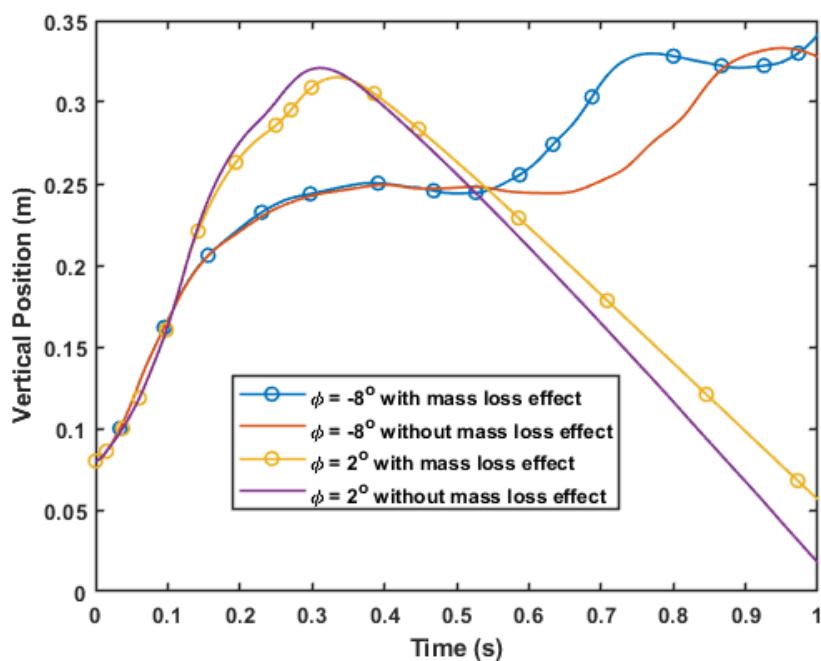


*Figure 5.17. A detail presentation about the firebrand's vertical position's change with respect to the time in the flow field for mass loss effect based on the drag with lift model.*

The figure shows the change of trajectory of the firebrand before and after considering the mass loss effect. It is clear that at the beginning, the mass loss effect is limited. At the beginning of lofting, the line on considering the mass loss effect and the line that does not consider the mass loss effect is covered by each other. As time goes by, the firebrand becomes lighter due to the combustion's mass loss effect, and the

159

acceleration of the firebrand is increased due to the lower mass of the firebrand. Then, the line considering the mass loss effect tends to be above the line that neglects the mass loss effect.
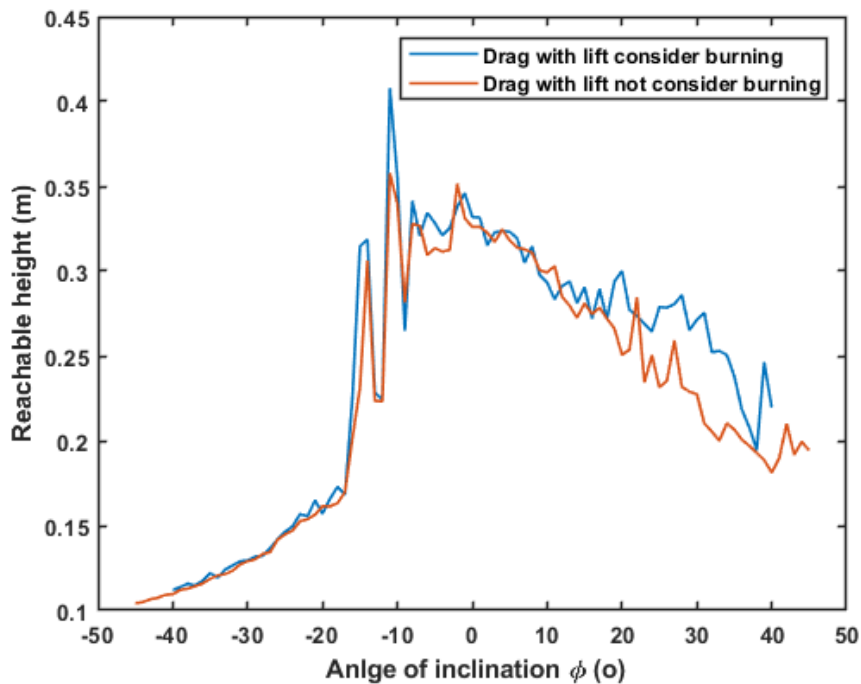


*Figure 5.18. The comparison of the maximum reachable height with a different initial angle of inclination for drag with lift model with and without mass loss effect.*

Also, by collecting the maximum reachable height for every angel of inclination of $[-45, 45^o]$, the figure could be plotted. In the figure, a comparison of the maximum reachable height for the drag-with-lift model that considers the mass loss effect to the model for drag-with-lift that does not consider the mass loss effect has been placed. Due to a lighter firebrand from the mass loss effect, the maximum reachable height tends to be higher in most cases. But in certain cases, the mass loss effect will negatively affect the maximum reachable height. That is because the lighter firebrand will obtain a higher acceleration under the same net forces, no matter which direction.

Thus, if the net force is pointed downward, then a lighter firebrand will obtain a higher acceleration that points downward. From the previous analysis, it is clear that the aerodynamic lift force is not always a positive factor in the firebrand's lofting. Then in the situation that the aerodynamic lift effect is a negative factor to the firebrand's lofting, the mass loss effect will enhance the such negative effect.

# 6. Conclusions and findings

In the thesis, based on different aspects of the investigation of the firebrand's lofting mechanism, the conclusions could be summarized in two sections, the experimental study of the firebrand lofting mechanism and the numerical study of the firebrand's lofting mechanism.

## 6.1. Experimental study of lofting mechanism

In this part, a brand-new experimental setup that investigates the firebrand's lofting mechanism is developed, including a new scaler parameter that describes the destruction of a certain type of firebrand. After then, it also did some investigation by using the Particle Image velocimetry (PIV) technique.

From the experiment of the firebrand lofting mechanism, it is found that:

1.  The fire whirl has a significant additional impact on the firebrand's lofting mechanism.

2.  The additional effect is positively related to the aspect ratio of the firebrand.

3.  The cross-section area of the firebrand sample is also positively related to that additional effect.

4.  From the analysis of the experimental result, it is pointed out that the aerodynamic lift might be the reason for that additional impact.

And from the PIV result of the flow field test for fire whirl. A group of flow field properties for fire whirl is also given, which are related to the fire whirl's additional impact on the firebrand's lofting mechanism. The properties are:

162

1. The central zone of the fire whirl contains the highest vertical velocity and horizontal velocity.

2. The central zone's vertical velocity is higher than the horizontal velocity by more than one magnitude.

3. The residual zone of the fire whirl generator's vertical velocity could be assumed to be 0, while the horizontal velocity could not.

## 6.2. Numerical study of lofting mechanism

In the numerical study of the firebrand's lofting mechanism, a brand-new model has been introduced to predict the firebrand's lofting mechanism, together with a brand-new semi-theoretical approach to solving the governing equation. A brand-new indirect method to measure the direction of aerodynamic forces in a three-dimensional axis has also been discussed. Then the firebrand lofting model was utilized in a simulated fire whirl calculated by LES simulated-based software FDS. A group of the model has been introduced to study the firebrand's lofting mechanism qualitatively and quantitatively in a fire whirl.

From the comparison of the aerodynamic forces, it is found that:

1. The aerodynamic effect is not able to be neglected for the firebrand lofting mechanism in a fire whirl.

2. The model that considered the aerodynamic lift and aerodynamic drag at the same time is more sensitive to the change of angle of inclination.

3. The more complicated models are not always increasing the maximum reachable height for a firebrand in a certain flow field.

4. For a relatively large negative inclined angle of a rectangular plate-like firebrand, $\varphi < -40^o$, the spherical assumption model will obtain a larger maximum reachable height.

5. The aerodynamic lift effect will be positively affected to increase the maximum reachable height only in the range of $[-10^o, 10^o]$

6. The magnitude of the aerodynamic lift force is usually less than that of the aerodynamic drag, but they are in the same magnitude.

For the investigation of the tumbling effect, it is found that:

1. The current aerodynamic momentum model only affects the firebrand's lofting in a limited magnitude.

2. The model that considered both aerodynamic drags and lifts is more sensitive to the introduction of the tumbling effect than that of the drag-only model.

3. The variation of the inclined angle is not affected by which models to use in the calculation of the firebrand's trajectory.

4. The tumbling effect might not always be a positive impact.

For the study of the mass loss effect of the firebrand, it is found that:

1. In a relatively short period of time transportation of firebrand's motion, the mass loss effect is not obvious.

2. The model that considered the mass loss effect usually obtains a larger maximum reachable height compared to those that do not take the mass loss effect into account.

# 7. Future work

Based on the conclusion and finding from this thesis, future work could be considered into two aspects, the experimental study of the firebrand lofting mechanism and the numerical study of the firebrand's lofting mechanism.

## 7.1. Experimental studying

As discussed in the previous paragraph, the experiment is fully based on one type of material of the sample of the firebrand. Only one size of the fire whirl generator was utilized in the experiment. On the other hand, the controlled variables for the fire whirl's effect only consider the aspect ratio and cross-section area. Thus, the corresponding future works could be:

1. The material of the sample for the firebrand:

   - Only the light paper pieces were utilized as the paper sample, and such light paper pieces have a huge limitation in size. For a relatively larger size, the sample tends to be curved during transportation. And it is relatively too thin compared to real firebrands.

   - The burning property of paper is not the same as the wooden firebrand. Thus, it is lofting behaviours that might act differently with respect to the real firebrand in real wildland fire.

2. Fire whirl generator:

166

- Only one size of the fire whirl generator was utilized in the experiment. And the generated fire whirl is relatively weak, which prevents other materials of the sample from being lofted by the fire whirl.

- In the PIV measurement, another size of the fire whirl generator has been utilized. However, those fire whirl generator is not yet being utilized in the firebrand's lofting experiment.

- Only the on-source fire whirl generator has been utilized to study the lofting mechanism. In order to study the relationship between the spinning of the fire whirl to the lofting mechanism, an off-source fire whirl generator should be utilized in the experiment

3. Other controlled variables:

- Due to the limitation of the paper sample, only a few aspects of the sample could be investigated. With a larger fire whirl, another material of firebrand might be able to be lofted. Then the other properties, such as the shape, density, and thickness, could be taken into account in the experiment.

## 7.2. Numerical study of the lofting mechanism

In this thesis, a brand-new model that calculates the firebrand's lofting has been built. As a brand-new model, it is true that there are a few limitations of these models on the investigation of the firebrand's lofting mechanism in a fire whirl.

1. The current calculation of the firebrand's motion is just based on one instance of the fire whirl. The phenomenon of fire whirl is quite acoustic, and the LES result is transient. Therefore, a future model should calculate the

transportation of the firebrand and calculate the fire whirl simultaneously but not in a separate step (In progress).

2. The rectangular disk-shaped firebrand is utilized to pair with the experimental sample of the firebrand. In the future, more shapes and more geometry of the firebrand should be utilized to calculate the firebrand's lofting.

3. The current aerodynamic momentum equation is not perfectly fit for a real firebrand, future works on the modelling of the aerodynamic momentum that is applied to the firebrand.

# Publication

1. Yuchen Zhang, Ahemd Albadi and Yang Zhang (2022), Experimental Study of Firebrand Lofting Mechanism in a Fire Whirl Induced Flow Field. Proceddings of 28th International Colloquium on the Dynamics of Explosions and Reactive Systems, Paper number. 74.

2. Yuchen Zhang, and Yang Zhang (2022), Statistical investigation on firebrand behaviour in a simulated 3D fire whirl. Proceddings of 28th International Colloquium on the Dynamics of Explosions and Reactive Systems, Paper number. 32.

3. Wang, Q., Zhu, P., Mei, X. H., Foroughi, V., Casal, J., Planas, E., Albadi, A., Zhang, Y. C., & Zhang, Y. (2023). Experimental study of horizontally lifted high-speed nonpremixed flame jets. *Experimental Thermal and Fluid Science*, *140*. https://doi.org/10.1016/J.EXPTHERMFLUSCI.2022.110774

# Conference

1. Yuchen Zhang, 2022, Experimental Study of Firebrand Lofting Mechanism in a Fire Whirl Induced Flow Field. 28th International Colloquium on the Dynamics of Explosions and Reactive Systems (ICDERS 2022), Naples, Italy, Oral presentation.

2. Yuchen Zhang, and Yang Zhang (2022), Statistical investigation on firebrand behaviour in a simulated 3D fire whirl. 28th International Colloquium on the Dynamics of Explosions and Reactive Systems (ICDERS 2022), Naples, Italy, Oral presentation.

# Reference List

[1]. A. B. Basset (1961) [1888], *Treatise on hydrodynamics*, vol. 2, Cambridge: Deighton, Bell and Co., Chapter 22

[2]. A. MURASZEW (1977), The Fire Whirl Phenomenon, 34, 29-45(1979).

[3]. A. MURASZEW (1977), Trajectory of Firabrands in and out of fire whrils. Combustion and Flame, 30, 321-324(1977).

[4]. *About the Campaign | Smokey Bear*. (n.d.). Retrieved September 28, 2022, from https://smokeybear.com/en/smokeys-history/about-the-campaign

[5]. Albini, F. A. (2007). Transport of Firebrands by Line Thermals †. *Http://Dx.Doi.Org/10.1080/00102208308923662*, *32*(5–6), 277–288. https://doi.org/10.1080/00102208308923662

[6]. Albini, F. A., & Brown, J. K. (1996). Mathematical modeling and predicting wildland fire effects. *Combustion, Explosion and Shock Waves 1997 32:5*, *32*(5), 520–533. https://doi.org/10.1007/BF01998574

[7]. Ali Tohidi, Michael J. Gollner, and Huahua Xiao, "Fire Whirls", Annual Review of Fluid Mechanics 2018

[8]. Anthenien, R., Tse, S. and Carlos Fernandez-Pello, A. (2006). On the trajectories of embers initially elevated or lofted by small scale ground fire plumes in high winds. *Fire Safety Journal*, 41(5), pp.349-363.

[9]. Barbosa, P., Amatulli, G., Boca, R., Camia, A., Kucera, J., Libertà, G., San-Miguel-Ayanz, J., Schmuck, G., Schulte, E., & Dierks, H.-H. (2007). Forest fires in Europe 2006. In *Scientific and Technical Reports*. Joint Research Centre - Institute for Environment and Sustainability. Office for Official Publications of the European

Communities. http://dx.doi.org/10.1016/B978-0-12-410434-1.00005-1

[10]. Barowy, A. M. (2010). *Heat and Smoke Transport in a Residential-Scale Live Fire Training Facility: Experiments and Modeling*. Worcester Polytechnic Institute. https://digital.wpi.edu/concern/etds/5425k983w?locale=en

[11]. C. Sanchez Tarifa. On the fligh paths and lifetimes of burning particles of wood. *Tenth symposium on Combustion 1965*, pp.1021-1037

[12]. *California wildfires: Camp fire becomes state's deadliest with 42 people killed | California | The Guardian*. (n.d.). Retrieved September 28, 2022, from https://www.theguardian.com/us-news/2018/nov/12/california-wildfire-latest-camp-woolsey-fires-refugees

[13]. *Canada wildfire: 1,600 structures already destroyed in massive blaze in Fort McMurray, officials say - ABC News*. (n.d.). Retrieved September 28, 2022, from https://www.abc.net.au/news/2016-05-05/wildfire-fort-mcmurray-canada-hundreds-of-structures-destroyed/7385418

[14]. Cruz, M. G., & Alexander, M. E. (2019). Comments on "Evaluating Crown Fire Rate of Spread Predictions from Physics-Based Models." *Fire Technology 2019 55:6*, *55*(6), 1919–1925. https://doi.org/10.1007/S10694-019-00856-2

[15]. Deardorff, J. W. (1974). Three-dimensional numerical study of the height and mean structure of a heated planetary boundary layer. *Boundary-Layer Meteorology 1974 7:1*, *7*(1), 81–106. https://doi.org/10.1007/BF00224974

[16]. Emmons, H. W., & Ying, S. J. (1967). The fire whirl. *Symposium (International) on Combustion*, *11*(1), 475–488. https://doi.org/10.1016/S0082-0784(67)80172-3

[17]. Emmons, H. W., & Ying, S. J. (1967). The fire whirl. *Symposium (International)*

*on Combustion*, *11*(1), 475–488. https://doi.org/10.1016/S0082-0784(67)80172-3

[18]. F., M., & Winterwerp, J. C. (2007). An experimental study into the evolution of the size distribution of kaolinite flocs. *Proceedings in Marine Science*, *8*, 55–73. https://doi.org/10.1016/S1568-2692(07)80006-4

[19]. Fair, G.M., and J.C. Geyer. 1954. Water Supply and Wastewater Disposal. John Wiley and Sons, New York, 973 pp.

[20]. Filkov, A., Prohanov, S., Mueller, E., Kasymov, D., Martynov, P., Houssami, M. el, Thomas, J., Skowronski, N., Butler, B., Gallagher, M., Clark, K., Mell, W., Kremens, R., Hadden, R. M., & Simeoni, A. (2017). Investigation of firebrand production during prescribed fires conducted in a pine forest. *Proceedings of the Combustion Institute*, *36*(2), 3263–3270. https://doi.org/10.1016/J.PROCI.2016.06.125

[21]. *Fire Safety Guidance Note 4 Issued by the Safety Section Fire Safety Risk Assessment*. (2013).

[22]. GANESH, N., ARUNVINTHAN, S., & NADARAJA PILLAI, S. (2019). Effect of surface blowing on aerodynamic characteristics of tubercled straight wing. *Chinese Journal of Aeronautics*, *32*(5), 1111–1120. https://doi.org/10.1016/J.CJA.2019.02.006

[23]. Grayson, M., Pang, W. C., & Schiff, S. (2012). Three-dimensional probabilistic wind-borne debris trajectory model for building envelope impact risk assessment. *Journal of Wind Engineering and Industrial Aerodynamics*, *102*, 22–35. https://doi.org/10.1016/J.JWEIA.2012.01.002

[24]. Hartl, K. A., & Smits, A. J. (2016). Scaling of a small scale burner fire whirl.

172

*Combustion and Flame*, *163*, 202–208. https://doi.org/10.1016/J.COMBUSTFLAME.2015.09.027

[25]. Hartl, K. A., & Smits, A. J. (2016). Scaling of a small scale burner fire whirl. *Combustion and Flame*, *163*, 202–208. https://doi.org/10.1016/J.COMBUSTFLAME.2015.09.027

[26]. Hartl, K. A., & Smits, A. J. (2016). Scaling of a small scale burner fire whirl. *Combustion and Flame*, *163*, 202–208. https://doi.org/10.1016/J.COMBUSTFLAME.2015.09.027

[27]. Hartl, K. A., & Smits, A. J. (2019). Stereo PIV measurements in fire whirls. *Experiments in Fluids*, *60*(1), 1–16. https://doi.org/10.1007/S00348-018-2661-6/FIGURES/16

[28]. Hartl, K., Wang, P., Smits, A., Hartl, K., Wang, P., & Smits, A. (2014). Experimental investigation of the velocity field of a laboratory fire whirl. *APS*, D34.004. https://ui.adsabs.harvard.edu/abs/2014APS..DFDD34004H/abstract

[29]. Himoto, K., & Tanaka, T. (2005). Transport Of Disk-shaped Firebrands In A Turbulent Boundary Layer. *Fire Safety Science*, *8*, 433–444. https://doi.org/10.3801/IAFSS.FSS.8-433

[30]. Hoerner, S.F. (1965) Fluid-Dynamic Drag. Published by the Author, 3-6.

[31]. Holmes, J. D., Letchford, C. W. and Lin, N. (2006) 'Investigations of plate-type windborne debris - Part II: Computed trajectories', *Journal of Wind Engineering and Industrial Aerodynamics*, 94(1), pp. 21–39. doi: 10.1016/j.jweia.2005.10.002.

[32]. Holmes, J., Letchford, C. and Lin, N. (2006). Investigations of plate-type windborne debris—Part II: Computed trajectories. *Journal of Wind Engineering and Industrial Aerodynamics*, 94(1), pp.21-39.

[33]. Hölzer, A., & Sommerfeld, M. (2008). New simple correlation formula for the drag coefficient of non-spherical particles. *Powder Technology*, *184*(3), 361–365. https://doi.org/10.1016/J.POWTEC.2007.08.021

[34]. J. V. Boussinesq (1885), "Sur la résistance qu'oppose un fluide indéfini au repos, sans pesanteur, au mouvement varié d'une sphère solide qu'il mouille sur toute sa surface, quand les vitesses restent bien continues et assez faibles pour que leurs carrés et produits soient négligeables", *Comptes Rendus de l'Académie des Sciences*, **100**: 935–937

[35]. J.D. Anderson, Fundamentals of Aerodynamics (6th edition), McGraw-Hill Education, New York, 2017.

[36]. J.P.WOYCHEESE (1999), Combustion model for wooden brands, Fire research and Engineering. 53-59

[37]. Jain, S., Sitaram, N., & Krishnaswamy, S. (2015). Effect of reynolds number on aerodynamics of airfoil with gurney flap. *International Journal of Rotating Machinery*, *2015*. https://doi.org/10.1155/2015/628632

[38]. Jiayun Song, Naian Liu, (2017) The wind effect of the transport and burning of firebrand. Fire Technology, 53, 1555-1568, 2017

[39]. *Jul 18, 64 CE: Great Fire of Rome | National Geographic Society*. (n.d.). Retrieved September 28, 2022, from https://education.nationalgeographic.org/resource/great-fire-rome

[40]. Koo, Eunmo; Pagni, Patrick J.; Weise, David R.; Woycheese, John P. 2010. Firebrands and spotting ignition in large-scale fires. International Journal of Wildland Fire 19(7) 818-843

[41]. Koo, Eunmo; Pagni, Patrick J.; Weise, David R.; Woycheese, John P. 2010.

Firebrands and spotting ignition in large-scale fires. International Journal of Wildland Fire 19(7) 818-843

[42]. Lazaro, B. J., & Lasheras, J. C. (1992). Particle dispersion in the developing free shear layer. Part 2. Forced flow. *Undefined*, *235*, 179–221. https://doi.org/10.1017/S0022112092001083

[43]. Lee, S. (n.d.). *Computational investigation of flahover mechanisms using fire dynamics simulator (fds)*. Retrieved September 28, 2022, from https://hdl.handle.net/2142/24363

[44]. Lee, Shao-lin. "Axisymmetrical Turbulent Swirling Jet." (1965).

[45]. Luke R.H. and McArthur A.G., "Bushfires in Australia", Australian Government Publishing Service, Canberra, 1978.

[46]. Manzello, S. L., & Suzuki, S. (2012). The new and improved NIST Dragon's LAIR (Lofting and Ignition Research) facility. *Fire and Materials*, *36*(8), 623–635. https://doi.org/10.1002/FAM.1123

[47]. Manzello, S. L., & Suzuki, S. (2013). Experimentally simulating wind driven firebrand showers in wildland-urban interface (WUI) fires: Overview of the NIST firebrand generator (NIST dragon) technology. *Procedia Engineering*, *62*, 91–102. https://doi.org/10.1016/J.PROENG.2013.08.047

[48]. Manzello, S. L., & Suzuki, S. (2021). Ignition vulnerabilities of combustibles around houses to firebrand showers: Further comparison of experiments. *Sustainability (Switzerland)*, *13*(4), 1–14. https://doi.org/10.3390/SU13042136

[49]. Manzello, S. L., Suzuki, S., & Hayashi, Y. (2012). Enabling the study of structure vulnerabilities to ignition from wind driven firebrand showers: A summary of experimental results. *Fire Safety Journal*, *54*, 181–196.

https://doi.org/10.1016/J.FIRESAF.2012.06.012

[50]. Manzello, S. L., Suzuki, S., & Nii, D. (2017). Full-Scale Experimental Investigation to Quantify Building Component Ignition Vulnerability from Mulch Beds Attacked by Firebrand Showers. *Fire Technology*, *53*(2), 535–551. https://doi.org/10.1007/S10694-015-0537-3

[51]. Manzello, S. L., Suzuki, S., Gollner, M. J., & Fernandez-Pello, A. C. (2020). Role of firebrand combustion in large outdoor fire spread. *Progress in Energy and Combustion Science*, *76*. https://doi.org/10.1016/J.PECS.2019.100801

[52]. Martin, J. E., & Meiburg, E. (1998). The accumulation and dispersion of heavy particles in forced two-dimensional mixing layers. I. The fundamental and subharmonic cases. *Physics of Fluids*, *6*(3), 1116. https://doi.org/10.1063/1.868283

[53]. McArthur, A.G. Fire Behaviour in Eucalypt Forests; Technical Report; Forestry and Timber Bureau: Canberra, Australia, 1967

[54]. McGrattan, K. B., McDermott, R. J., Weinschenk, C. G., & Forney, G. P. (2013). *Fire Dynamics Simulator, Technical Reference Guide, Sixth Edition*. https://doi.org/10.6028/NIST.SP.1018

[55]. Meneveau, C., & Lund, T. S. (1998). The dynamic Smagorinsky model and scale-dependent coefficients in the viscous range of turbulence. *Physics of Fluids*, *9*(12), 3932. https://doi.org/10.1063/1.869493

[56]. Ortiz, X., Rival, D. and Wood, D. (2015). Forces and Moments on Flat Plates of Small Aspect Ratio with Application to PV Wind Loads and Small Wind Turbine Blades. *Energies*, 8(4), pp.2438-2453.

[57]. Ortiz, X., Rival, D. and Wood, D. (2015). Forces and Moments on Flat Plates of

Small Aspect Ratio with Application to PV Wind Loads and Small Wind Turbine Blades. *Energies*, 8(4), pp.2438-2453.

[58]. Pramaote, H (2003). Development of particle image velocimetry (piv) for wall shear stress estimation within a 50cc penn state artificial heart ventricular chamber, PhD thesis, The Pennsylvania State University, Access from: https://etda.libraries.psu.edu/files/final_submissions/4977

[59]. Pudasaini, S. P. (2019). A fully analytical model for virtual mass force in mixture flows. *International Journal of Multiphase Flow*, *113*, 142–152. https://doi.org/10.1016/J.IJMULTIPHASEFLOW.2019.01.005

[60]. Raju, N., & Meiburg, E. (1995). The accumulation and dispersion of heavy particles in forced two-dimensional mixing layers. Part 2: The effect of gravity. *Undefined*, *7*(6), 1241–1264. https://doi.org/10.1063/1.868581

[61]. Richter, A., & Nikrityuk, P. A. (2012). Drag forces and heat transfer coefficients for spherical, cuboidal and ellipsoidal particles in cross flow at sub-critical Reynolds numbers. *International Journal of Heat and Mass Transfer*, *55*(4), 1343–1354. https://doi.org/10.1016/J.IJHEATMASSTRANSFER.2011.09.005

[62]. Sanjeevi, S. K. P., Dietiker, J. F., & Padding, J. T. (2022). Accurate hydrodynamic force and torque correlations for prolate spheroids from Stokes regime to high Reynolds numbers. *Chemical Engineering Journal*, *444*, 136325. https://doi.org/10.1016/J.CEJ.2022.136325

[63]. Sanjeevi, S. K. P., Kuipers, J. A. M., & Padding, J. T. (2018). Drag, lift and torque correlations for non-spherical particles from Stokes limit to high Reynolds numbers. *International Journal of Multiphase Flow*, *106*, 325–337. https://doi.org/10.1016/J.IJMULTIPHASEFLOW.2018.05.011

[64]. Sanjeevi, S. K. P., Padding, J., Sanjeevi, S. K. P., & Padding, J. (2017). The drag and lift of different non-spherical particles from low to high Re. *APS*, G36.006. https://ui.adsabs.harvard.edu/abs/2017APS..DFDG36006S/abstract

[65]. *Sir George Cayley - Historic UK*. (n.d.). Retrieved September 28, 2022, from https://www.historic-uk.com/HistoryUK/HistoryofBritain/Sir-George-Cayley/

[66]. Smagorinsky, J., Smagorinsky, & J. (1963). General Circulation Experiments with the Primitive Equations. *MWRv*, *91*(3), 99. https://doi.org/10.1175/1520-0493(1963)091

[67]. Smith, Diane M. "Sustainability and the Origins of Wildland Fire Research." Environment & Society Portal, *Arcadia* (2015), no. 13. Rachel Carson Center for Environment and Society. https://doi.org/10.5282/rcc/7185.

[68]. *Spotting Fire Behavior | NWCG*. (n.d.). Retrieved September 28, 2022, from https://www.nwcg.gov/publications/pms437/crown-fire/spotting-fire-behavior

[69]. Statistics | National Interagency Fire Center. (n.d.). Retrieved September 24, 2022, from https://www.nifc.gov/fire-information/statistics

[70]. *Stokes, G. G. (1851). "On the effect of internal friction of fluids on the motion of pendulums". Transactions of the Cambridge Philosophical Society. 9, part ii: 8–106.*

[71]. *Stokes, George (1851). "On the Effect of the Internal Friction of Fluids on the Motion of Pendulums". Transactions of the Cambridge Philosophical Society. **9**: 8–106. Bibcode:1851TCaPS...9....8S.*

[72]. Suzuki, S., & Manzello, S. L. (2017). Experimental investigation of firebrand accumulation zones in front of obstacles. *Fire Safety Journal*, *94*, 1–7.

https://doi.org/10.1016/J.FIRESAF.2017.08.007

[73]. Suzuki, S., & Manzello, S. L. (2017). Experiments to provide the scientific-basis for laboratory standard test methods for firebrand exposure. *Fire Safety Journal*, *91*, 784–790. https://doi.org/10.1016/J.FIRESAF.2017.03.055

[74]. Suzuki, S., Brown, A., Manzello, S. L., Suzuki, J., & Hayashi, Y. (2014). Firebrands generated from a full-scale structure burning under well-controlled laboratory conditions. *Fire Safety Journal*, *63*, 43–51. https://doi.org/10.1016/J.FIRESAF.2013.11.008

[75]. Terfous, A., Hazzab, A., & Ghenaim, A. (2013). Predicting the drag coefficient and settling velocity of spherical particles. *Powder Technology*, *239*, 12–20. https://doi.org/10.1016/J.POWTEC.2013.01.052

[76]. Tohidi, A., & Kaye, N. B. (2017). Comprehensive wind tunnel experiments of lofting and downwind transport of non-combusting rod-like model firebrands during firebrand shower scenarios. *Fire Safety Journal*, *90*, 95–111. https://doi.org/10.1016/J.FIRESAF.2017.04.032

[77]. Tohidi, A., & Kaye, N. B. (2017). Stochastic modeling of firebrand shower scenarios. *Fire Safety Journal*, *91*, 91–102. https://doi.org/10.1016/J.FIRESAF.2017.04.039

[78]. Tohidi, A., Kaye, N. and Bridges, W. (2015). Statistical description of firebrand size and shape distribution from coniferous trees for use in Metropolis Monte Carlo simulations of firebrand flight distance. Fire Safety Journal, 77, pp.21-35.

[79]. Tohidi, A., Kaye, N., Tohidi, A., & Kaye, N. (2016). Experimental &amp; Numerical Modeling of Non-combusting Model Firebrands' Transport. *APS*, M12.001. https://ui.adsabs.harvard.edu/abs/2016APS..DFDM12001T/abstract

[80]. Tohidi, Ali, "Experimental and Numerical Modeling of Wildfire Spread via Fire Spotting" (2016). All Dissertations. 1681. https://tigerprints.clemson.edu/all_dissertations/168

[81]. Wadhwani, Rahul (2019) Physics-based simulation of short-range spotting in wildfires. PhD thesis, Victoria University. From https://vuir.vu.edu.au/40025/

[82]. Weber, R. O. (1991). Toward a Comprehensive Wildfire Spread Model. *International Journal of Wildland Fire*, *1*(4), 245–248. https://doi.org/10.1071/WF9910245

[83]. Wildland Fire. (n.d.). Retrieved September 23, 2022, from https://www.washoecounty.gov/em/Hazards/Wildland%20Fire.php

[84]. Williams, J. R., & Berndt, H. D. (1977). Sediment Yield Prediction Based on Watershed Hydrology. Transactions of the ASAE, 20, 1100-1104. https://doi.org/10.13031/2013.35710

[85]. Yin, C., Rosendahl, L., Knudsen Kær, S. and Sørensen, H. (2003). Modelling the motion of cylindrical particles in a nonuniform flow. *Chemical Engineering Science*, 58(15), pp.3489-3498.

[86]. Yow, H. N., Pitt, M. J., & Salman, A. D. (2005). Drag correlations for particles of regular shape. *Advanced Powder Technology*, *16*(4), 363–372. https://doi.org/10.1163/1568552054194221

[87]. Zastawny, M., Mallouppas, G., Zhao, F. and van Wachem, B. (2012). Derivation of drag and lift force and torque coefficients for non-spherical particles in flows. *International Journal of Multiphase Flow*, 39, pp.227-239.

[88]. Zastawny, M., Mallouppas, G., Zhao, F. and van Wachem, B. (2012). Derivation of drag and lift force and torque coefficients for non-spherical particles in

flows. *International Journal of Multiphase Flow*, 39, pp.227-239.

[89]. Zhou, K., Suzuki, S., & Manzello, S. L. (2015). Experimental Study of Firebrand Transport. *Fire Technology*, *51*(4), 785–799. https://doi.org/10.1007/S10694-014-0411-8

[90]. 災害教訓の継承に関する専門調査会報告書, 2006, 内閣府

[91]. Sharples, J. J., & Hilton, J. E. (2020). Modeling Vorticity-Driven Wildfire Behavior Using Near-Field Techniques. *Frontiers in Mechanical Engineering*, *5*, 69. https://doi.org/10.3389/FMECH.2019.00069/BIBTEX

[92]. Tohidi, A., & Kaye, N. B. (2017). Aerodynamic characterization of rod-like debris with application to firebrand transport. *Journal of Wind Engineering and Industrial Aerodynamics*, *168*, 297–311. https://doi.org/10.1016/J.JWEIA.2017.06.019

[93]. Storey, M. A., Price, O. F., Bradstock, R. A., & Sharples, J. J. (2020). Analysis of variation in distance, number, and distribution of spotting in southeast Australian wildfires. *Fire*, *3*(2), 1–21. https://doi.org/10.3390/FIRE3020010

[94]. Zhou, Hangxu (2020) *Interaction of big particles with flow- A study of the spotting distances of the firebrands by modelling and simulations.* PhD thesis, University of Sheffield.

[95]. Zhang, Jing (2022) *The Study of Combustion and Emission Characteristics of Partially Cracked Ammonia and Chemiluminescent Emission for Hydrocarbon Fuel Based on the Chemical Kinetic Mechanisms.* PhD thesis, University of Sheffield.

[96]. Lai, Yufeng (2021) *The Study of Fire Spread on an Inclined Wooden Surface by Multiple Spectrum Imaging Systems and Diagnostical Techniques.* PhD thesis,

University of Sheffield.

[97].Wang, Xiao (2021) *The development and utilization of low-cost near infrared imagers for fire detection and diagnostics.* PhD thesis, University of Sheffield.

[98].Muraszew, A., Fedele, J.B., Kuby, W.C., (1979) The Fire Whirl Phenomenon, Combustion and Flame 34: 29-45, http://dx.doi.org/10.1016/0010-2180(79)90077-4

[99].P. Wang, X. Liu and L. Chen, "Experimental Study on Flame Wander of Small-scale Fire Whirl based on Video Image Analysis," *2019 9th International Conference on Fire Science and Fire Protection Engineering (ICFSFPE)*, 2019, pp. 1-4, doi: 10.1109/ICFSFPE48751.2019.9055760.

[100].Wang, P., Liu, N., Zhang, L., Bai, Y., & Satoh, K. (2015). Fire Whirl Experimental Facility with No Enclosure of Solid Walls: Design and Validation. *Fire Technology*, *51*(4), 951–969. https://doi.org/10.1007/S10694-014-0435-0

[101].Wang, P., Liu, N., Liu, X., & Yuan, X. (2018). Experimental Study on Flame Wander of Fire Whirl. *Fire Technology*, *54*(5), 1369–1381. https://doi.org/10.1007/S10694-018-0734-Y

# Statement of COVID-19 impact

The author's PhD started in November 2018. The first year of the author's PhD study is focused on the literature review and discovering the research gap related to the topic of combustion. After passing the Confirmation review, the pandemic of COVID-19 comes. Plenty of restrictions on accessing the resources from the University of Sheffield existed then. Soon, in April 2020, the author returned to China to avoid the sharply spread virus. During this period, the experimental study of the thesis's research had to stop. Therefore, the author's PhD research was forced to focus on theoretical and analytical study. Adjusting the research goal requires an additional literature review. Therefore, the literature review was undertaken during the first few months after the author returned to China.

The author initially planned to study in China for around six months remotely. However, the travel restriction in China soon begins. There is no way to be back in the UK as planned. Therefore, the author has to stay in China to continue the investigation.

With the help of international collaboration with Northeastern University in China, part of the authors' experimental study, such as the PIV test to the flow field of fire whirl, could be undertaken. However, due to the limited resources, other experimental investigations are still unable to undertake as scheduled.

The numerical investigation began in 2021 after a few months of literature review. In that study, an open-source Fire Dynamic Simulator was utilized to simulate the flow field of the fire whirl. As the CFD usually requires a high capacity of computing power, An High-Performance Computer system is required in the simulation. However, due

to internet censorship in China, the condition of the connection with Sheffield's HPC is poor. The numerical investigation is also highly affected in China.

At the end of 2021, the travel restriction in China is not as restrictive as they used to be in the previous few years. Therefore, the author went back to Sheffield. However, since that is already the last year of PhD study, The author focuses mainly on thesis writing but not new research.

All in all, most of the author's PhD career is limited to accessing the university's resources. Even in that condition, the author is still doing the research in both experimental and numerical aspects. Therefore, the outcome of the author's study is severely affected. There are plenty of future works for firebrand's lofting mechanism that the author could not finish within the PhD period. In the following career lift of doing research, the author will continue focusing on this topic to gain a further conclusion.